GENETIC AND MOLECULAR DISSECTION OF NEURONAL INTERCELLULAR SIGNALING IN FRAGILE X SYNDROME

By

Chunzhu Song

Dissertation
Submitted to the Faculty of the
Graduate School of Vanderbilt University
in partial fulfillment of the requirements
for the degree of

DOCTOR OF PHILOSOPHY

in

Biological Sciences
August 11, 2023
Nashville, Tennessee

Approved:

Julian Hillyer, Ph.D. (Chair)

Kendal Broadie, Ph.D. (Advisor)

James Patton, Ph.D.

Qiangjun Zhou, Ph.D.

David Miller, Ph.D.

DEDICATION

This dissertation is dedicated to my father Jin-Cheng Song, who is always my strong mental support for my brave scientific dream.

ACKNOWLEDGEMENTS

Backtracking these five years, I still remember the first day when I arrived at Vanderbilt. My first impression of the campus is green, quiet, and beautiful. While I lost direction in a maze-like building, I love the academic atmosphere that conveyed by the labs along the hallway. My faith to the Vanderbilt scientific training starts from an attracting picture wall on the third floor of MRB III. It has lots of journal's cover pictures with encouraging words: *coming soon… your cover*. I then decided to work in my best at Vanderbilt to publish my own research on a prestigious journal.

The basic training in my first year was intense, painful, but fulfilled. Lots of courses, homework, assignments, group discussion, and lab rotation make me barely have time to stop running my brain. As it was also my first year studying in the US, language barrier indeed increased difficulty in the study and communication. To overcome this obstacle, I recorded almost every lecture at daytime and listened again after work at night. Meanwhile, I kept pushing myself to be familiar in speaking all professional items in English. This experience raised a humor for me that I, an international student who have passed the Test of English as a Foreign Language (TOEFL) and Graduate Record Examination (GRE) before arriving in the US, still need to study the English that is different from what I learned for years. Having the chance of rotating in four labs with entirely different research topics, my technique skills and scientific view are expanded especially in my beloved molecular and biochemical biology, providing me a solid foundation to efficiently study and process my Ph.D projects. I appreciate all the lab training and courses in the first year enlightened my critical thinking. Importantly, I learned a lesson from my first-year experience that never giving up in front of new life challenges.

Entering the second year in PhD Program, I officially started my thesis research after I joined the Broadie lab. Here, I would like to thank Professor Kendal Broadie for accepting me to join the lab. Due to my blank experience in neuroscience, I began to learn basic knowledge in neurobiology by using a simple synaptic model, *Drosophila* larval neuromuscular junction, to explore intercellular signaling. Since it was also my first time to use the *Drosophila* model, I spent around three months with the help from Kendal to figure out *Drosophila* genetics, receptor immunohistochemical staining, *Drosophila* developmental stages, neuromuscular junction structure, as well as *Drosophila* genetic tools. It was a starting stage with lots of frustration in failure and overwhelm. Graduate school courses and exams, together with teaching and grading undergraduate lab, making me hard to have enough time to focus on lab research at daytime. To troubleshoot experiments, I started to work in lab at nights and luckily overcame all obstacles no matter in techniques or working pace. After this phase, I went through a happy stage where most of experimental results started to become stable with a clearer research aim until Covid 19 pandemics came. . Staying at home was a hard-won time for me to 100% focus on studying, which allowed me to fully prepare and finally pass my qualify exam, although I had to delay my bench work. I appreciate the tight guidance from Kendal and the help from lab members as well as committee members in that period. Situations that are beyond expectation are not always negative. Instead, it depends on how we plan and use it.

In graduate school, having a good publication is not easy. When I studied my first project, several issues occurred: two opposite results versus previous publication, and a phenocopy with overexpression and RNAi for the same gene *coracle*. Although reviewers suggested several reasonable experiments for the manuscript, it was still an unexpected long journey to genetically prove the conflicts with previous publications. I still remember the frustration when a chromosome

recombination failed because of the inefficient genetic tool, which I worked for more than two months with lots of screening. As a saying in biological studies: although we have fully prepared plans before the experiment, it is impossible to always have the expected results after testing. It was lucky for me to have Emma, our research specialist in the lab, help me make chromosome recombination so that I was able to continue measuring downstream results and have solid evidence provided to reviewers. I also would like to thank my peer colleague Shannon for helping in electrophysiological test, whose results provide unbiased evidence to support my conclusion. Even though I encountered obstacles in the first project, I still learned a lot of essential knowledge in neuroscience, intercellular signaling, and a lesson that never afraid of challenging the conclusion in previous publication.

Rainbows are always after clouds. Falling into a valley could discover a new avenue if we keep open-minded. My first project somehow inspired me to transfer my interest to transcellular communication in the central nervous system. Initially, the major reason to transferred research direction was not only I tried to avoid complicated genetic recombination (it turned out a too naïve thought later), but also the difficulty that I have met in handling molecular and biochemical study with less protein/RNA levels at the tiny neuromuscular junction structure. To apply my advantages at molecular biology, using brains, the tissue possesses more total protein/RNA levels, to explore the molecular mechanism in Fragile X Syndrome became an ideal choice. I therefore began testing the direct molecular interaction between neuronal Fragile X Mental Retardation Protein (FMRP) and pMad, a remaining question from my first project. Coincidently, a previous graduate student Dominic published research about developmental neuron clearance regulated by glia. It therefore attracted my attention to put my neuronal signaling network into the big picture of neuron-glia interaction. With more article reading, I noticed massive researchers focus on the role of glial

signaling in neuronal clearance but barely saw reports to explore how neuronal signaling regulates glial activity. Moreover, the previous report showed neuronal FMRP plays primary roles in glial engulfment but left the related molecular mechanisms to be determined. Thus, all these information induced my huge curiosity to deeply dig the mechanisms of FMRP-mediated neuron-to-glia signals for neuronal removal by combining my tested neuronal signaling network. At the beginning of the project, I naively used mushroom body, a relatively big brain area to store memory, to explore this intercellular interaction. However, the circuits in mushroom body are barely remodeled in juvenile adult brains. Kendal then suggested using other three types of neurons with obvious remodeling behavior in my study. After several tests, we decided to continue using the PDF-Tri neuron, which is easy to manipulate and has a clearer background in the lab, to study neuron-to-glia communication. The biggest challenge in this research is conducting a strict timing due to the rapid developmental reduction in total RNA/protein levels and neuronal removal. I spent several weeks determining the best way to synchronize *Drosophila* adults and the best time window to measure molecular and cellular differences. My second work went fast, although some obstacles were still unavoidable. To meet the requirements of graduation for my training, I started to work at days and nights, most of time until midnights. Including revision in the PNAS, the whole project was spent only one year with the fact that I work hard. Meanwhile, I also hugely appreciate all well-developed *Drosophila* genetic tools especially Gal4/UAS system and rapid generation of *Drosophila* models, as well as the generous support from Kendal. Otherwise, it is impossible for me to run multiple tests in a short time. While my initial goal to start this project was trying to escape from classic genetics, I gradually realized the truth that genetics as a method is unavoidable even in brain and molecular studies. To force myself to face it, I independently operated genetic recombination to combine Gal4/UAS and LexA/LexAOP systems together in

same individuals for the test of glial Rab7 volume with different neuronal signal RNAi. Although this process still took a long period (about two months), I eventually overcame my fear and obtained the expected flies for a follow-up experiment.

Altogether, PhD is not an easy degree as what we need to tackle is not only scientific questions. However, PhD training is a precious experience that strengths me in both science and life. Over these years, I have too many appreciation words for the colleagues surrounding me. My most important colleague is my adviser Professor Kendal Broadie. I sincerely appreciate the training and guidance from Kendal for these four years. He is very patient in teaching basic knowledge of neuroscience and *Drosophila* model after I join the lab. Although I have barriers in languages as an international student, he still edited and revised all my manuscripts in detail. Kendal always provides guidance at an appropriate time point so that I can efficiently solve problems. Moreover, he is generous in supporting students with any possible experiment and meanwhile easy to access through emails. Kendal is never stingy in providing resources and personnels to students for the important networking. He is also sweating to make an ice cream gamble for experimental results. Apart from the mentorship in lab, he even shares his useful advice in job hunting. Kendal always immediately sent out strong recommendation letters for my postdoctoral application. I therefore received lots of interviews and eventually obtained postdoctoral offers from the labs at both Harvard Medical School and Stanford University affiliated with Howard Hughes Medical Institute. I will learn Kendal's good quality as a mentor to train my future students. In the lab, I would like to thank previous and current members for providing communication and suggestions for my research work, especially Emma Rushton who teaches me *Drosophila* genetics, Dominic Vita provides suggestions and scientific communication, and Shannon Leahy provides help in lab meeting notes and lab event organization. I sincerely appreciate all the committee members for

their training and suggestions. The members also spent big efforts in recommending me for my postdoctoral application, which is another reason I can receive a good postdoc appointment. Out of school, I thank my friends and family who are open to talk with me, especially my father always gives strong mental support over these years. Finally, I would like to thank myself for keeping hard-working, learning, and thinking. Importantly, even though I encountered lots of difficulties in graduate school, I am proud that I never gave up chasing higher scientific goals and pursuing my dream to become an excellent faculty in the future. I am also proud that I keep stepping up stairs each year to build up my multiple capabilities. I will continue challenging ground-breaking science during the postdoc career with the knowledge, intensity, and professionalism that I have been passed by at Vanderbilt.

TABLE OF CONTENTS

LIST OF FIGURES

LIST OF TABLES

LIST OF ABBREVIATION

AICD	Amyloid Precursor Protein Intracellular Domain
AMPA	α-amino-3-hydroxy-5-methyl-4-isoxazolepropionic Acid
APP	Amyloid Precursor Protein
APPL	Amyloid Precursor Protein-like
AZ	Active Zone
BDSC	Bloomington Drosophila Stock Center
BMP	Bone Morphogenetic Protein
BMPR	Bone Morphogenetic Protein Receptor
Brp	Bruchpilot
BSA	Bovine Serum Albumin
Cac	Cacophony
CaCl2	Calcium Chloride
CCAP	Crustacean Cardioactive Peptide
CED-1	Cell Death Abnormality Protein 1
ChIP	Chromatin Immunoprecipitation
CNS	Central Nervous System

Cora	Coracle
Dlg	Disc Large
DNA	Deoxyribonucleic Acid
DPE	Day Post-Eclosion
Drpr	Draper
EDTA	Ethylenediaminetetraacetic Acid
EGF	Epidermal Growth Factor
EJC	Excitatory Junction Current
EMI	Elastin Microfibril Interfacer
ER	Endoplasmic Reticulum
Evi	Evenness Interrupted
FERM	Four-Point-one-Ezrin-Radixin-Moesin
FMR1	Fragile X Mental Retardation 1
FMRP	Fragile X Mental Retardation Protein
FXS	Fragile X Syndrome
Fz	Frizzled
GAPDH	Glyceraldehyde 3-phosphate Dehydrogenase

Gbb	Glass Bottom Boat
GFP	Green Fluorescent Protein
GluRIIA	Glutamate Receptor Type II A
GluRIIB	Glutamate Receptor Type II B
GluRIIC	Glutamate Receptor Type II C
GluRIID	Glutamate Receptor Type II D
GluRIIE	Glutamate Receptor Type II E
HEPES	N-2-hydroxyethylpiperazine-N'-2-ethanesulfonic Acid
HRP	Horseradish Peroxidase
ILP	Insulin-like Peptide
InR	Insulin Receptor
IP	Immunoprecipitation
JNK	c-Jun N-terminal Kinase
KCl	Potassium Chloride
KH	K Homology
LIMK1	Lin11/Isl1/Mec3 Domain Kinase 1
LRP	Lipoprotein Receptor-related Proteins

LSM	Laser-Scanning Confocal Microscopy
mEJC	Miniature Excitatory Junction Current
MgCl2	Magnesium Chloride
Mmp1	Matrix Metalloproteinase 1
mRNA	Messenger Ribonucleic Acid
NaCl	Sodium Chloride
NEDD4	Neural Precursor Cell Expressed Developmentally Down-Regulated Protein 4
NES	Nuclear Export Sequence
NIM	Nimrod
NLS	Nuclear Localization Sequence
NMJ	Neuromuscular Junction
NT	Neurotransmitter
OE	Overexpression
pAkt	Phosphorylated Protein Kinase B
PBS	Phosphate-Buffered Saline
PCR	Polymerase Chain Reaction
PDF	Pigment Dispersing Factor

PDK	3-Phosphoinositide-Dependent Kinase
PFA	Paraformaldehyde
PHLPP	PH Domain Leucine-Rich Repeat Protein Phosphatase
PI3K	Phosphatidylinositol 3-Kinase
pMad	Phosphorylated Mothers Against Decapentaplegic
PNS	Peripheral Nervous System
PP2A	Protein Phosphatase 2a
Prtp	Pretaporter
PS	Phosphatidylserine
qPCR	Quantitative Polymerase Chain Reaction
RGG	Arginine-Glycine-Glycine
RIM	Rab3-Interacting Molecule
RIM-BP	RIM-Binding Protein
RIP	Immunoprecipitation
RNA	Ribonucleic Acid
RNAi	RNA Interference
RNP	Ribonucleoprotein

ROR	Receptor Tyrosine Kinase-Like Orphan Receptor
RT	Room Temperature
Ryk	Tyrosine (Y) Kinase
sAPPL	Secreted APPL
SILAC	Stable Isotope Labeling by Amino Acids In Cell Culture
SIM	Structured Illumination Microscopy
SIMU	Six-Microns-Under
SMAD	*C. elegans* Small (Sma) Mothers Against Decapentaplegic
SNARE	Soluble N-Ethylmaleimide-Sensitive Factor-Attachment Protein Receptor
SREC	Scavenger Receptor from Endothelial Cells
SSR	Subsynaptic Reticulum
Stau	Staufen
SV	Synaptic Vesicle
SYD	Synaptic Defective
TEVC	Two-Electrode Voltage-Clamp
tRNA	Transfer Ribonucleic Acid
t-SNARE	Target Soluble N-Ethylmaleimide-Sensitive Factor-Attachment Protein Receptor

UTR	Untranslated Region
VDRC	Vienna Drosophila Resource Center
VGCC	Voltage Gated Ca^{2+} Channels
VNC	Ventral Nerve Cord
v-SNARE	Vesicular Soluble N-Ethylmaleimide-Sensitive Factor-Attachment Protein Receptor
Wg	Wingless
Wit	Wishful Thinking
Wls	Wntless
Wnt	Wingless + INT-1
YFP	Yellow Fluorescent Protein
ZO-1	Zonula Occludens-1

CHAPTER I

Overview of Dissertation

Fragile X Syndrome (FXS) is an inherited intellectual disability associated with autism spectrum disorder caused by a total loss of Fragile X Mental Retardation Protein (FMRP; Rajaratnam et al., 2017; Razak et al., 2020). FMRP has key roles in cell-to-cell communication during synaptogenesis and synaptic remodeling (Friedman et al., 2013; Pan and Broadie, 2007a; Song and Broadie, 2023). To mediate the intercellular communication, the RNA-binding FMRP regulates the level of proteins that are associated with transcellular signaling cascades by binding intracellular transcripts (Friedman et al., 2013; Song and Broadie, 2023). Intercellular signaling in the nervous systems is fundamental in axonal wiring (Guy et al., 2015), circuit formation (Demarque et al., 2002), and synapse elimination (Sharma et al., 2019; Vita et al., 2021). Disruption of this signaling results in misregulated neurodevelopment (Chan et al., 2020), aberrant neurotransmission (Soto et al., 2018), and neuroinflammation (Turola et al., 2012), which ultimately results in a host of neurological diseases, such as FXS. With the advantages of well-developed genetics and rapid generation time in the *Drosophila* model, I first studied FMRP-dependent intercellular signaling in the formation of synaptic terminals (boutons), focusing on neuron-to-muscle crosstalk at the Drosophila larva glutamatergic neuromuscular junction (NMJ; Song et al., 2022). In the second half of my thesis, I study FMRP-dependent intercellular signaling in brain circuit remodeling, focusing on neuron-to-glia communication in developmental neuron clearance in the adult juvenile central nervous system (CNS; Song and Broadie, 2023). Both projects demonstrate novel FMRP-mediated molecular mechanisms that regulate transcellular signaling pathways. In this overview, I will introduce the initiation and inspiration of these two facets of my thesis research.

The aim of my initial research is to understand how FMRP at the NMJ participates in synaptic formation in motor neurons. As a developmental protein, FMRP is widely expressed in a majority of cell types in different tissues within restricted time windows (Cheever et al., 2010; Tamanini et al., 1997; Tessier and Broadie, 2011; Verheij et al., 1993). In both mammals and *Drosophila*, FMRP has a particularly high expression level in neurons (Roth et al., 2021; Tessier and Broadie, 2011). Therefore, there has been a focus on exploring the function of neural FMRP, but much less study of FMRP in other tissues, such as muscle. The Broadie lab uses a *Drosophila* larval NMJ to study the control of muscle movement, and to map synaptic signaling networks regulating synaptic architecture and neurotransmission (Pan and Broadie, 2007a; Zhang et al., 2001). Previous lab studies showed loss of FMRP in neurons induces overgrown NMJ presynaptic boutons, condensed synaptic vesicle pools, and strengthened synaptic transmission (Pan et al., 2008; Zhang et al., 2001). The lab also reported overexpression of FMRP in muscle causes decreased presynaptic bouton formation and accumulation of postsynaptic glutamate type II A receptor (GluRIIA) (Pan and Broadie, 2007a). GluRIIA-containing ionotropic receptors are located opposite on presynaptic active zones, and are known to play roles in the reverse regulation (retrograde signaling) of presynaptic development (Kamimura et al., 2019; Sulkowski et al., 2016). However, FMRP interaction with this signaling mechanism was unknown.

To address this question, I started testing if postsynaptic FMRP interacts with the GluRIIA pathway. Previously, studies show a double-strand RNA-binding protein (dsRBP) Staufen interacts with the scaffold Coracle signaling to regulate GluRIIA accumulation on the postsynaptic muscle (Chen et al., 2005; Gardiol and St Johnston, 2014). Staufen has important roles in regulating bound mRNA localization, mRNA stability, mRNA translation, and ribonucleoprotein (RNP) assembly (Heraud-Farlow and Kiebler, 2014). Neuronal Staufen also colocalizes with

FMRP in somatic P bodies, indicating their potential interaction in mRNA degradation and translational control (Barbee et al., 2006). Downstream Coracle (mammalian Four-Point-one-Ezrin-Radixin-Moesin (FERM) protein homolog) binds to filamentous (F) actin and to the GluRIIA C-terminus, acting to tether receptors to the cytoskeleton in the postsynaptic domain (Chen et al., 2005; McClatchey, 2014). In my work, I established an FMRP-Staufen-Coracle-GluRIIA signaling cascade in muscles that transcellularly modulate presynaptic bouton formation (Figure 1.1). To test FMRP RNA-binding functions, my RNA immunoprecipitation showed FMRP binds staufen mRNA to stabilize transcript levels (Figure 1.1). Downstream, the RNA-binding Staufen protein binds coracle mRNA to inhibit the translation of the Coracle scaffold, linking GluRIIA-containing receptor to the underlying actin cytoskeleton actin (Figure 1.1). Muscle-targeted FMRP, Staufen, and Coracle RNAi cause elevated GluRIIA levels and bouton formation, consistent with mutant phenotypes (Song et al., 2022). Elevated GluRIIA transcellularly activates non-canonical Bone Morphogenetic Protein (BMP) signaling to induce presynaptic bouton growth via increased phosphorylation of Mothers against decapentaplegic (pMad) around active zones (Kamimura et al., 2019; Sulkowski et al., 2016). To phosphorylate Mad around active zones, the BMP type II receptor Wishful Thinking (Wit) is non-canonically over activated and then transduces its phosphate to the targeted Mad proteins (Moulton et al., 2020; Sulkowski et al., 2016; Vanlandingham et al., 2013). This process does not require an increased Wit ligand, Glass bottom boat (Gbb) (Sulkowski et al., 2016). I therefore tested presynaptic pMad levels with muscle-targeted RNAi and mutants to find that reducing muscle FMRP, Staufen, and Coracle elevates presynaptic pMad accumulation around active zones (Figure 1.1). Together, these results suggest a muscle FMRP-Staufen-Coracle signaling cascade suppresses postsynaptic GluRIIA levels, which, in turn, intercellularly inhibits presynaptic pMad accumulation to repress bouton formation.

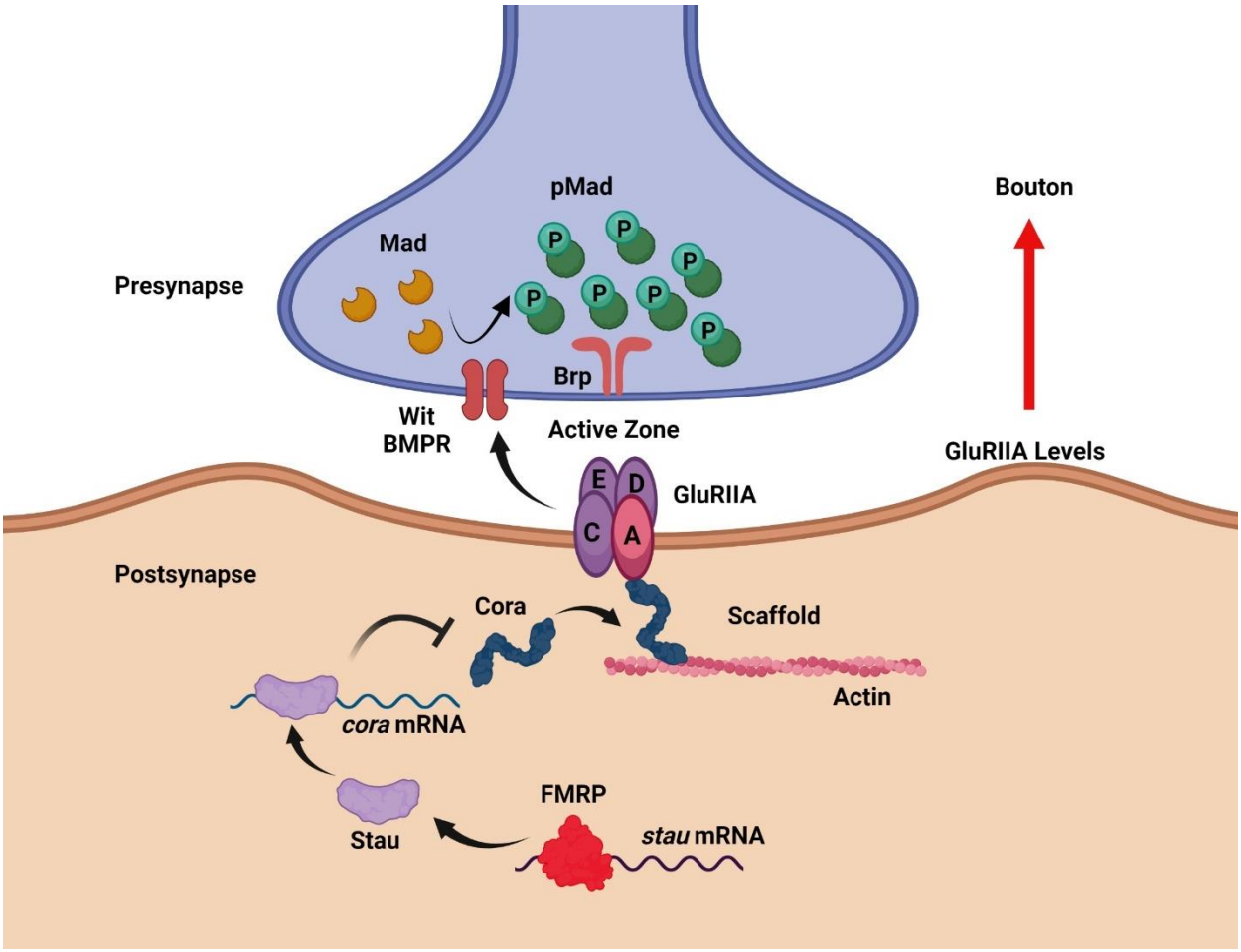

Figure 1.1 Postsynaptic FMRP negatively regulates glutamate receptors to limit presynaptic synaptogenesis (Song, et al., 2022).

In the *Drosophila* larval neuromuscular junction postsynaptic compartment (bottom), FMRP directly binds to *staufen* (*stau*) mRNA to promote translation. Staufen, in turn, binds *coracle* (*cora*) mRNA to inhibit translation. Coracle acts as an actin scaffold to anchor glutamate receptor type II A (GluRIIA) opposing the presynaptic active zone scaffolded by Bruchpilot (Brp). GluRIIA accumulation induced by loss of postsynaptic FMRP activates trans-synaptic signaling via the BMP receptor (BMPR) Wishful Thinking (Wit) to drive Mad phosphorylation (pMad) around presynaptic active zones. This noncanonical GluRIIA-BMPR signaling results in presynaptic bouton formation. Figure created with BioRender (BioRender.com).

In the second half of my Ph.D training, I switched to studying cell-to-cell communication from the *Drosophila* larval NMJ to the adult brain. Specifically, I started to explore neuronal FMRP-dependent neuron-glia crosstalk in neuronal pruning within developmental brains. Neuronal pruning is a process that extra neuronal structures and synaptic connections are eliminated in immature nervous system, in order to form properly functional circuitries (Low and Cheng, 2006; Santos and Noggle, 2011). The intriguing question of neuronal pruning requires intercellular interaction between targeted neurons and glia acting as directed phagocytes (Morizawa et al., 2022; Paolicelli et al., 2011; Raiders et al., 2021; Sakai, 2020).During neurodevelopment, both mammalian and *Drosophila* brain remodeling includes the clearance of unneeded neurons to form mature circuits (Raiders et al., 2021; Schafer et al., 2012; Sekar et al., 2016). To remove these neurons, glia engulf them, followed by intracellular digestion within an endosolysosomal network (Kessissoglou et al., 2020). Both mammals and *Drosophila* have diversified glial cell types in the central nervous system (CNS) and peripheral nervous system (PNS). Focusing on glial subtypes in the CNS, mammals have oligodendrocytes, astrocytes, ependymocytes, radial glia, Schwann cells, enteric glial cells, satellite cells, and microglia (Hanani and Spray, 2020; Jäkel and Dimou, 2017; Nazareth et al., 2021; Rasband, 2016). In the *Drosophila* brain, glia are classified into surface glia (to form blood-brain barrier), neuropil glia (axon ensheathment and pruning) and cortex glia (gas and nutrition exchange) (Ou et al., 2014). Current popular glia "stars" in studying neuronal pruning are astrocytes and a brain resident macrophage microglia, which can be induced by engulfment by neuron-released "eat me" signals such as a phospholipid phosphatidylserine (PS) (Dejanovic et al., 2022; Lala et al., 2022; Sokolova et al., 2021). Both *Drosophila* and mammals have astrocytes but only mammals have microglia. This clearance process is highly conserved from humans to *Drosophila*, allowing me to explore FMRP-

modulated neuron-glia interactions for brain circuit remodeling using the powerful *Drosophila* genetic model.

FXS has been well-characterized to show reduced neuronal clearance (Gatto and Broadie, 2011; Razak et al., 2020; Song and Broadie, 2023; Vita et al., 2021). The Broadie Lab identified the pigment dispersing factor (PDF)-Tripeptidergic neuron population to be developmentally-transient, with a failure to prune in the *Drosophila* FXS disease model (Gatto and Broadie, 2011; Vita et al., 2021). Our previous lab studies show neuronal FMRP, rather than glial FMRP, regulates the glial phagocytosis for PDF-Tri neuron removal in adult juvenile brains (Vita et al., 2021), indicating a neuron-to-glia signaling mechanism during neuronal pruning. However, the related transcellular signaling network remained elusive. Inspired by my first research project, I started by testing if neuronal pMad signaling plays a role in the glial phagocytosis defect in the FXS disease model (Figure 1.2). Reducing neuronal pMad blocks the clearance of PDF-Tri neurons in the juvenile brain, suggesting impaired glial activity. As mammalian FMRP reportedly binds SMAD (mammal Mad homologue) transcripts (Ascano et al., 2012), I next found neuronal FMRP binds *mad* mRNA to destabilize the bound transcripts, which consequently suppresses pMad levels in neurons (Figure 1.2). However, both loss of neuronal FMRP and pMad block PDF-Tri neuron clearance, contrary to expectation. I therefore aimed to discover a misregulated downstream mechanism that results in this phenocopy. As a transcription factor, pMad positively regulates transcription of insulin receptor (InR) to facilitate the assembly of mature InRs in neuronal plasma membrane (Deignan et al., 2016). Yet, loss of FMRP increases InR expression, supporting inhibited regulation from FMRP to pMad signaling (Figure 1.2). These findings suggested InR is not the misregulated molecular player. I therefore continued measuring if FMRP-pMad signaling mediates the levels of phosphorylated protein kinase B (pAkt), a downstream molecule that

positively regulated by InR (Fazakerley et al., 2019; Gross and Bassell, 2012; Kang et al., 2018; Vinayagam et al., 2016) Consistently, knockdown of both neuronal FMRP and pMad elevates pAkt levels inside PDF-Tri neurons. Genetically correcting neuronal pAkt levels within neuronal *mad* RNAi background restores normal PDF-Tri neuron removal, suggesting pAkt is the convergent downstream regulative signal (Figure 1.2). To test intercellular communication from neurons to glia in this clearance mechanism, I tested the neuron-secreted "eat me" signal Pretaporter (Prtp; Kuraishi et al., 2009) and cleavable Amyloid Precursor Protein-like (APPL; Kessissoglou et al., 2020). Prtp is an Endoplasmic Reticulum (ER) protein that will be translocated to plasma membrane in apoptotic cells to bind glial phagocytotic receptor Draper, inducing glia engulf the dying cell (Kuraishi et al., 2009). The single-transmembrane APPL has a cleavable extracellular N terminus, which can be phagocytized by glia to regulate glial endolysosomal activity (Kessissoglou et al., 2020). My results show Prtp signaling is tightly managed by the neuronal FMRP-pMad-InR-pAkt cascade, whereas APPL has additional roles in regulating neuron-glial cross talk (Figure 1.2). These discoveries provide insights into an FMRP-dependent control pathway for neuron-to-glia communication in neuronal pruning from developing brain circuits, which opens a new molecular mechanism avenue with the potential for devising FXS therapeutic treatments.

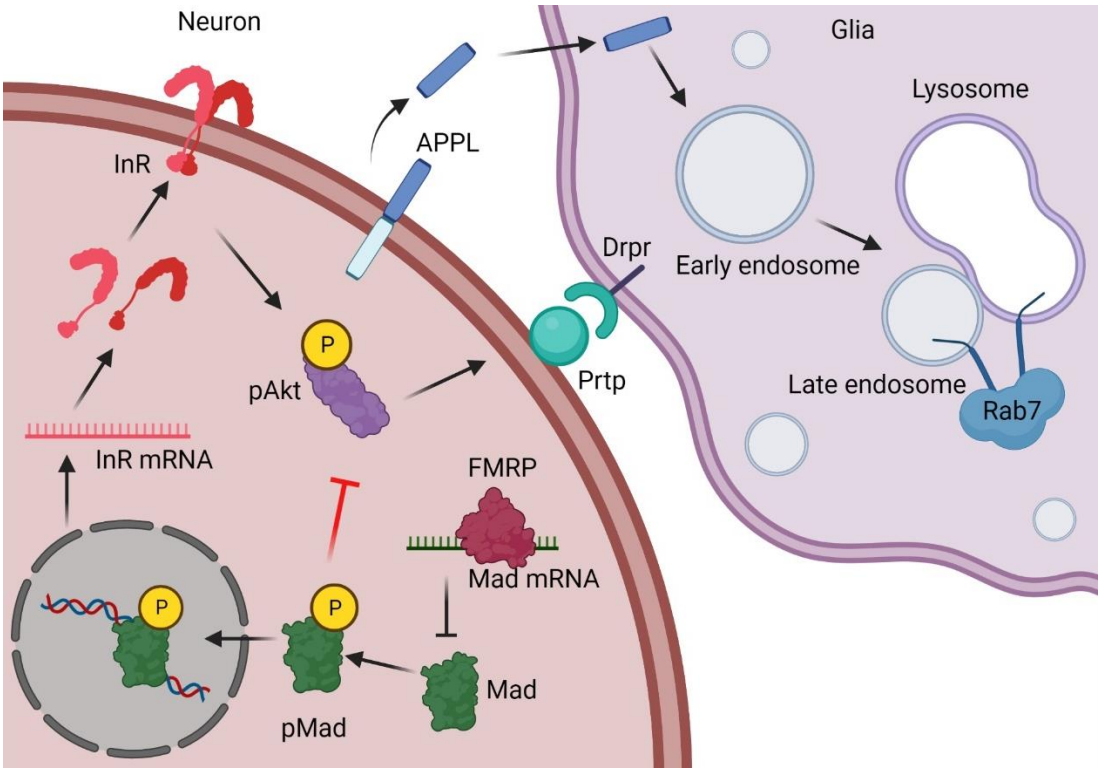

Figure 1.2 A neuronal FMRP-pMad-InR-pAkt signaling network regulates Prtp and APPL neuron-to-glia signaling during brain circuit pruning (Song and Broadie, 2023).

Neuronal FMRP binds *mad* transcripts to restrict the transcription factor pMad signaling. pMad promotes InR transcription, but inhibits pAkt signaling, to regulate downstream Draper ligand Prtp and APPL intercellular communication for glial phagocytosis during neuron pruning from the juvenile brain. Glial activation is measured through endolysosomal Rab7 volume. Figure created with BioRender (BioRender.com)

1.1 Fragile X Syndrome

Fragile X syndrome (FXS) is the most common heritable cause of intellectual and autism spectrum disabilities, and X-linked disorder with approximately 1 in 4000 males and 1 in 8000 females affected (Crawford et al., 2001; Garber et al., 2008). The first clinical indication is delayed neurodevelopment, typically with delayed speech by age 2 (Garber et al., 2008). FXS children

display autism-like features, such as hand flapping, hand biting, gaze avoidance, tactile defensiveness, and hyperarousal to sensory stimuli (Brown et al., 1986; Hagerman et al., 1986). In most of FXS patients, the 5' untranslated region (UTR) of *fragile X mental retardation 1* gene (*FMR1*) has expanded CGG repeats (>200) that cause promoter hypermethylation, inducing epigenetic transcriptional silencing with a total loss of encoded Fragile X Mental Retardation Protein (FMRP) (Pieretti et al., 1991; Verkerk et al., 1991). *FMR1* is widely expressed, but especially enriched in brain neurons (Ashley et al., 1993). A few reported disease cases are point mutations (for example, Gly266GLu (G266E), Ile304Asn (I304N)) in the FMRP RNA-binding domains (RBDs), which impair the canonical FMRP mRNA translational regulation function (Starke et al., 2022).The human *FMR1* gene is at Xq27.3 and consists of 17 exons (Tabolacci and Neri, 2017). FMRP contains multiple domains important for function, including two Tudor domains that interact with RNA, chromatin and other proteins; a nuclear localization sequence (NLS) and nuclear export sequence (NES); two K homology (KH) domains (KH1, KH2) and an arginine-glycine-glycine (RGG) rich motif, which all mediate RNA binding (Figure 1.3) (Bassell and Warren, 2008; Richter and Zhao, 2021). While a suspected third KH domain (KH0) has been identified by using X-ray crystallography (Myrick et al., 2015), its RNA-binding capabilities have not been well tested. In mammals, FMRP has two paralogs, Fragile X Related 1 (FXR1) and FXR2, with separable functions (Drozd et al., 2018). However, only FMRP has highly conserved structure and function in multiple species. *Drosophila* FMRP shares ~60% similarity in total amino acid sequence and 70-80% identity in RNA-binding domains compared to human FMRP (Drozd et al., 2018; Tessier and Broadie, 2011). Additionally, *Drosophila* FMRP has conserved function as humans. Expressing human *FMR1* in *Drosophila* FXS model fully rescues both molecular and cellular defects in neurons (Coffee et al., 2010).

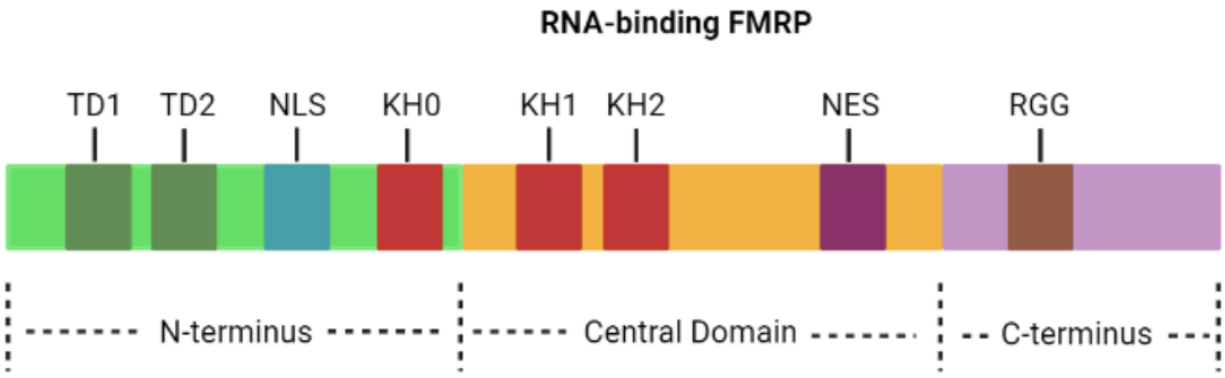

Figure 1.3 FMRP functional domains (D'Annessa et al., 2019).

The N-terminus contains two Tudor motifs (TD1, TD2), a nuclear localization sequence (NLS), and a predicted RNA-binding K homology (KH0) motif. The central domain contains two KH motifs (KH1, KH2) and a nuclear export sequence (NES). The C-terminus contains an RNA-binding arginine-glycine-glycine (RGG) rich motif. Figure created with BioRender (BioRender.com).

Based on the pathology of FXS, a few *Drosophila* disease models have been created to block the expression of *Drosophila FMR1* (*dfmr1*). In the Broadie Lab, we have primarily used the *dfmr1*$^{\Delta 50M}$ mutant, with a total loss of FMRP made by P-element imprecise excision deletion (Zhang et al., 2001) to study the mechanisms of dysregulated neurodevelopment within a FXS disease model. This model shares numerous similar symptoms with human FXS patients, including delayed neurodevelopment (Doll and Broadie, 2015; Song et al., 2022), overgrown neuronal structures (i.e., dendrites and axon terminals) (Pan and Broadie, 2007b; Pan et al., 2004; Zhang et al., 2001), increased neurotransmission (Zhang et al., 2001), hyperactivity (Doll et al., 2017), hypersensitivity to stimuli like odors (Golovin et al., 2019; Golovin et al., 2021), and defects in learning and memory (Bolduc et al., 2008; Gatto and Broadie, 2009; Siller and Broadie, 2011).

With the enormous advantages of *Drosophila* genetics, this disease model has provided numerous fundamental insights into FXS molecular mechanisms and potential targets for FXS treatments.

1.2 *Drosophila* Larval Neuromuscular Junction Synapse Model

Drosophila has a glutamatergic neuromuscular junction (NMJ) that assembles with a presynaptic axon terminal (arrayed synaptic boutons) separated by an extracellular synaptic cleft from the postsynaptic muscle with type II ionotropic glutamate receptors (iGluRs) (Figure 1.4). To form the presynaptic terminal, a motor neuron pathfinds from the ventral nerve cord (VNC) to contact a specific target muscle, with the axon tip growth cones branching to form bouton varicosities with the assembled machineries for glutamate neurotransmitter release (Cammarata et al., 2016; Lowery and Vactor, 2009). In the presynaptic compartment, the Bruchpilot (Brp) scaffold recruits Ca^{2+} channels (pore-forming Cacophony (Cac) subunit) together with synaptic defective 1 (SYD-1) and SYD-2/Liprin-α scaffolds to form a "T" bar structure at a presynaptic active zone (AZ), regulating synaptic vesicle pool size (Chou et al., 2020; Fouquet et al., 2009; Hallam et al., 2002; Kittel et al., 2006). On the postsynaptic side, the scaffold Disc Large (Dlg) within the subsynaptic reticulum (SSR) system of tubular-lamellar membrane folds envelops the presynaptic bouton (Parnas et al., 2001; Sone et al., 2000; Wan et al., 2000). Ionotropic glutamate receptors type IIA (GluRIIA) and type IIB (GluRIIB) cluster opposite of the AZ to receive the glutamate neurotransmitter (Chou et al., 2020; DiAntonio et al., 1999; Marrus and DiAntonio, 2004; Petersen et al., 1997). GluRIIA and GluRIIB classes are defined by a variable A/B subunit together with three other essential subunits; GluRIII/GluRIIC, GluRIID, and GluRIIE (Featherstone et al., 2005; Qin et al., 2005). These subunits share 44% amino acid identity (Currie et al., 1995; Petersen et al., 1997). GluRIIA has demonstrated unique functions modulating excitability properties for the control of activity-dependent glutamate release, calcium

permeability and presynaptic architecture (Bogdanik et al., 2004; Kamimura et al., 2019; Petersen et al., 1997). The pore region sequence critical for GluRIIA Ca^{2+} permeability (MQQ) is highly conserved in vertebrate α-amino-3-hydroxy-5-methyl-4-isoxazolepropionic acid (AMPA) /kainate receptors, while GluRIIB sequence is divergent (Petersen et al., 1997; Schuster et al., 1991).

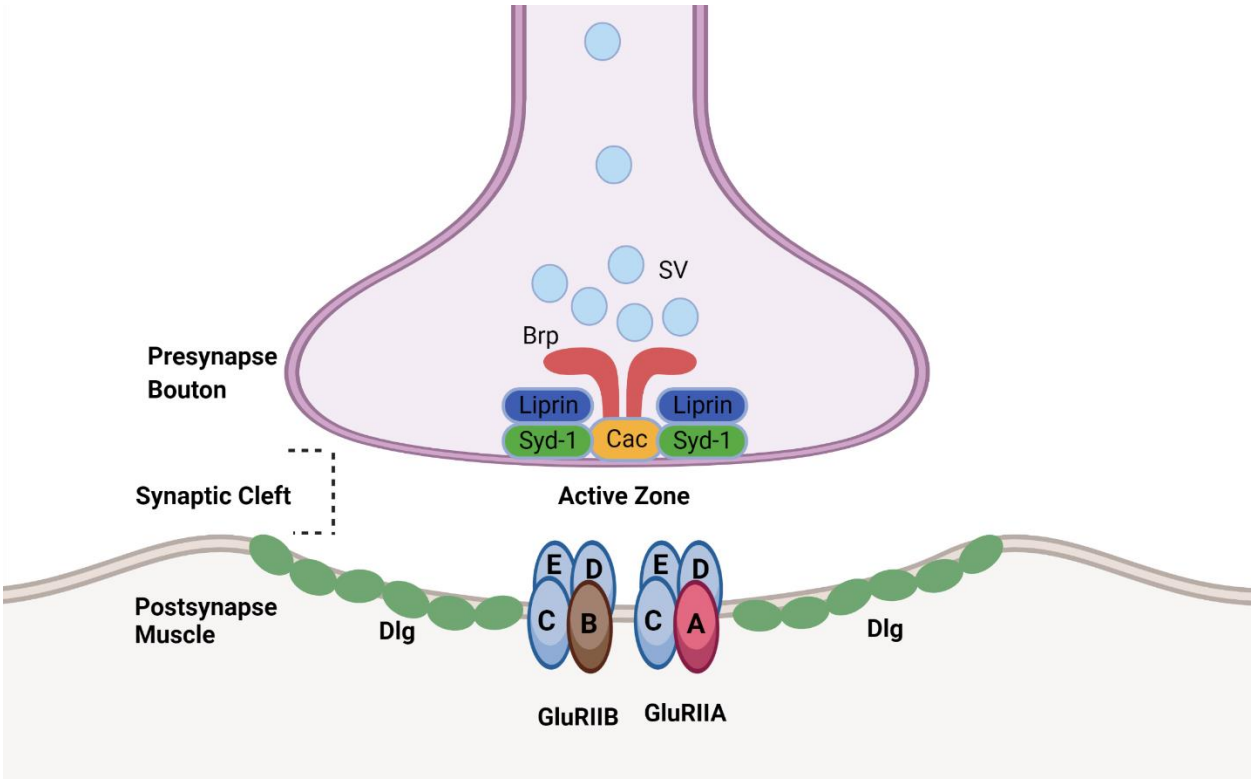

Figure 1.4 *Drosophila* neuromuscular junction structure and molecular organization.

In the presynaptic bouton, the synaptic vesicle (SV) pools are trafficked to fuse on the active zone for fusion and release of glutamate neurotransmitter. The active zone "T-bar" is assembled from Bruchpilot (Brp), Cacophony (Cac), synaptic defective 1 (SYD-1) and SYD-2/Liprin-α. in the postsynaptic muscle, the scaffold Disc Large (Dlg) surrounds the bouton to stabilize synaptic architecture. The 4-subunit type II glutamate receptors A and B (GluRIIA and GluRIIB) are located opposing the active zone. Figure created with BioRender (BioRender.com).

Based on the difference in size, SSR characters, neurotransmitter identity and synaptic vesicle composition, *Drosophila* NMJ boutons are classified into three types: Type I, II, and III, with the type I boutons further divided into type Ib (large) and Is (small) according to size and SSR enrichment (Figures 1.5) (Atwood et al., 1993; Guangming et al., 2020; Menon et al., 2013). While both Type II and III boutons have no surrounding SSR, they still contain active zones for neurotransmission (Figures 1.5). In wildtype animals, different types of boutons are organized into different chains to compose the presynaptic branch arbor. During development, synaptogenesis produces immature mini boutons (satellite boutons) that bud from mature boutons and presumably mature in separate mature boutons (Song et al., 2022).

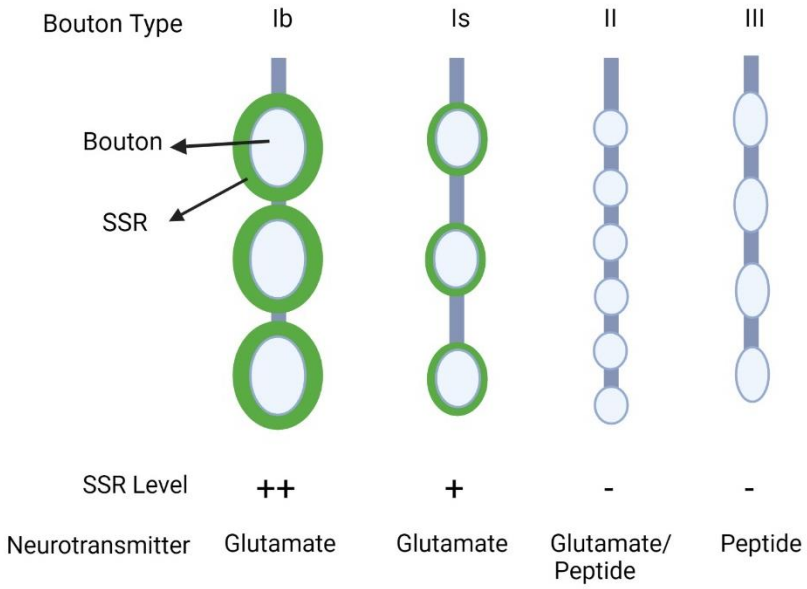

Figure 1.5 Different synaptic bouton types at the *Drosophila* neuromuscular junction (Menon et al., 2013).

Different bouton types have different SSR levels, neurotransmitter, and bouton size. Figure created with BioRender (BioRender.com).

Synaptic vesicle exocytosis mediates the release of neurotransmitters (Figure 1.6), and is highly conserved between *Drosophila* and mammals (Courtney et al., 2019; Sauvola and Littleton, 2021; Weimer and Jorgensen, 2003; Xue et al., 2009). The small GTPase Rab3 on synaptic vesicles interacts with a Rab3-interacting molecule (RIM) together with a UNC13 and RIM-binding protein (RIM-BP) to tether voltage gated Ca^{2+} channels (VGCC) at the AZs (Chou et al., 2020; Das et al., 2013; Kaeser et al., 2011; Mittelstaedt and Schoch, 2007). Synaptotagmin-1 (SYT-1) acts as an integral synaptic vesicle protein to binds Ca^{2+} and mediate fusion at AZs (Littleton et al., 1993; Quiñones-Frías and Littleton, 2021; Stenmark, 2009). The vesicular Soluble N-ethylmaleimide-Sensitive Factor-Attachment Protein Receptor (v-SNARE) tightly wrapping around a target SNARE (t-SNARE) to drive fusion (Dhara et al., 2020; Hutagalung and Novick, 2011; Kidokoro, 2003; Vats and Galli, 2022; Wang et al., 2017). To form a SNARE complex, the v-SNARE Synaptobrevin is zippered with t-SNARE Syntaxin and Synaptosomal-Associated Protein 25 (SNAP25) on the presynaptic membrane, whose process is chaperoned by UNC13 and UNC18 priming proteins (Das et al., 2013; Kaeser et al., 2011; Quiñones-Frías and Littleton, 2021). The released neurotransmitter (e.g., glutamate at *Drosophila* NMJ) in synaptic cleft either binds GluRIIA and GluRIIB to activate receptor channel opening (Featherstone et al., 2005), or is reuptaken by the presynapse and glia (Peng et al., 2019; Rival et al., 2006). This process mediates rapid intercellular communication (Figure 1.6).

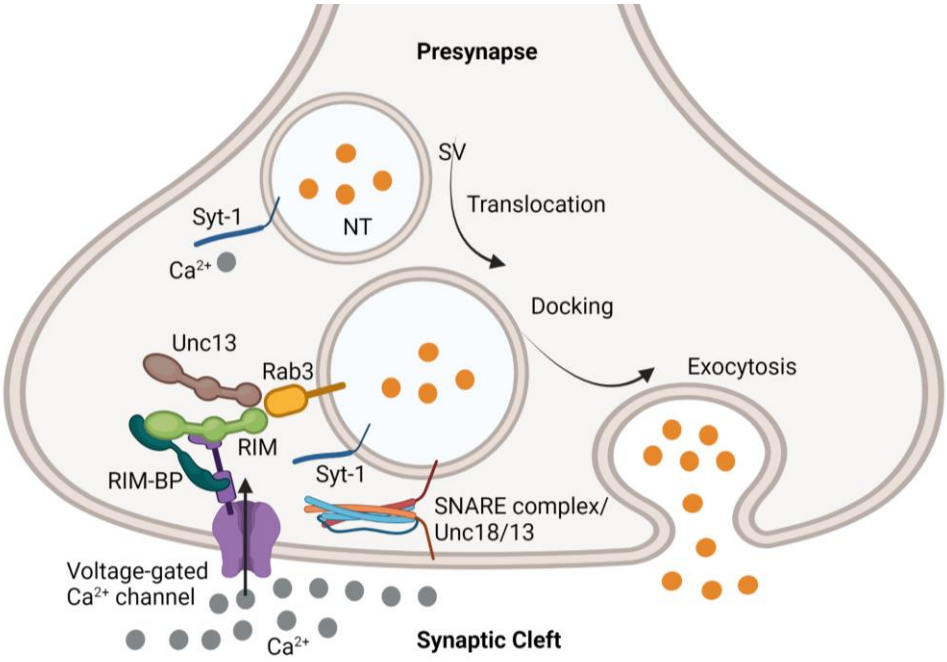

Figure 1.6 Synaptic vesicle exocytosis.

The synaptic vesicle (SV) with loaded neurotransmitter (NT) is activated to fuse after Synaptotagmin-1 (SYT-1) binds Ca^{2+}. To dock the vesicle, a protein complex consisted by the activated small GTPase Rab3, Rab3-interacting molecule (RIM), RIM-binding protein (RIM-BP) and UNC13 interact with the voltage-gated Ca^{2+} channel. UNC13 and UNC18 regulate t-SNARE and v-SNARE wrapping together to mediate exocytosis. Figure created with BioRender (BioRender.com).

1.3 Circuit Remodeling in the *Drosophila* Adult Brain

To study the general principles of brain development, *Drosophila* is a relatively simple model of 100,000+ neurons compared to the 10s of billions of neurons in humans (Scheffer et al., 2020). Like in humans, the *Drosophila* adult central nervous system (CNS) is composed of both neurons and glia, whose intercellular interactions are crucial to maintain normal brain development and function (Awasaki et al., 2011; Boulanger and Dura, 2022; Rahman et al., 2022; Stogsdill and Eroglu, 2017). In normal development, neuronal dendrites and axons in the numerous *Drosophila*

brain neuropils form complex synaptic connections, while different types of glia are integrated in different regions to mediate circuit remodeling through removal of redundant neurons (Kremer et al., 2017; Scheffer et al., 2020).

From embryo to adulthood, the *Drosophila* nervous system requires enormous remodeling to build neuronal circuit architectures and refine circuits based on environmental sensory input (Figure 1.7) (Dalva, 2010; Hart, 2019; Wegner et al., 2022). In the post-eclosion stage (juvenile adulthood; <5 days post-eclosion (dpe)), brain circuits are highly sensitive to fluctuations in the environment (i.e., temperature, light, odor) (Gatto and Broadie, 2011; Golovin et al., 2019). This time window is therefore a critical period for brain development. Disrupting this normal neuron remodeling in humans results in detrimental consequences such as neuroinflammation (Bernaus et al., 2020; Juliani et al., 2021), memory defects (Boulanger et al., 2021; Nelson et al., 2008), dysregulated circadian clock (Fernandez et al., 2020; Ikeno and Nelson, 2015; Sivachenko et al., 2013), and vulnerable psychological resilience (Fox et al., 2020; Licznerski and Duman, 2013; Wu et al., 2021). In *Drosophila*, several identified neuron classes are developmentally-transient and removed during this early-life critical period, including bursicon neurons, Crustacean Cardioactive Peptide (CCAP) neurons, and pigment dispersing factor (PDF)-Trineurons (Gatto and Broadie, 2011; Golovin et al., 2019). One of the possible reasons to remove these neurons is their redundancy, with the possibility of interfering with normal information flow. Unneeded neurons release “eat me” signals to activate phagocytotic glia to engulf neuron bodies and processes (Kuraishi et al., 2009; Song and Broadie, 2023). For example, the membrane lipid phosphatidylserine (PS) and endoplasmic reticulum (ER)-derived protein Pretaporter (Prtp) are two reported “eat me” signals that are exposed on the apoptotic cell surface (Kuraishi et al., 2009; Sokolova et al., 2021). Several signals like these reportedly bind the glial engulfment receptor

Draper (Drpr, human Scavenger Receptor from Endothelial Cells (SREC) (Adachi et al., 1997)) to transcellularly activate glial phagocytosis to remove apoptotic neurons cells (Kuraishi et al., 2009; Nagata et al., 2016; Song and Broadie, 2022; Song and Broadie, 2023).

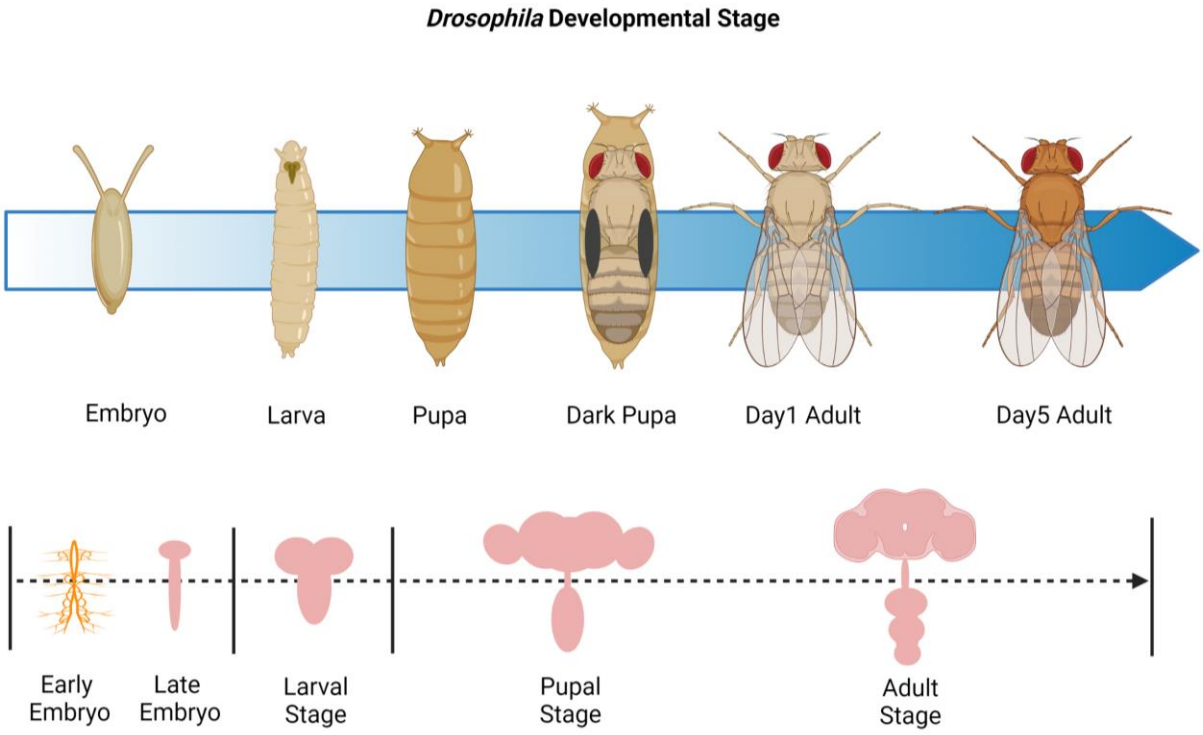

Figure 1.7 Morphology of *Drosophila* and its brain in different developmental stages.

From embryo to adulthood (top), Drosophila nervous systems (below) undergo numerous remodeling to form different architecture, synaptic connections, and neuronal circuits. Figure created with BioRender (BioRender.com).

Intercellular signaling for neuron-to-glia communication usually involves multiple intracellular and extracellular cascade networks to regulate cellular process. For example, insulin and insulin-like peptide (ILP) signaling participates in neuron-glia transcellular interaction via both direct regulation to glia activity and indirect mediation through neuronal "eat me" molecules (Vita et al., 2021). In the *Drosophila* juvenile brain, reducing the glial insulin receptor (InR)

directly suppresses glial phagocytosis for normal PDF-Tri neuron pruning (Figure 1.8) (Vita et al., 2021). It was suggested that neuron-secreted ILPs regulate glial engulfment through binding glial InR. Neuronal InR, however, is required to inhibit the release of neuronal "eat me" Prtp, which, in turn, intercellularly hinders glial activity for neuronal removal (REFS). Neuronal Bone Morphogenetic Protein (BMP) signaling interacts with the InR-dependent cascade to promote neuronal Prtp release (REFS) while the glial BMP pathway regulates glia formation for neuron remodeling (Scholze et al., 2014; See et al., 2007). However, lots of mechanisms regarding this neuron-glia intercellular signaling in neuron-glial interaction have not been well studied. It will be therefore essential to continue exploring their detailed mechanisms related to the neuron-glia transcellular communication during brain circuit remodeling.

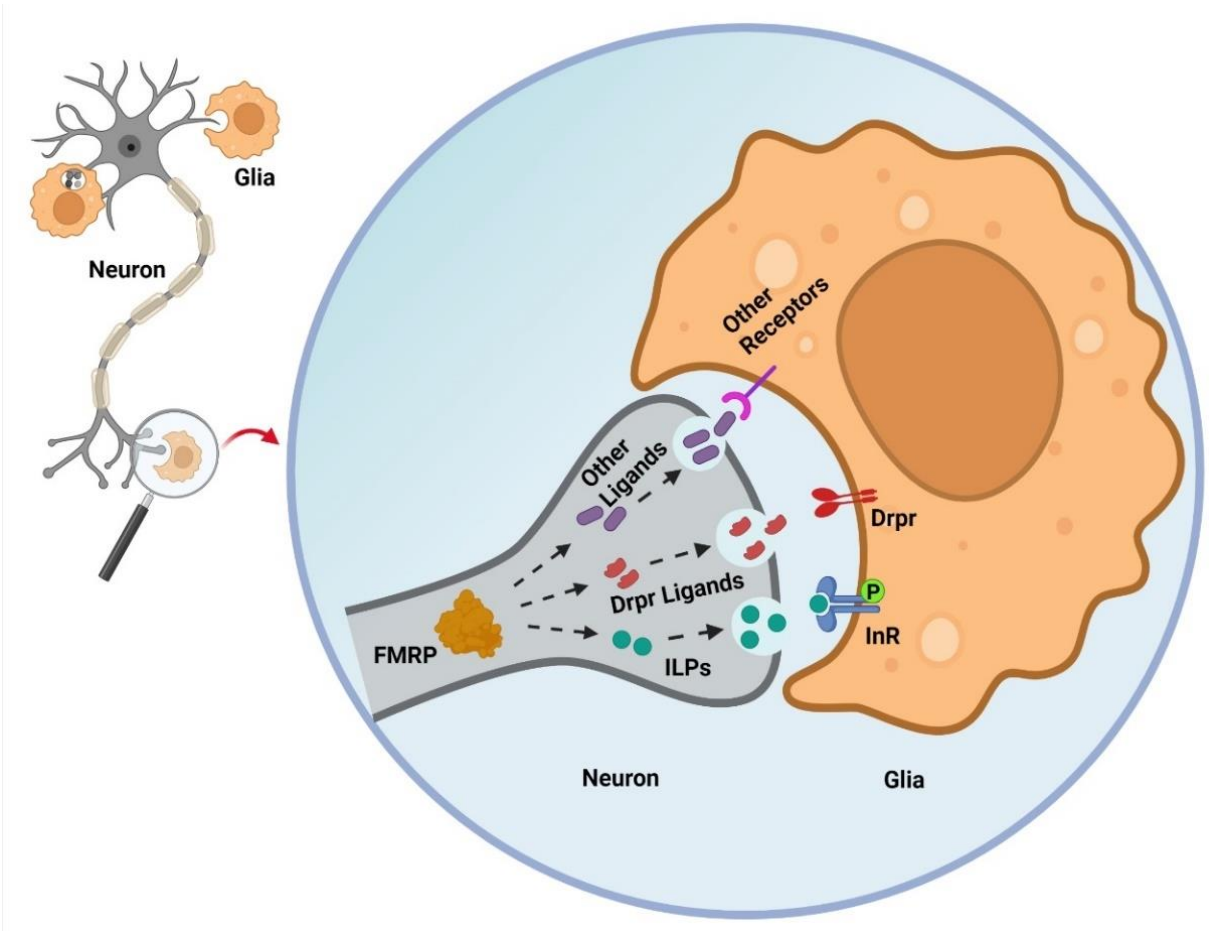

Figure 1.8 Secreted signals regulated by neural FMRP to guide glial phagocytosis clearance (Song and Broadie, 2022).

In juvenile *Drosophila* brain PDF-Tri neurons, FMRP is proposed to promote the secretion of insulin-like peptides (ILPs) that drive glial insulin receptor phosphorylation (InR-P) to trigger glial phagocytosis of neuronal processes. In glia, the Draper phagocytosis receptor (Drpr) expression is elevated by loss of neuronal FMRP. The neuronal Drpr ligand Pretaporter is involved in this FMRP-dependent mechanism. Other potential ligands (for example, phosphatidylserine) have not yet been tested. Neuronal FMRP may regulate numerous other "find me" and "eat me" secreted neural signals that recruit glia and instruct glial phagocytosis, ranging from individual synapses to whole brain neurons.

In this dissertation, I focus on two independent research works related to intercellular communication for the NMJ synaptogenesis and brain neuronal pruning underlying FXS. In chapter II, I describe my first project that has been published in the *Development*. This work reports that the NMJ postsynaptic FMRP interacts with Staufen-Coracle signaling to limit GluRIIA levels, which transcellular deactivates non-canonical BMP signaling cascade to restrict presynaptic pMad levels, consequently limiting bouton formation. These discoveries reveal a novel molecular mechanism of muscular FMRP-mediated GluRIIA accumulation and presynaptic development. Chapter III describes my second research that was published in the *Proceedings of the National Academy of Sciences* to discuss neuronal FMRP intercellularly regulates glial phagocytosis for developmental neuron removal. My study shows FMRP in neurons walks through pMad to inhibit pAkt signaling, which further modulates neuronal-released Prtp and APPL to intercellularly signal glia for the PDF-Tri neuron pruning. These findings provide a new insight into the molecular mechanism of neuronal FMRP-dependent neuron-to-glia cross talk during normal neurodevelopment. All mechanisms in both of my studies are critical for normal and diseased synaptic formation and circuit remodeling.

CHAPTER II

RNA-binding FMRP and Staufen sequentially regulate the Coracle scaffold to control synaptic glutamate receptor and bouton development

Chunzhu Song[1], Shannon N. Leahy[1], Emma M. Rushton[1] and Kendal Broadie[1,2,3,*]

Department of Biological Sciences[1], Department of Cell and Developmental Biology[2], Kennedy Center for Research on Human Development[3], and Vanderbilt Brain Institute[4], Vanderbilt University and Medical Center, Nashville, Tennessee, 37235, USA

This research is published in the *Development*.

PMID: 35394012

2.1 Abstract

Both mRNA-binding Fragile X mental retardation protein (FMRP; Fmr1) and mRNA-binding Staufen regulate synaptic bouton formation and glutamate receptor (GluR) levels at the Drosophila neuromuscular junction (NMJ) glutamatergic synapse. Here, we tested whether these RNA-binding proteins act jointly in a common mechanism. We found that both *dfmr1* and *staufen* mutants, and trans-heterozygous double mutants, displayed increased synaptic bouton formation and GluRIIA accumulation. With cell-targeted RNA interference, we showed a downstream Staufen role within postsynaptic muscle. With immunoprecipitation, we showed that FMRP binds *staufen* mRNA to stabilize postsynaptic transcripts. Staufen is known to target actin-binding, GluRIIA anchor Coracle, and we confirmed that Staufen binds to *coracle* mRNA. We found that FMRP and Staufen act sequentially to co-regulate postsynaptic Coracle expression, and showed that Coracle, in turn, controls GluRIIA levels and synaptic bouton development. Consistently, we found that *dfmr1, staufen* and *coracle* mutants elevate neurotransmission strength. We also identified that FMRP, Staufen and Coracle all suppress pMad activation, providing a trans-synaptic signaling linkage between postsynaptic GluRIIA levels and presynaptic bouton development. This work supports an FMRP–Staufen–Coracle–GluRIIA–pMad pathway regulating structural and functional synapse development.

Keywords: FMRP, Fragile X syndrome, Synaptogenesis, Synapse, Neuromuscular junction, Neurotransmission

2.2 Introduction

Fragile X syndrome (FXS) is a common heritable cause of intellectual and autism spectrum disorders (Crawford et al., 2001). FXS patients typically exhibit a fragile X mental retardation 1 (FMR1) 5′ untranslated region (UTR) CGG repeat expansion (typically $\geqslant$200), which causes epigenetic transcriptional silencing via FMR1 promoter hypermethylation (Garber et al., 2008; Hansen et al., 1992; Verkerk et al., 1991). The fragile X mental retardation protein (FMRP; FMR1) product is a very broadly expressed (e.g. neurons, muscles) mRNA-binding translation regulator (Drozd et al., 2018), which binds target transcripts via K homology (KH) domains and arginine-glycine rich (RGG) box (Blackwell and Ceman, 2011; Kenny and Ceman, 2016; Myrick et al., 2015; RAMOS et al., 2003). FMRP regulates protein translation to modulate synaptic architecture (bouton/spine number) and glutamate receptor (GluR) levels (Comery et al., 1997; Connor et al., 2011). In the Drosophila FXS disease model, *dfmr1* mutants likewise exhibit increased synaptic bouton formation and Glutamate receptor IIA (GluRIIA) levels at the neuromuscular junction (NMJ) model glutamatergic synapse (Pan and Broadie, 2007a; Zhang et al., 2001). The molecular mechanism of FMRP-mediated synaptic regulation remains elusive; however, FMRP has been increasingly linked to other mRNA-binding proteins (Kenny et al., 2020; PRICE et al., 2006; Zhang et al., 2017). A key hypothesized partner is Staufen, a double-strand RNA-binding protein (dsRBP) repeatedly associated with FMRP function via both biochemical and genetic interaction studies (Barbee et al., 2006; Chu et al., 2019; Yu et al., 2012).

Staufen plays crucial roles in regulating mRNA localization, stability, translation and ribonucleoprotein (RNP) assembly (Dugré-Brisson et al., 2005; Micklem et al., 2000; Park and Maquat, 2013). In *Drosophila*, Staufen colocalizes with FMRP in neural RNP granules that mediate mRNA translational repression and mRNA decay, with genetic interaction regulating

long-term memory consolidation (Barbee et al., 2006; Bolduc et al., 2008). Like FMRP, Staufen controls both synaptic bouton formation and GluRIIA levels at the Drosophila NMJ (Gardiol and St Johnston, 2014). In this mechanism, Staufen works by regulating local translation of the 4.1 ezrin-radixin-moesin (FERM) scaffold Coracle in the muscle postsynaptic domain (Gardiol and St Johnston, 2014). Consistently, mammalian Staufen also binds Coracle homolog 4.1 mRNA and is predicted to regulate its local translation (Furic et al., 2008). Coracle is suggested to link F-actin to GluRIIA C-termini to scaffold receptors within the postsynaptic membrane (Chen et al., 2005; McClatchey, 2012). Importantly, intercellular interaction between postsynaptic GluRIIA and the presynaptic bone morphogenic protein (BMP) receptor Wishful thinking (Wit) generates phosphorylated Mothers against decapentaplegic (pMad) retrograde trans-synaptic signaling to regulate presynaptic bouton formation (Chou et al., 2020; Sulkowski et al., 2014; Sulkowski et al., 2016). Based on these studies, we hypothesized that FMRP works with Staufen to regulate postsynaptic Coracle scaffolding, which in turn acts to control postsynaptic GluRIIA accumulation and thereby GluRIIA-dependent presynaptic bouton development.

To interrogate this layered hypothesis, we first tested NMJ bouton number and GluRIIA levels in *dfmr1* and *staufen* single mutants and RNA interference (RNAi) lines, to find that both FMRP and Staufen negatively regulate synaptic bouton formation and GluRIIA accumulation. We next made trans-heterozygous double mutants (*dfmr1/+; staufen/+*) to find that FMRP and Staufen operate in the same pathway to control synaptic development. Subsequently, we used RNA immunoprecipitation (RIP) to show that FMRP binds *staufen* mRNA to regulate transcript abundance in the postsynaptic muscle, and that Staufen in turn binds *coracle* mRNA. Consistently, Coracle expression in the NMJ postsynaptic domain was elevated in both *dfmr1* and *staufen* mutants, as well as in trans-heterozygous double mutants. We found that postsynaptic Coracle

overexpression (OE) and loss of function similarly increase bouton number and GluRIIA levels. Consistently, we employed NMJ electrophysiology recordings to show that *dfmr1*, *staufen* and *coracle* mutants all display increased synaptic strength. Moreover, postsynaptic knockdown of *dfmr1*, *staufen* and *coracle* all caused elevated presynaptic pMad levels, consistent with activation of GluRIIA–Wit retrograde trans-synaptic signaling to drive presynaptic bouton formation. Taken together, these findings suggest that FMRP and Staufen work sequentially to inhibit the Coracle scaffold controlling GluRIIA levels in postsynaptic domain, and that postsynaptic GluRIIA levels in turn signal presynaptic bouton development. This work provides insights into the molecular pathway by which FMRP regulates synapse formation, identifying potential new FXS treatment targets.

2.3 Results

2.3.1 FMRP and Staufen negatively regulate synaptic bouton formation and GluRIIA levels

At the *Drosophila* NMJ, we have previously reported that viable *dfmr1* nulls ($dfmr1^{50M}$) exhibit elevated synaptic bouton formation and GluRIIA levels (Pan and Broadie, 2007a; Zhang et al., 2001). By contrast, *staufen* nulls are embryonic lethal owing to essential mRNA localization and translation roles (St Johnston et al., 1991), and a viable *staufen* mutant over a genomic deficiency [$stau^{HL}/Df(2R)Pcl7B$] reportedly develops fewer NMJ boutons and lower GluRIIA levels (Gardiol and St Johnston, 2014). The $stau^{HL}$ mutant contains a T-A point mutation in dsRNA-binding domain 5 (Figure 2.1A) that blocks local translation (Gardiol and St Johnston, 2014). As a first step, we re-tested $dfmr1^{50M}$ and $stau^{HL}$ mutants compared with matched genetic background controls (w^{1118}) for bouton number and GluRIIA level. We then tested trans-heterozygotes ($dfmr1^{50M}$ /+; $stau^{HL}$ /+) for a predicted interaction within the same pathway. We

assayed wandering third-instar NMJs double labeled with anti-horseradish peroxidase (HRP) (Jan and Jan, 1982; Pan and Broadie, 2007a), which recognizes neural presynaptic membrane, and anti-Discs large (DLG; Dlg1) (Kamimura et al., 2019; Menon et al., 2013), which recognizes muscle subsynaptic reticulum (SSR). Both total NMJ boutons and developing satellite boutons were counted in muscle 4 terminals in abdominal segment A3. The same genotypes were double labeled with anti-HRP and anti-GluRIIA (Pan and Broadie, 2007) at the same NMJ. GluRIIA labeling intensity was quantified at HRP-thresholded boutons.

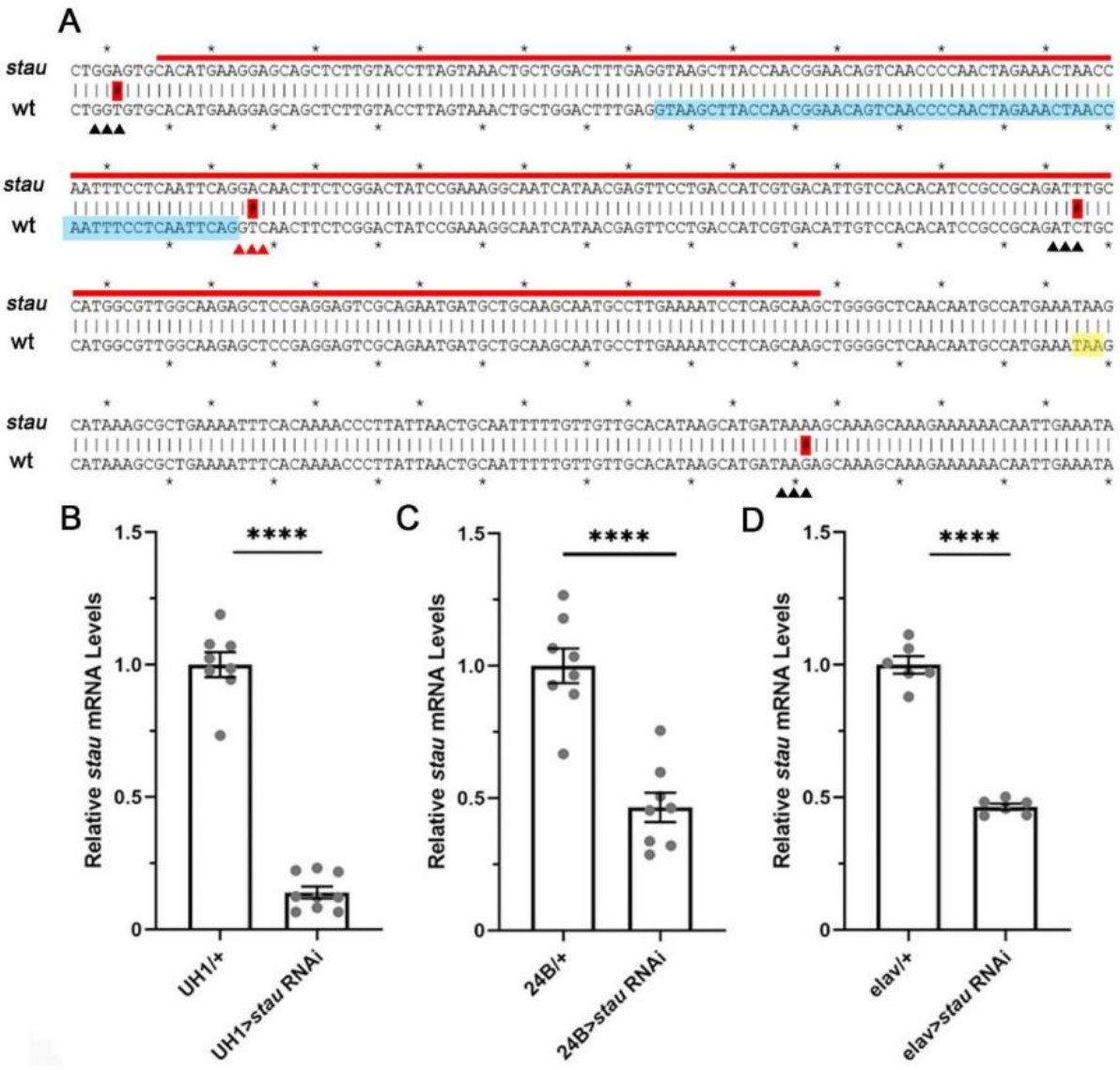

Figure 2.1 Mutant *staufen*^{HL} sequence and *staufen* RNAi knock-down efficiency

(A) The *staufen*^{HL} mutant sequence compared to wildtype sequence (http://flybase.org/). The double strand RNA-binding domain 5 (dsRBD5, red underline) contains a single intron (blue shading). In the mutant, silent mutant codon (black triangles) and nonsense mutant codon (red triangles) with mutated nucleotide (red shading) upstream of the stop codon (yellow shading). (B-D) Larval qPCR measurements of *staufen* RNAi efficiency with ubiquitous UH1-Gal4 (B), muscle-targeted 24B-Gal4 (C) and neuron-targeted elav-Gal4 (D). Significance is indicated at $p<0.0001$ (****) based on student's t-tests.

Compared with the genetic background control (w^{1118}), $dfmr1^{50M}$ mutants showed supernumerary synaptic bouton formation (Figure 2.2A, top). The quantified total bouton number was significantly elevated (mean±s.e.m.: control 19.10±1.77, *dfmr1* 31.42±1.67; P<0.0001; Figure 2.2C), with a parallel increase in satellite boutons (number/NMJ: control 0.86±0.27, *dfmr1* 2.65±0.47; P=0.003; Figure 2.2 D). Similarly, $stau^{HL}$ mutants also developed consistently more NMJ boutons compared with w^{1118} genetic controls (Figure 2.2A, bottom). Quantification showed that the total NMJ bouton number was significantly increased in *staufen* mutants compared with controls (control 20.85±0.78, $stau^{HL}$ 29.25±2.15; P=0.0003; Figure 2.2C), with satellite boutons also elevated (control 0.89±0.21, $stau^{HL}$ 4.64±0.72; P<0.0001; Figure 2.2D). Assaying synaptic GluRIIA levels, *dfmr1* mutants exhibited a clear increase throughout the NMJ terminal (Figure 2.2B, top). GluRIIA fluorescence levels normalized to control were significantly higher in *dfmr1* mutants (control 1.00±0.08, $dfmr1^{50M}$ 1.616±0.11; P=0.0002; Figure 2.2E). Likewise, GluRIIA levels were also increased in the *staufen* mutants compared with matched controls (Figure 2.2B). Compared with levels in genetic controls, the normalized GluRIIA fluorescence levels in the *staufen* mutants were also significantly elevated (control 1.00±0.04, $stau^{HL}$ 1.24±0.06; P=0.0014; Figure 2.2B,E). These results indicate that FMRP and Staufen similarly regulate synaptic development.

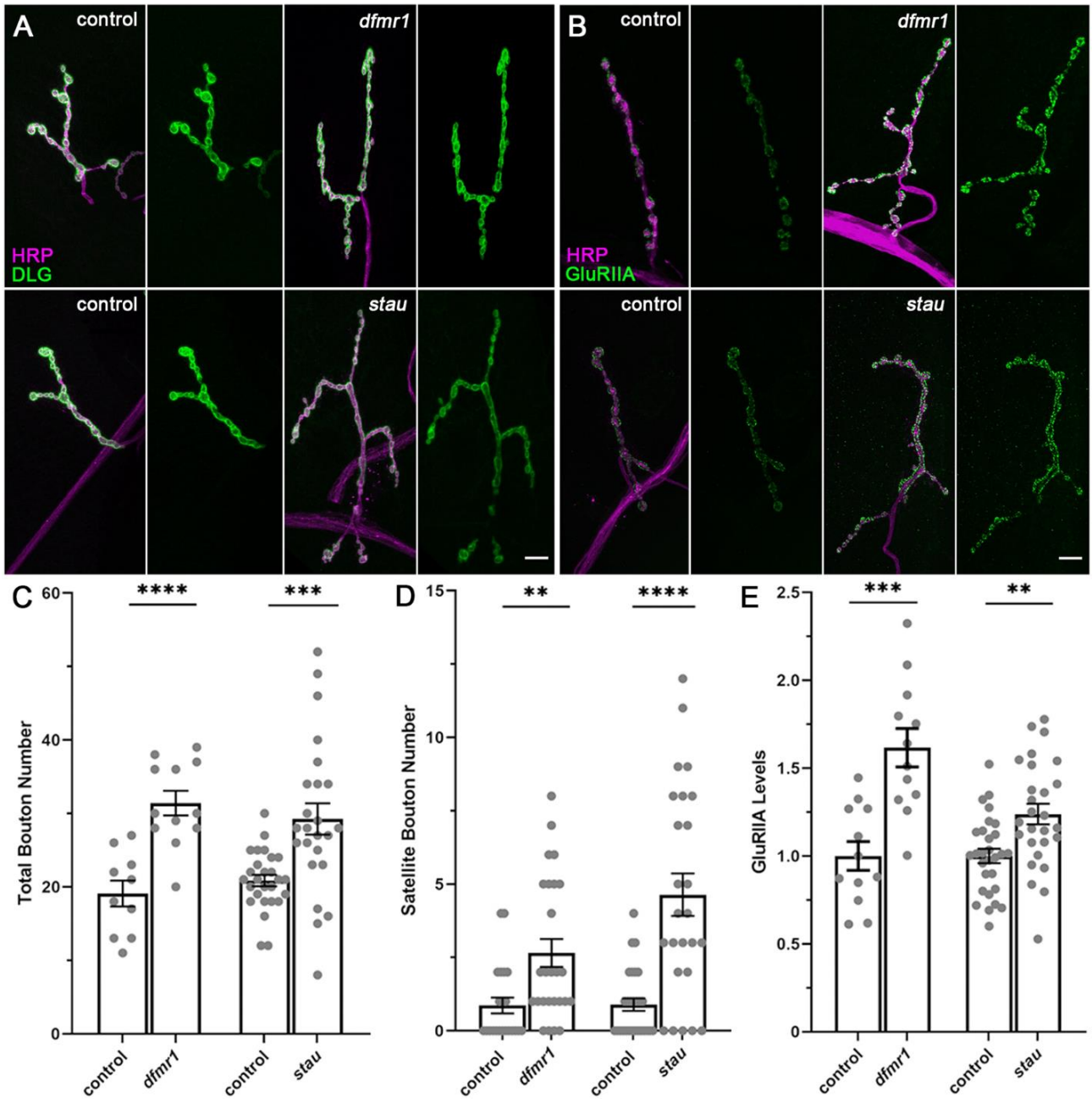
A
control
dfmr1
HRP
DLG
control
stau
B
control
dfmr1
HRP
GluRIIA
control
stau
C
Total Bouton Number
****
***
0
20
40
60
control
dfmr1
control
stau
D
Satellite Bouton Number
**
****
0
5
10
15
control
dfmr1
control
stau
E
GluRIIA Levels
***
**
0
0.5
1.0
1.5
2.0
2.5
control
dfmr1
control
stau

Figure 2.2 FMRP and Staufen both limit neuromuscular junction (NMJ) bouton formation and GluRIIA levels.

Larval NMJ synaptic terminals compared between genetic background control (w^{1118}), *dfmr1* ($dfmr1^{50M}$) and *staufen* ($stau^{HL}$) mutants. (A) Double labeling for the presynaptic anti-horseradish peroxidase (HRP; magenta) and the postsynaptic anti-Discs large (DLG; green), with overlap shown in white. (B) Double labeling for HRP (magenta) and anti-Glutamate receptor IIA (GluRIIA; green), with overlap shown in white. (C) Quantification of total synaptic bouton number in muscle 4 type 1 NMJ terminals, with each mutant and control paired for side-by-side comparisons. (D) Quantification of satellite bouton number only within each type 1 synaptic terminal. (E) Quantification of GluRIIA fluorescence intensity normalized to genetic background control. In all figures, graphs show dot plots of all individual data points and histogram bars of the mean±s.e.m., with statistical comparisons using unpaired two-tailed Student's t-tests. **P<0.01, ***P<0.001 and ****P<0.0001. Scale bars: 10 μm.

To further test *staufen* phenotypes, we next used *staufen* RNAi as an independent knockdown method (Figure 2.3B-D). Studies with quantitative PCR (qPCR) showed ~90% *staufen* mRNA loss with global UH1-Gal4 driving UAS-*staufen* RNAi [Vienna Drosophila Resource Center (VDRC) 106645; Figure 2.1B]. Consistent with the above *staufen* mutants, *staufen* RNAi elevated both presynaptic bouton formation (Figure 2.3A, top) and postsynaptic GluRIIA levels (Figure 2.3A, bottom). Quantification of the knockdown showed that UH1>*stau* RNAi (VDRC 106645) increased all measurements, including total bouton number (UH1/+ 23.33±1.09, UH1>*stau* RNAi 28.87±1.30; P=0.004; Figure 2.3B), satellite boutons (UH1/+ 1.33±0.43, UH1>*stau* RNAi 2.93±0.50; P=0.0273; Figure 2.3C) and GluRIIA levels (UH1/+ 1.00±0.06, UH1>*stau* RNAi 1.28±0.07; P=0.0038; Figure 2.3D). We repeated these analyses with an independent *staufen* RNAi line [Bloomington Drosophila Stock Center (BDSC) 31247]. Consistent with the above results, this second RNAi similarly caused a significant increase in synaptic bouton number (UH1/+ 24.33±0.79, UH1>*stau* RNAi 32.36±1.815, P=0.0004) and GluRIIA levels (UH1/+ 1.00±0.07, UH1>*stau* RNAi 1.66±0.16; P=0.0041). Thus, $stau^{HL}$ and two independent *staufen* RNAi lines (VDRC 106645 and BDSC 31247) confirmed the same NMJ development phenotypes. We therefore conclude that Staufen loss increases synaptic bouton formation and GluRIIA levels, consistent with FMRP requirements.

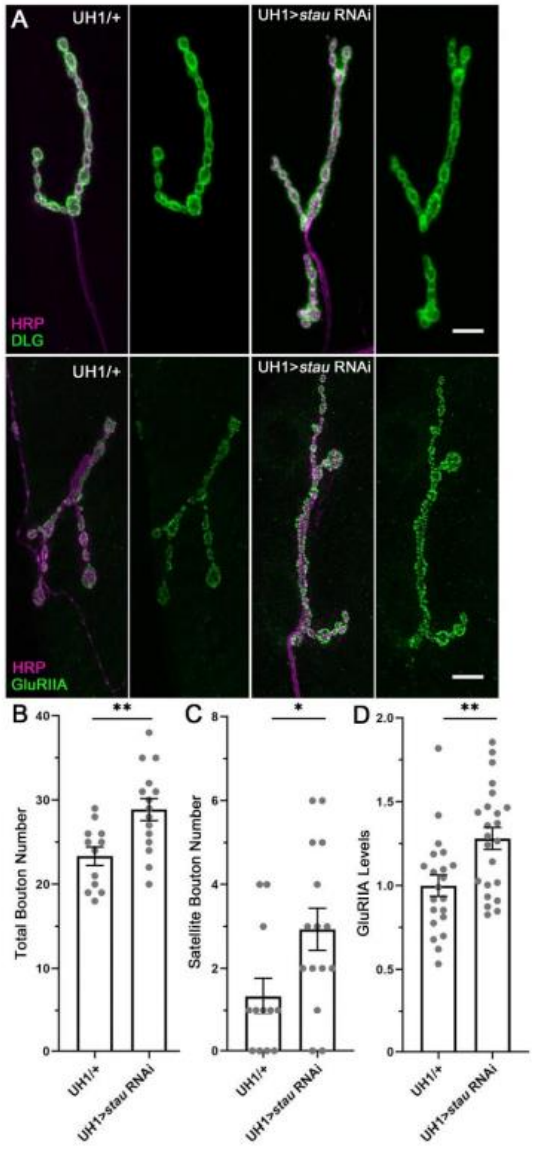

Figure 2.3 *staufen* RNAi increases synaptic bouton formation and GluRIIA levels.

Larval NMJ structure and GluRIIA levels compared between transgenic control (UH1/+) and *staufen* knockdown (UH1-*stau* RNAi). (A) Double labeling for presynaptic anti-HRP (magenta) and either postsynaptic DLG (green, top) or GluRIIA (green, bottom). Scale bar: 10 μm. Quantification of total synaptic bouton (B) and satellite bouton (C) number. (D) Quantification of GluRIIA fluorescence intensity normalized to genetic background control. Significance is indicated at $p<0.05$ (*) and $p<0.01$ (**) based on student's t-tests.

To test the hypothesis that FMRP and Staufen co-regulate NMJ development in a common pathway, we next made *dfmr1* and *staufen* double mutants. Homozygous double mutants were early larval lethal, but $dfmr1^{50M}$/+; $stau^{HL}$/+ trans-heterozygotes were viable and could be tested. Similar to $dfmr1^{50M}$ and $stau^{HL}$ single mutants, we found a clear elevation of total boutons in the trans-heterozygotes. Quantification showed bouton increases in *dfmr1* (control 17.91±0.89, *dfmr1*/+ 25.88±1.81) and *staufen* (control 19.00±0.70, *stau*/+ 26.91±1.56) heterozygotes, and the trans-heterozygotes (control 17.56±1.17, *dfmr1/+; stau/+* 28.70±1.55; P<0.0001; Figure 2.4A, bottom). We next tested GluRIIA to find similar levels in *dfmr1/+* and *stau/+* heterozygotes compared with controls, but elevated levels in *dfmr1/+; stau/+* trans-heterozygotes (Figure 2.4A). Quantified GluRIIA levels were not changed in either *dfmr1/+* or *stau/+* single heterozygotes compared with control (Figure 2.4A,B), but were significantly increased in trans-heterozygotes (normalized control 1.00±0.08, *dfmr1/+; stau/+* 1.28±0.12; P=0.047; Figure 2.4A,B). These findings showed that reducing FMRP and Staufen in parallel elevated synaptic GluRIIA levels, suggesting that the two RNA-binding proteins (RBPs) work in a common mechanism. Overall, we conclude that FMRP and Staufen negatively regulate synaptic development in the same direction, and to a similar degree, by functioning in the same pathway.

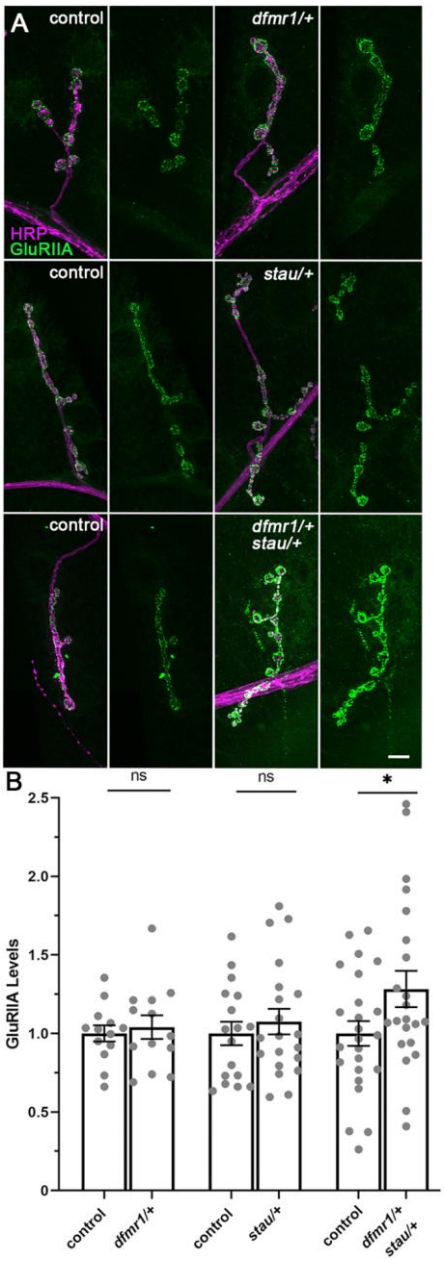

Figure 2.4 FMRP and Staufen work together to co-regulate synaptic GluRIIA levels.

Larval NMJ synaptic terminals in controls (w^{1118}) compared with the single heterozygous *dfmr1* ($dfmr1^{50M}$/+) and *staufen* ($stau^{HL}$/+) mutants, and the double trans-heterozygous combination ($dfmr1^{50M}$/+; $stau^{HL}$/+). (A) Double labeling for presynaptic HRP (magenta) and GluRIIA (green) with each mutant condition paired to genetic background control. Scale bar: 10 μm. (B) Quantification of GluRIIA fluorescence intensity normalized to control. ns, not significant (for both single heterozygous conditions); *P<0.05 (for the double trans-heterozygous mutant).

2.3.2 Postsynaptic Staufen regulates GluRIIA levels and presynaptic bouton development

Cell-targeted RNAi studies have established that FMRP inhibits GluRIIA levels only postsynaptically (Pan and Broadie, 2007), but suppresses bouton development in both postsynaptic and presynaptic cells (Friedman et al., 2013; Zhang et al., 2001). Likewise, Staufen subcellularly localizes in the postsynaptic domain, to function postsynaptically in muscle, controlling mRNA localization and local translation (Gardiol and St Johnston, 2014). These previous studies, as well as the above non-complementation genetic interaction tests, suggest that FMRP interacts with Staufen in the postsynaptic compartment to regulate GluRIIA levels and presynaptic bouton formation. Previous antibody labeling shows Staufen in the postsynaptic muscle region immediately surrounding NMJ termini, with Staufen not detectable in presynaptic boutons (Gardiol and St Johnston, 2014). We therefore hypothesized Staufen that has a specific muscle postsynaptic function. To test this hypothesis, we used muscle-specific 24B-Gal4 (Kim et al., 2021) and neuron-specific elav-Gal4 (Kan et al., 2021) to drive UAS-*staufen* RNAi (VDRC 106645; (Landskron et al., 2018). We also used postsynaptic 24B-Gal4 to drive wild-type UAS-*staufen* in both homozygous $stau^{HL}$ and $dfmr1^{50M}$ mutants. As above, synaptic bouton development was tested with presynaptic anti-HRP and postsynaptic anti-DLG double labeling, and GluRIIA levels with anti-HRP and anti-GluRIIA double labeling.

Compared with transgenic controls (24B-Gal4/+), muscle-targeted *staufen* RNAi (24B>*stau* RNAi) resulted in more synaptic boutons (Figure 2.5A, top). With quantification, total boutons were significantly increased in 24B>*stau* RNAi (24B/+ 21.94±1.23, RNAi 25.43±0.86; P=0.02; Figure 2.5C), with more developing satellite boutons (24B/+ 2.09±0.31, RNAi 3.46±0.34; P=0.0047; Figure 2.5D). By contrast, neural *staufen* knockdown (elav>*stau* RNAi) had no effect, with no change in bouton number (Figure 2.5A, bottom). Quantification showed no significant

difference in synaptic bouton formation between transgenic control (elav-Gal4/+) and neural *staufen* RNAi (P=0.91; Figure 2.5C), indicating that presynaptic Staufen has no detectable role. Assaying GluRIIA levels, muscle-targeted knockdown (24B>*stau* RNAi) resulted in clearly higher fluorescence than in the transgenic controls (24B-Gal4/+), with elevated GluRIIA levels at synaptic boutons (Figure 2.5B, top). Quantified GluRIIA measurements showed that muscle-targeted *staufen* RNAi strongly upregulated GluIIA levels compared with normalized controls (24B/+ 1.00±0.04, RNAi 1.33±0.05; P<0.0001; Figure 2.5E). By contrast, neural *staufen* knockdown (elav>*stau* RNAi) resulted in no detectable change in GluRIIA synaptic fluorescence (Figure 2.5B, bottom), with quantified results showing no role in determining GluRIIA levels (P=0.46; Figure 2.5E). These findings suggest that Staufen acts in the postsynaptic muscle to regulate NMJ development.

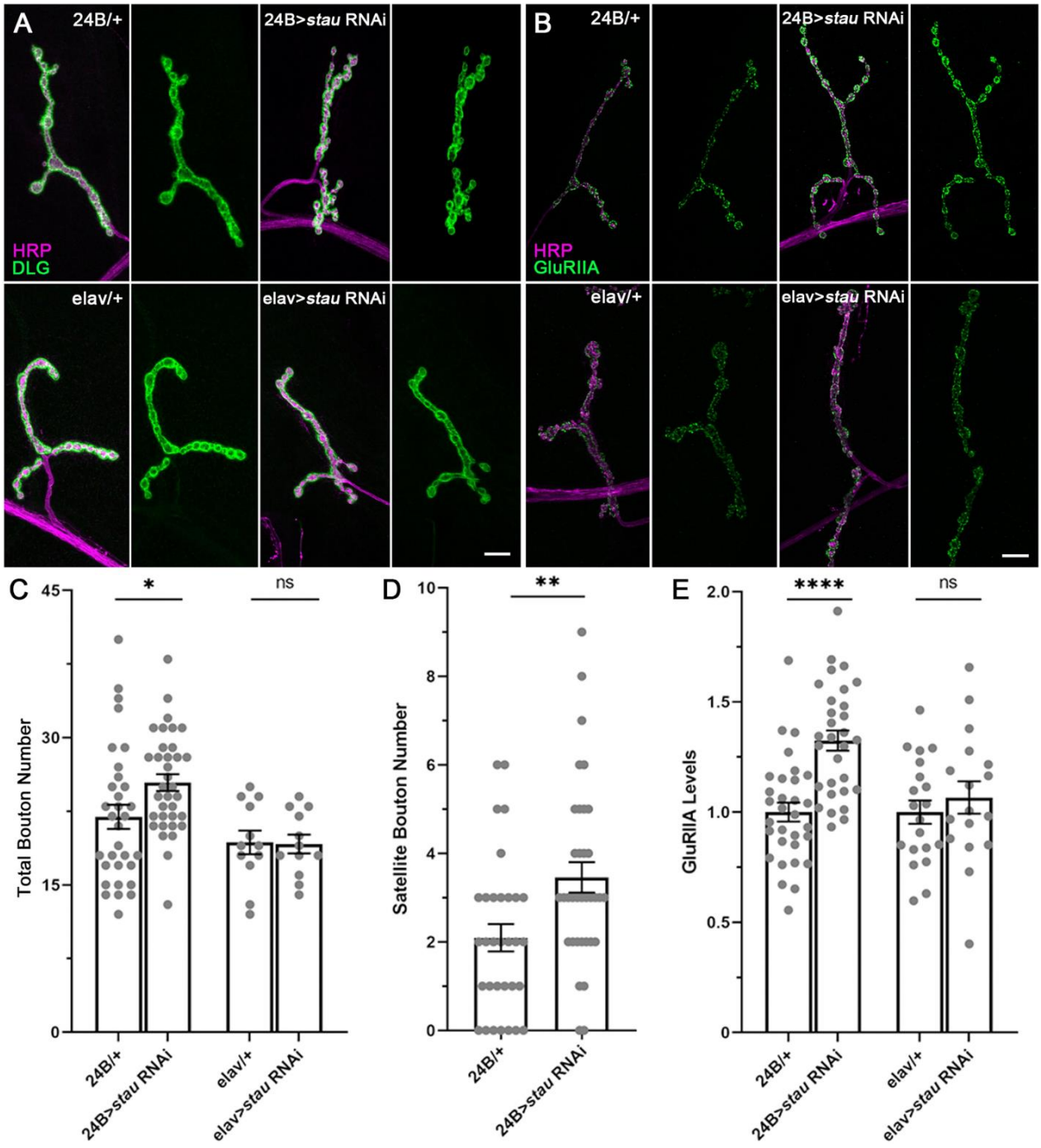
A
24B/+
24B>stau RNAi
HRP
DLG
elav/+
elav>stau RNAi
B
24B/+
24B>stau RNAi
HRP
GluRIIA
elav/+
elav>stau RNAi
C
Total Bouton Number
45
30
15
0
*
ns
24B/+
24B>stau RNAi
elav/+
elav>stau RNAi
D
Satellite Bouton Number
10
8
6
4
2
0
**
24B/+
24B>stau RNAi
E
GluRIIA Levels
2.0
1.5
1.0
0.5
0
****
ns
24B/+
24B>stau RNAi
elav/+
elav>stau RNAi

Figure 2.5 Postsynaptic Staufen regulates NMJ bouton formation and GluRIIA levels.

Larval NMJ synaptic terminals in transgenic controls compared with postsynaptic muscle Staufen RNAi (24B>*stau* RNAi) and presynaptic neuron Staufen RNAi (elav>*stau* RNAi). (A) Double labeling for HRP (magenta) and DLG (green), with the 24B-Gal4 control (left) and RNAi (right) shown in the top row and the elav-Gal4 control/RNAi in the bottom row. (B) Double labeling for HRP (magenta) and GluRIIA (green) for the same comparisons. (C,D) Quantification of total NMJ bouton number (C) and satellite bouton number (D) on muscle 4 for all four conditions. (E) Quantification of GluRIIA fluorescent intensity normalized to the transgenic controls. *P<0.05, **P<0.01 and ****P<0.0001; ns, not significant (for elav>*stau* RNAi). Scale bars: 10 μm.

To further test this conclusion, we next performed complementary *staufen* rescue experiments in the postsynaptic muscle. Compared with transgenic control (24B-Gal4/+), muscle UAS-*staufen* expression in *staufen*^{HL} (*stau*^{HL}) homozygous mutant (*stau*^{HL}; 24B>*stau*) showed strongly rescued synaptic development (Figure 2.6). With targeted postsynaptic UAS-*staufen*, the presynaptic bouton number was restored to the control level (24B/+ 23.80±0.86, *stau*^{HL}; 24B>*stau* 26.89±1.24), with no significant difference remaining (P=0.113). Assaying GluRIIA levels revealed an even stronger effect, with muscle-targeted rescue (*stau*^{HL}; 24B>*stau*) resulting in clearly reduced fluorescence compared with that of transgenic controls (24B-Gal4/+), showing lower GluRIIA levels at synaptic boutons (Figure 2.6A). Quantification revealed a >40% reduction in GluRIIA receptors normalized to transgenic controls (24B/+ 1.00±0.067, *stau*^{HL}; 24B>*stau* 0.57±0.04), which is a significant decrease (P<0.0001; Figure 2.6B). Consistent with this postsynaptic requirement, the same muscle *staufen* OE in the null *dfmr1* homozygous mutant (*dfmr1*; 24B>*stau*) suppressed GluRIIA expression to levels comparable with those of the transgenic control (normalized 24B/+ 1.00±0.07, *dfmr1*; 24B>*stau* 1.21±0.19; P=0.21). Taken together, these findings suggest that FMRP interacts with Staufen in the muscle postsynaptic domain to regulate GluRIIA levels.

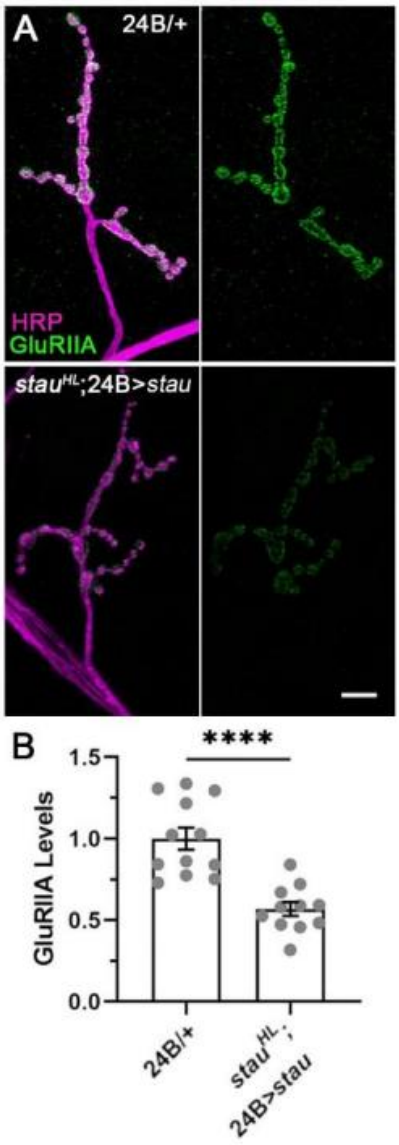

Figure 2.6 Postsynaptic muscle-targeted Staufen rescue decreases GluRIIA levels.

Larval NMJs labeled for GluRIIA comparing transgenic control (24B/+) with postsynaptic muscle UAS-*staufen* expression in *staufen*^{HL} (*stau*^{HL}) homozygous mutant background (*stau*^{HL}; 24B>*stau*). (A) Double labeling for both presynaptic anti-HRP (magenta) and anti-GluRIIA (green) in the 24B-Gal4/+ control (top) and muscle *staufen* rescue in the *stau*^{HL} mutant (bottom). GluRIIA labeling alone is shown on the right for both genotypes. Scale bar: 10 μm. (B) Quantification of the normalized GluRIIA fluorescence intensity. Significance is indicated at $p<0.0001$ (****).

2.3.3 FMRP binds *staufen* mRNA and downstream Staufen protein binds *coracle* mRNA

FMRP and Staufen both bind mRNA directly to regulate local protein translation (Bonnet-Magnaval, 2016; Laver et al., 2013; Liu et al., 2018; Tsang et al., 2019), and therefore could operate either in parallel or sequentially in protein-mRNA interactions limiting synaptic development. Importantly, FMRP has been predicted to bind *staufen* mRNA (D'Annessa et al., 2019), and we therefore hypothesized that FMRP regulates Staufen translation in a sequential mechanism. To test the predicted FMRP and *staufen* mRNA interaction, we used UH1-Gal4 to express UAS-*dfmr1*::YFP (Cziko et al., 2009), and then pulled down FMRP-RNA complexes from larval lysates using anti-YFP beads (Nagai et al., 2002; Rana et al., 2018). In parallel, non-tagged w^{1118} third-instar lysates served as the immunoprecipitation (IP) negative control. In both cases, α-Tubulin (αTub85E; FMRP does not bind) was the negative control and Futsch (a known FMRP target) was the positive control (Zhang et al., 2001). Immunoprecipitated mRNAs were reverse transcribed using random hexamers, followed by specific primer PCR amplification to produce ~200 bp PCR fragments (Table 2.1). Downstream of hypothesized mRNA binding, we also assayed *staufen* mRNA levels with qPCR measurements in *dfmr1* null mutants and with muscle-targeted *dfmr1* RNAi (Flockhart et al., 2006) to test the postsynaptic interaction in isolated muscle analyses.

Primer (forward)	**Sequence**	**Primer (reverse)**	**Sequence**
Staufen	GTAAACTGCTGGACTTTGAGGTC	Staufen	GCAGCATCATTCTGCGACTCC
GAPDH	CGTTCATGCCACCACCGCTA	GAPDH	CACGTCCATCACGCCACAA
Tubulin	ATTTACCCAGCACCACAAGTGT	Tubulin	GGCGATTGAGATTCATGTAGGTGG
Futsch	TTCCTGGATATTGCAGGACGG	Futsch	CTCGGGCAATGTGTGCCATA
Coracle	AAGAACAAGAAGGAGAAGGATGC	Coracle	CATTAACAGCCGCTCCTGCAG
Pal1	ACGACTGGGGCAAGAACTTTTTT	Pal1	CGTAGGATATGCCGGAGAAGG

Table 2.1 Primers used in this study.

The FMRP IP pulled down *staufen* mRNA from larval lysates (Figure 2.7A, IP, top). Consistently, the *futsch* mRNA positive control was precipitated in parallel, with no detectable binding to the α-tubulin mRNA negative control (Figure 2.7A). As expected, the genetic negative control w^{1118} (no YFP) showed no immunoprecipitated bands (Figure 2.7A, IP, bottom). These results indicated that FMRP binds to *staufen* mRNA from the wandering third instar, with the controls confirming the binding interaction specificity. RNA binding protects transcripts from degradation by increasing RNA stability, so we hypothesized that FMRP binding should increase *staufen* mRNA levels. To test this idea, we performed qPCR to measure *staufen* mRNA levels in genetic background controls (w^{1118}) compared with *dfmr1* nulls (Figure 2.7B). Quantification showed that *staufen* mRNA levels were significantly reduced in *dfmr1* mutants normalized to controls (control 1.00±0.05, *dfmr1* 0.68±0.08; P=0.002; Figure 2.7B). This finding suggested that FMRP stabilizes *staufen* mRNA through protein-RNA binding. To test postsynaptic roles, we used muscle 24B-Gal4 to drive *dfmr1* RNAi, and then isolated body muscles for mRNA extraction (Figure 2.7C). Quantified qPCR results showed that *staufen* mRNA levels were strongly downregulated in 24B>*dfmr1* RNAi muscles normalized to the transgenic control (24B/+ 1.00±0.09, RNAi 0.61±0.10; P=0.009; Figure 2.7C). These findings suggest that FMRP binding stabilizes *staufen* mRNA in the postsynaptic muscle.

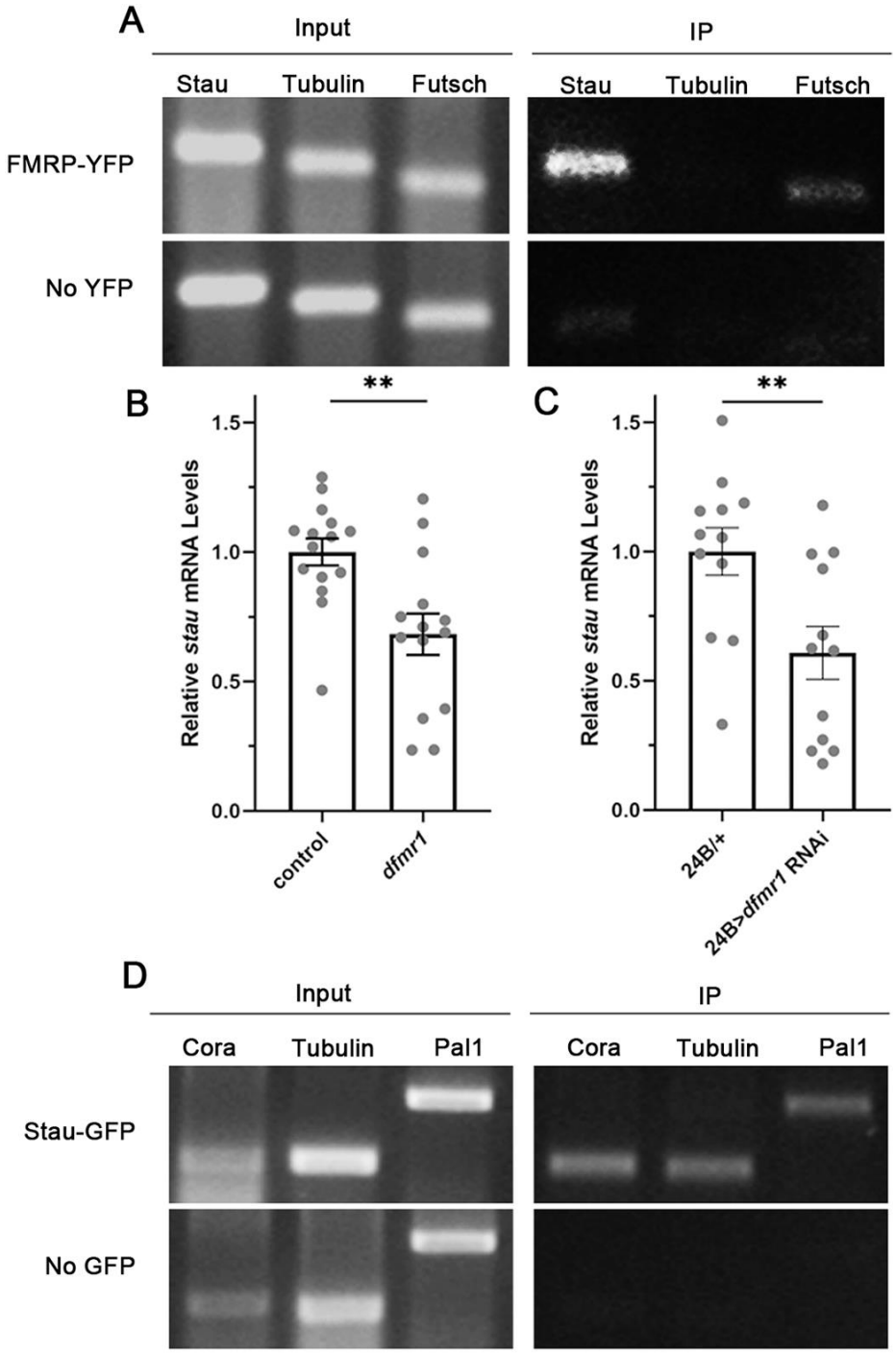
A
Input
IP
Stau
Tubulin
Futsch
Stau
Tubulin
Futsch
FMRP-YFP
No YFP
B
**
Relative stau mRNA Levels
1.5
1.0
0.5
0.0
control
dfmr1
C
**
Relative stau mRNA Levels
1.5
1.0
0.5
0.0
24B/+
24B>dfmr1 RNAi
D
Input
IP
Cora
Tubulin
Pal1
Cora
Tubulin
Pal1
Stau-GFP
No GFP

Figure 2.7 FMRP binds/stabilizes *staufen* mRNA and Staufen binds *coracle* mRNA.

Larval musculature RNA immunoprecipitation (RIP) assays for FMRP and Staufen show transcript binding interactions. (A) FMRP-YFP immunoprecipitated by anti-YFP (top) compared with w^{1118} negative control (no YFP, bottom). The input is shown on the left and the immunoprecipitate (IP) on the right, for Staufen, α-Tubulin (negative control) and Futsch (positive control). (B) qPCR measurements of *stau* mRNA levels in *dfmr1* mutant larvae normalized to genetic background control (w^{1118}). (C) Muscle *stau* mRNA levels with muscle-targeted *dfmr1* RNAi (24B>*dfmr1* RNAi) normalized to transgenic control (24B-Gal4/+). (D) Staufen-GFP immunoprecipitated by anti-GFP (top) compared with w^{1118} negative control (no GFP, bottom). The input (left) and IP (right) are shown for Coracle, α-Tubulin and Pal1. **P<0.01.

At the NMJ, postsynaptic Staufen is required for the localization and translation of *coracle* mRNA, which encodes a mammalian 4.1 ortholog functioning as a GluRIIA anchoring scaffold (Gardiol and St Johnston, 2014). To test Staufen and *coracle* mRNA interaction, we used UH1-Gal4 to drive UAS-*staufen*::GFP (Barbee et al., 2006; Laver et al., 2013) and pulled down RNA complexes from larval lysates using anti-GFP beads (Figure 2.7D). As above, w^{1118} (no GFP) was the IP negative control. As a positive control, Staufen binds α-tubulin mRNA (Laver et al., 2013), whereas peptidyl-α-hydroxyglycine-α-amidating lyase 1 (Pal1) mRNA reportedly is not bound by Staufen (Laver et al., 2013) and was therefore selected as a negative control. Staufen IP pulled down *coracle* mRNA, but also pulled down α-tubulin and Pal1 mRNA (Figure 2.7D). We also tested GAPDH (Gapdh2), RP49 (RpL32) and Gal4 mRNAs, and all of these were also immunoprecipitated. Repeated trials with increasing transfer RNA (tRNA) concentrations (300 μg, 600 μg, 900 μg, 1 mg) or even highly elevated tRNA (10 mg, 20 mg) all showed continued mRNA pulldown. Thus, Staufen binds *coracle* mRNA, but lacks binding specificity. Staufen is also predicted to bind *dfmr1* mRNA (Laver et al., 2013), but FMRP levels did not change in *staufen* mutant muscle (control 1.00±0.04, $stau^{HL}$ 0.91±0.07; P=0.30; Figure 2.8A,B). We therefore suggest that there is a directional pathway of FMRP binding *staufen* mRNA to control postsynaptic muscle levels, with Staufen in turn binding *coracle* mRNA.

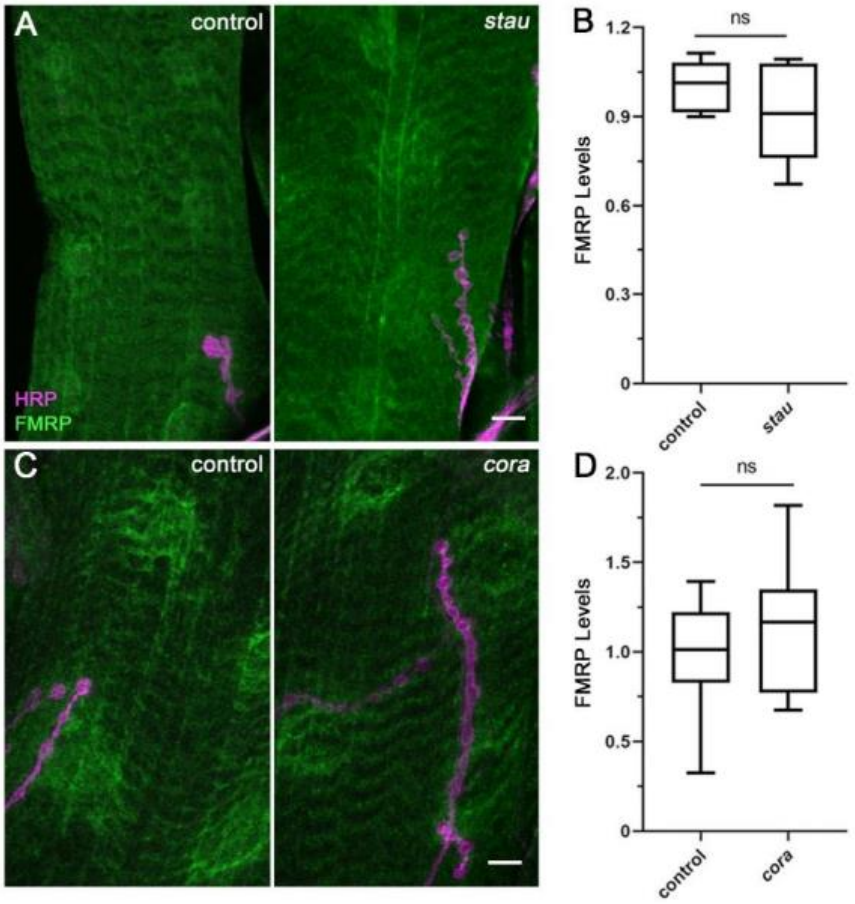

Figure 2.8 Neither *staufen* and *coracle* mutants affect muscle FMRP levels.

Larval muscles labeled for FMRP comparing genetic background control (w^{1118}) with *staufen* ($stau^{HL}$) and *coracle* (*cora*14) mutants. (A) Double labeling for anti-FMRP (green) and synaptic anti-HRP (magenta) in control versus *staufen* mutant. Scale bar: 10 μm. (B) Quantification of FMRP levels shows no significant (ns) change. (C) Double labeling for FMRP (green) + HRP (magenta) in control versus *coracle* mutant. Scale bar: 10 μm. (D) Quantification of FMRP levels shows no significant (ns) change.

2.3.4 FMRP and Staufen act sequentially to regulate postsynaptic Coracle expression

The Staufen dsRNA-binding domain 5 is specifically required for Coracle local translation (Gardiol and St Johnston, 2014). Disruption of this domain in *stau*^{HL} over the genomic deficiency [*stau*^{HL}/*Df(2R)Pcl7B*] reportedly impairs postsynaptic accumulation of Coracle protein via loss of local translation, without affecting *coracle* mRNA localization (Gardiol and St Johnston, 2014), suggesting that Staufen regulates local Coracle translation specifically within the NMJ postsynaptic domain. Coracle binds the GluRIIA C-terminus to scaffold receptors in the postsynaptic membrane, with tight stoichiometry between Coracle and GluRIIA levels within muscle (Chen et al., 2005). As FMRP and Staufen both repress GluRIIA accumulation, we hypothesized that both proteins should inhibit postsynaptic Coracle expression. To test how FMRP and Staufen might regulate Coracle, alone and in combination within the FMRP-Staufen pathway, we used an anti-Coracle antibody (Gomez et al., 2012) to measure levels in anti-HRP-labeled NMJs in wandering third instars. Coracle levels were measured in genetic background controls (w^{1118}), *dfmr1* and *staufen* homozygous mutants, *dfmr1/+* and *staufen/+* heterozygotes, and *dfmr1/+;stau/+* trans-heterozygous double mutants. The expression was quantified postsynaptically surrounding anti-HRP thresholded synaptic boutons, within a dilated 1 μm region of interest to capture the postsynaptic SSR domain.

Coracle encircled NMJ boutons, with a more intense ring in *dfmr1* mutants than in controls (Figure 2.9A). Quantification showed that normalized Coracle levels were significantly elevated in *dfmr1* mutants (control 1.00±0.18, *dfmr1* 1.68±0.13; P=0.0081; Figure 2.9B). To test possible feedback regulation, we assayed anti-FMRP in *coracle* mutant muscle, but found no detectable change (control 1.00±0.10, *cora* 1.14±0.12; P=0.36; Figure 2.8C,D), showing that FMRP acts upstream of Coracle. Compared with genetic controls (w^{1118}), *stau* mutants also had more intense

Coracle rings around boutons (Figure 2.9C). Quantification showed that *staufen* mutants also exhibited significantly more postsynaptic Coracle expression (control 1.00±0.08, *stau* 1.32±0.05; P=0.0018; Figure 2.9D). These findings indicate that FMRP and Staufen similarly limit Coracle in the NMJ postsynaptic domain. To test FMRP and Staufen action in the same pathway, we assayed *dfmr1/+; stau/+* trans-heterozygotes. Neither *dfmr1/+* nor *stau/+* single heterozygotes showed any detectable difference in Coracle levels compared with controls (Figure 2.10A-D). By contrast, the *dfmr1*/+; *stau*/+ trans-heterozygotes had clearly enhanced postsynaptic Coracle rings around NMJ boutons (Figure 2.9E). Quantification showed that the double mutant had a significant 50% increase in normalized Coracle levels compared with the control (control 1.00±0.14, *dfmr1/+; stau/+* 1.53±0.20; P=0.034; Figure 2.9F). We suggest that FMRP and Staufen act sequentially to inhibit Coracle GluRIIA-scaffold enrichment in the postsynaptic domain.

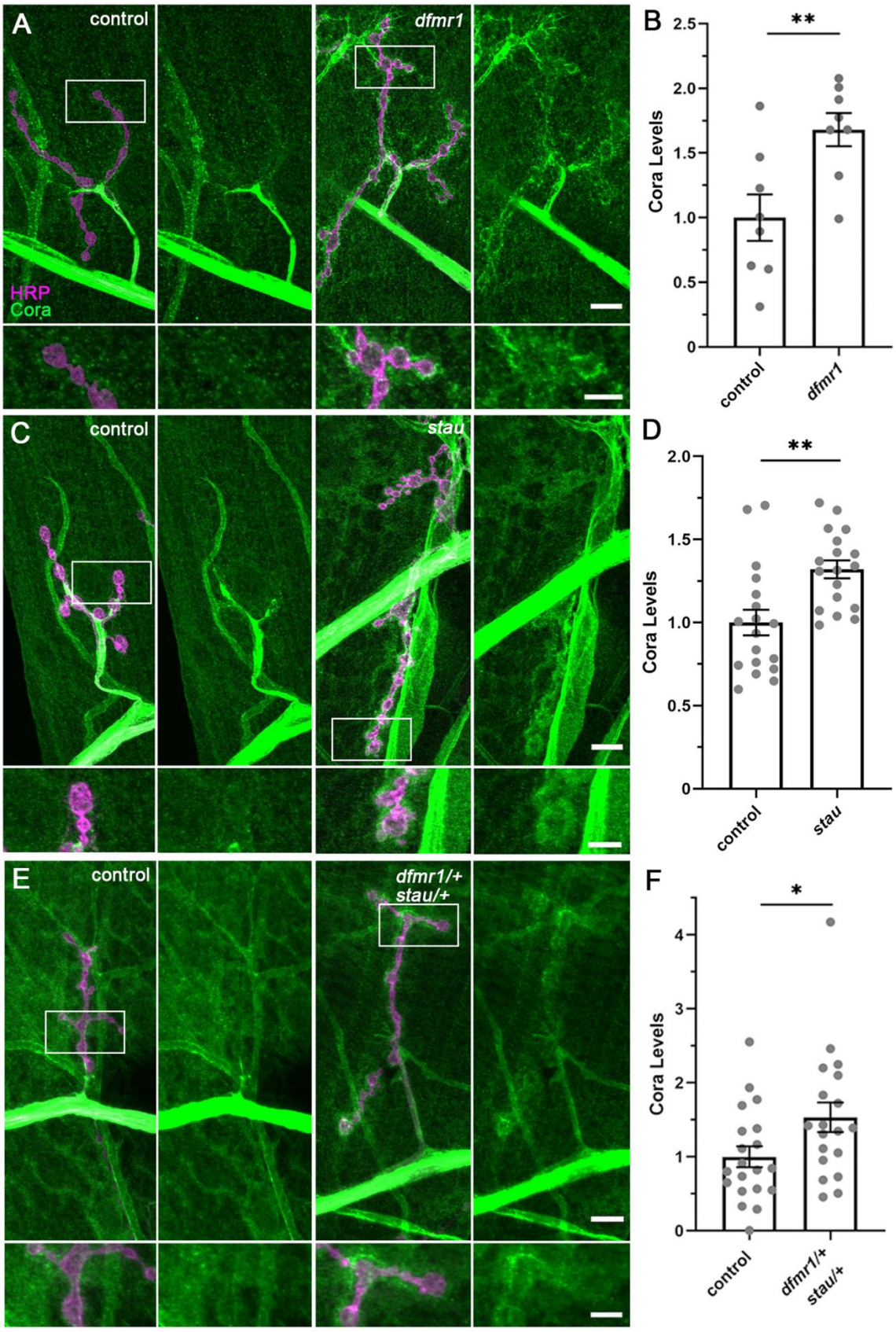
A
control
dfmr1
HRP
Cora
B
**
Cora Levels
2.5
2.0
1.5
1.0
0.5
0
control
dfmr1
C
control
stau
D
**
Cora Levels
2.0
1.5
1.0
0.5
0
control
stau
E
control
dfmr1/+
stau/+
F
*
Cora Levels
4
3
2
1
0
control
dfmr1/+
stau/+

Figure 2.9 FMRP and Staufen act to co-regulate postsynaptic Coracle expression.

Larval NMJ synaptic terminals labeled for Coracle in controls (w^{1118}), *dfmr1* ($dfmr1^{50M}$) and *staufen* ($stau^{HL}$) mutants, and double trans-heterozygotes ($dfmr1^{50M}$/+; $stau^{HL}$/+). Top rows show full muscle 4 NMJs (scale bars: 10 μm) and white-boxed regions are shown magnified below (scale bars: 5 μm). (A) Double labeling for presynaptic HRP (magenta) and Coracle (Cora; green) in control versus *dfmr1* mutant. (B) Postsynaptic Coracle levels are normalized to control. (C) Coracle labeling shown in a *staufen* mutant. (D) Postsynaptic Coracle levels normalized to control. (E) Coracle labeling shown in the double trans-heterozygote ($dfmr1^{50M}$/+; $stau^{HL}$/+). (F) Postsynaptic Coracle levels shown normalized to control. *P<0.05 and **P<0.01. The single heterozygotes ($dfmr1^{50M}$/+ and $stau^{HL}$/+) are shown in Figure 2.8.

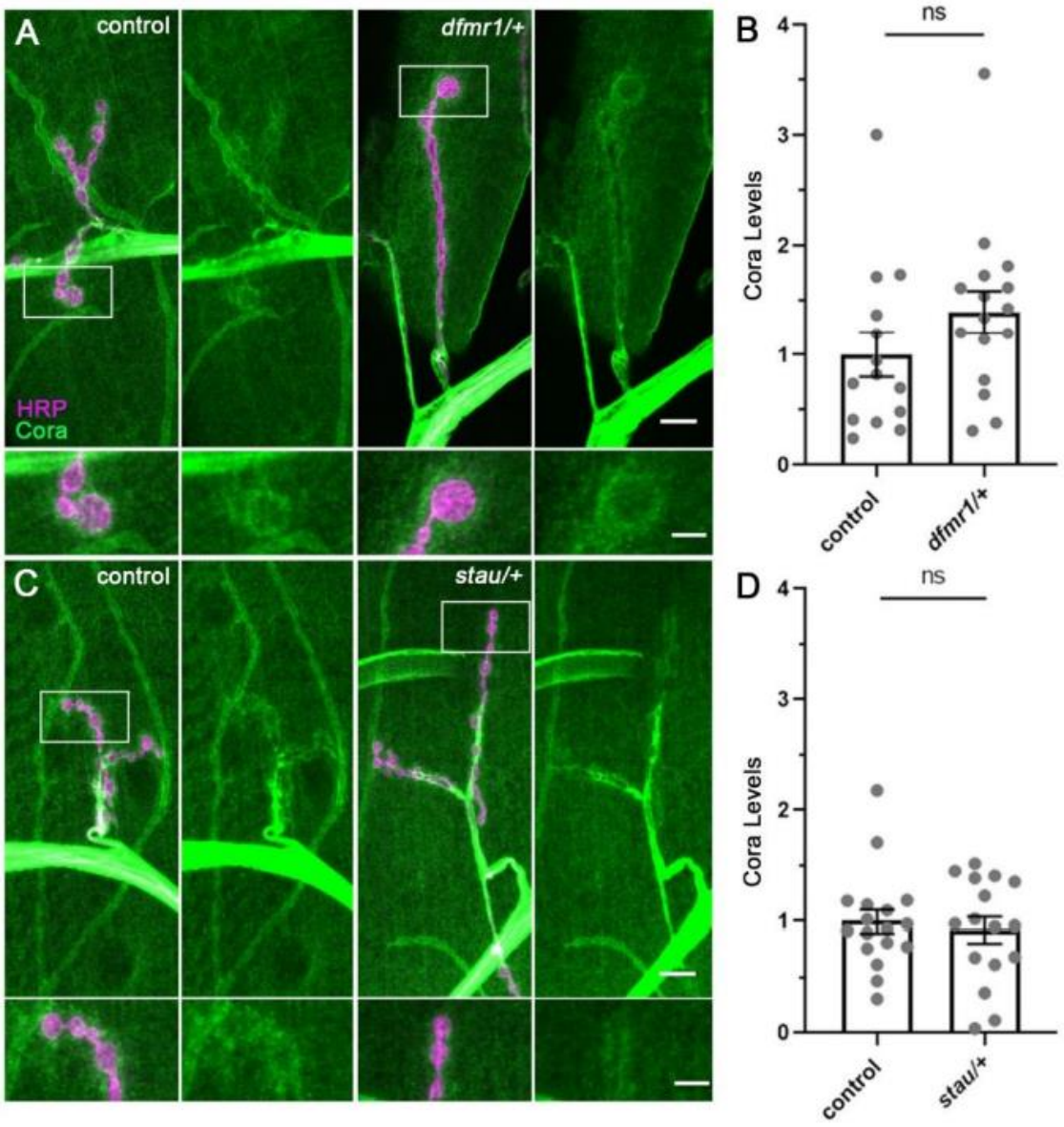

Figure 2.10 Heterozygous *dfmr1*/+ and *staufen*/+ do not affect Coracle levels.

Larval NMJs labeled for Coracle in controls (w^{1118}) compared to *dfmr1* ($dfmr1^{50M}$/+) and *staufen* ($stau^{HL}$/+) heterozygotes. Top rows show full muscle 4 NMJs (scale bar: 10 μm) with white-boxed regions shown magnified below (scale bar: 5 μm). (A) Double labeling for presynaptic HRP (magenta) and Coracle (Cora, green) in control versus *dfmr1* heterozygote. (B) Postsynaptic Coracle levels normalized to control show no significant (ns) change. (C) NMJ Coracle labeling shown in control versus *staufen* heterozygote. (D) Postsynaptic Coracle levels normalized to control show no significant (ns) change.

2.3.5 Postsynaptic Coracle regulates GluRIIA levels and presynaptic bouton formation

Null *coracle* mutants are embryonic lethal (Lamb et al., 1998), and total Coracle loss impairs GluRIIA accumulation at the embryonic NMJ (Chen et al., 2005). As a GluRIIA-binding scaffold, Coracle anchors receptors to underlying F-actin cytoskeleton in the postsynaptic domain (Chen et al., 2005). Consistently, our above results predicted that Coracle OE should be causally associated with an increase in postsynaptic GluRIIA levels. However, many scaffolds like Coracle show similar phenotypes with loss and OE (McCarthy, 2010), including scaffolds at intercellular junctions (Tokuda et al., 2014) and specifically at neuronal synapses (Fulterer et al., 2018). We therefore hypothesized that disrupting Coracle levels in either direction could generate elevated GluRIIA levels and, secondarily, supernumerary bouton formation. To test this hypothesis, we assayed in parallel a larval viable *coracle* hypomorphic mutant (*cora*14; (Khadilkar et al., 2017; Lamb et al., 1998)) and muscle-targeted 24B-Gal4 *coracle* RNAi (Jiang et al., 2019), as well as *coracle* OE (Ward IV et al., 1998). For all three conditions and matched controls, we used double labeling with presynaptic anti-HRP and postsynaptic anti-DLG to assay NMJ architecture and quantify synaptic bouton number. We also double labeled with anti-HRP and anti-GluRIIA to assay synaptic GluRIIA expression and quantify receptor level based on fluorescence intensity.

Both *coracle* mutants and muscle-targeted *coracle* RNAi produced enlarged NMJs with more synaptic boutons (Figure 2.11A). Quantification showed that bouton numbers increase in *coracle* mutants (control 21.00±1.10, $cora^{14}$ 32.86±1.79; P<0.0001) and with muscle *coracle* RNAi (24B/+ control 19.20±1.06, RNAi 26.21±1.69; P=0.0014; Figure 2.11B). NMJ bouton formation was also elevated by muscle-specific *coracle* OE (Figure 2.11A, bottom). Quantification showed that bouton number was significantly elevated by 24B-Gal4-targeted *coracle* OE (24B/+ 21.33±0.64, *cora* OE 30.00±1.12; P<0.0001; Figure 2.11B). Thus, both Coracle loss and gain in

the postsynaptic muscle similarly restricts presynaptic development. Similarly, *coracle* mutants, muscle-targeted *coracle* RNAi and OE all had more postsynaptic GluRIIA than controls (Figure 2.11C). Quantification showed that normalized GluRIIA levels were significantly higher in *coracle* mutants (control 1.00±0.05, $cora^{14}$ 1.32±0.10; P=0.0085) and muscle-specific 24B-Gal4>*cora* RNAi (24B/+ 1.00±0.06, RNAi 1.30±0.13; P=0.03; Figure 2.11D) than in controls. Supporting our hypothesis, quantification likewise showed that normalized GluRIIA levels were highly elevated by *coracle* OE in muscle (24B/+ 1.00±0.06, *cora* OE 1.35±0.096; P=0.004; Figure 2.11D). Taken together, these results suggest that postsynaptic FMRP restricts Staufen to restrict Coracle to restrict GluRIIA levels and thus presynaptic bouton formation, with loss and gain of Coracle phenocopying each other within this GluRIIA regulative mechanism.

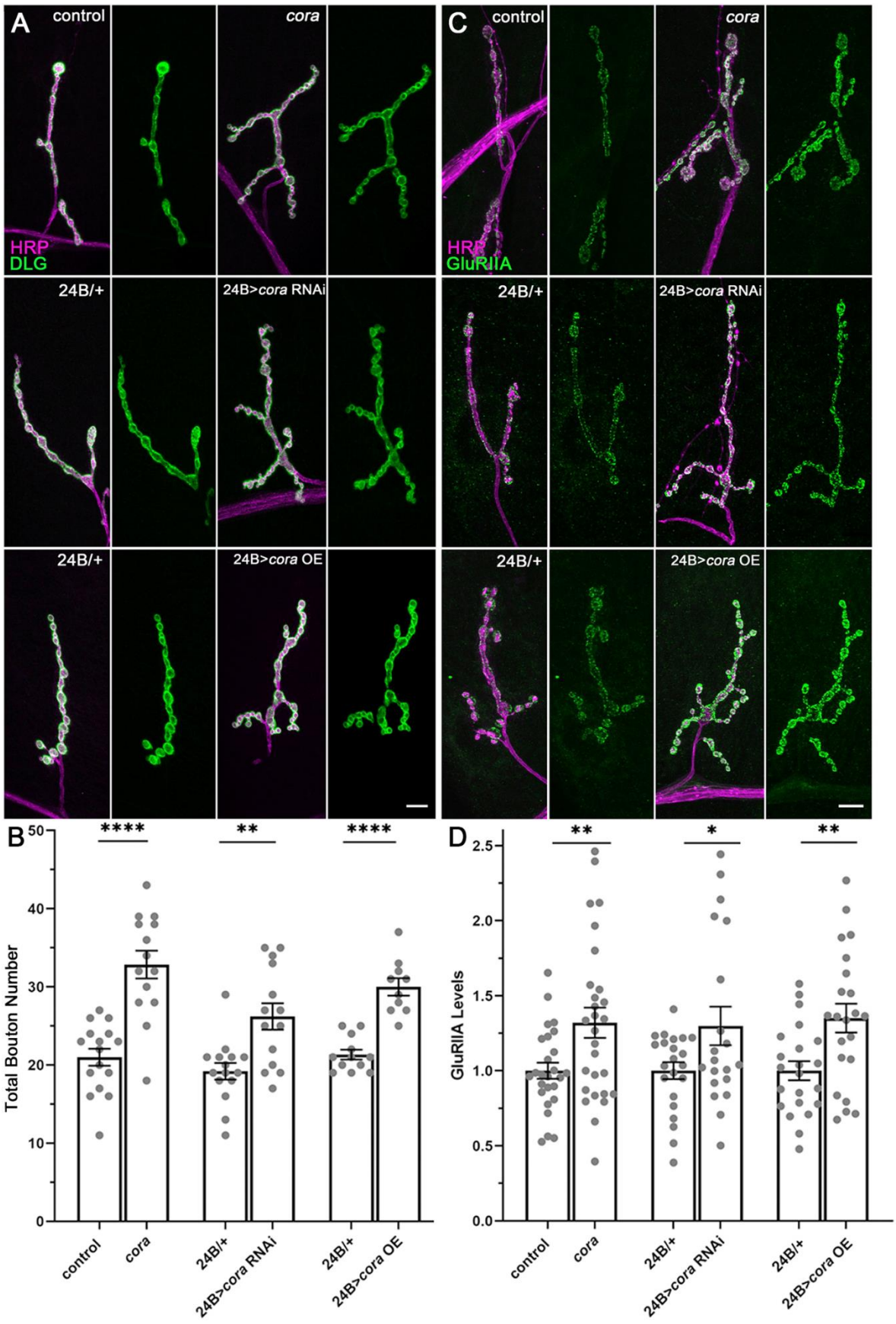
A
control
cora
HRP
DLG
24B/+
24B>cora RNAi
24B/+
24B>cora OE
C
control
cora
HRP
GluRIIA
24B/+
24B>cora RNAi
24B/+
24B>cora OE
B
Total Bouton Number
****
**
****
0
10
20
30
40
50
control
cora
24B/+
24B>cora RNAi
24B/+
24B>cora OE
D
GluRIIA Levels
**
*
**
0.0
0.5
1.0
1.5
2.0
2.5
control
cora
24B/+
24B>cora RNAi
24B/+
24B>cora OE

Figure 2.11 Postsynaptic Coracle regulates NMJ bouton growth and GluRIIA levels.

Larval NMJ synaptic terminal structure and GluRIIA levels compared between genetic background controls (w^{1118}), *coracle* (*cora*14) mutants, postsynaptic *coracle* knockdown (24B>*cora* RNAi) and postsynaptic *coracle* overexpression (24B>*cora* OE). (A) Double labeling for presynaptic HRP (magenta) and postsynaptic DLG (green) in all genotypes. (B) Quantification of synaptic bouton number at the muscle 4 NMJ. (C) Double labeling for HRP (magenta) and GluRIIA (green) in all the above genotypes. (D) Quantification of GluRIIA fluorescence intensity normalized to controls. *P<0.05, **P<0.01 and ****P<0.0001. Scale bars: 10 μm.

2.3.6 FMRP, Staufen and Coracle all negatively regulate synaptic functional differentiation

Clustered postsynaptic GluRIIA channels mediate excitatory ion influx during neurotransmission (Han et al., 2015; Müller and Davis, 2012). GluRIIA levels are thus positively correlated with enhanced excitatory synaptic strength (Petzoldt et al., 2014). We therefore hypothesized that impairment of the FMRP–Staufen–Coracle pathway should elevate function. To test this hypothesis, two-electrode voltage-clamp (TEVC) recordings in *dfmr1*, *staufen* and *coracle* mutants were compared with those in genetic background controls (w^{1118}). Evoked excitatory junction current (EJC) amplitude provides a measure of overall NMJ neurotransmission efficacy dependent on postsynaptic GluRs precisely juxtaposed to the presynaptic active zone glutamate release sites (Clarke et al., 2012; Hong et al., 2020; Marrus and DiAntonio, 2004). To make EJC recordings, suprathreshold stimuli (0.5 ms) were applied with a motor nerve suction electrode at 0.2 Hz (Kopke et al., 2020). Ten sequential evoked traces were recorded in 1 mM [Ca2+] and averaged to generate each data point (Kopke et al., 2020). Miniature EJC (mEJC) recordings assay spontaneous synaptic vesicle fusion events, with frequency indicating presynaptic fusion probability and amplitude correlated with postsynaptic GluR function (Harris and Littleton, 2015). In these recordings, mEJCs were analyzed at 10 kHz in continuous gap-free configuration (Kopke et al., 2020).

Compared with the EJC amplitude of the genetic control (w^{1118}), *dfmr1, staufen* and *coracle* mutants all showed consistently elevated EJC amplitudes (Figure 2.12A). Relative to the control EJC amplitude (126.9±11.75 nA), NMJ synaptic strength was significantly greater in *dfmr1* (190.0±19.19; P=0.0069), *staufen* (185.0±11.24; P=0.0091) and *coracle* (206.7±12.59; P=0.0002) mutants (Figure 2.12B), consistent with their GluRIIA accumulation. Spontaneous mEJC events failed to reveal any obvious changes in these mutants (Figure 2.12C). The mEJC frequency was

not detectably altered, and quantification showed no change in mutants (*staufen*: P=0.92; *coracle*: P=0.67; Figure 2.12D), indicating that synapse number and presynaptic vesicle fusion probability were unaltered. The mEJC amplitude was also unchanged in mutants (Figure 2.12C), and quantification showed no change in mutants (*staufen*: P=0.41; *coracle*: P=0.93; Figure 2.12E), indicating that GluR conductance was unaffected. Similar EJC-specific phenotypes have been repeatedly reported at the *Drosophila* NMJ (e.g. Wang et al., 2017), which might reflect postulated differences between evoked and spontaneous fusion mechanisms (Horvath et al., 2020; Kavalali, 2015) or compensatory interactions between GluRIIA number and conductance (Petzoldt et al., 2014; Renden and Broadie, 2003). We conclude that FMRP, Staufen and Coracle all repress postsynaptic GluRIIA accumulation and functional neurotransmission strength, but we still need a mechanistic link to the increase in presynaptic bouton formation via this pathway.

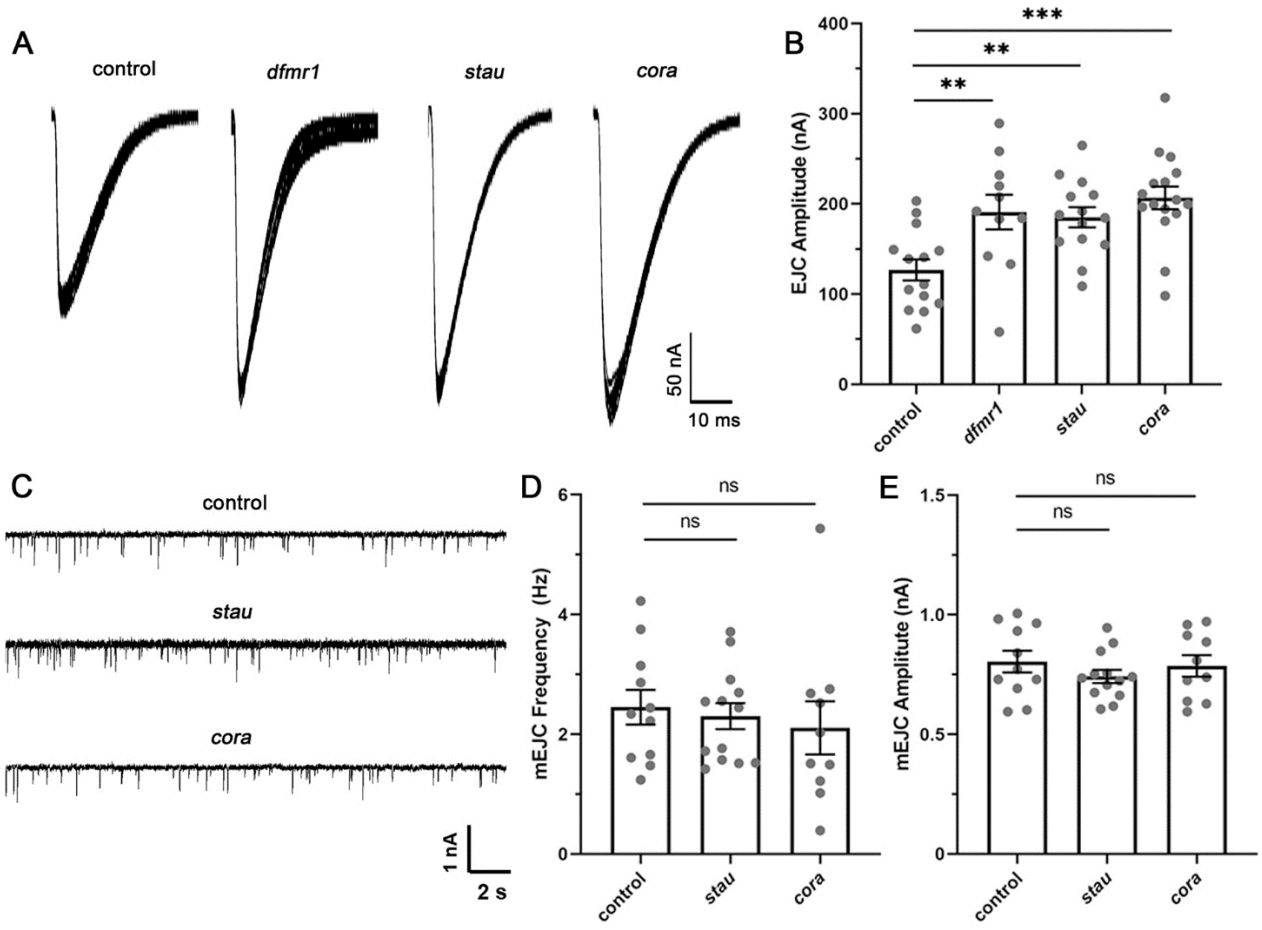

Figure 2.12 FMRP, Staufen and Coracle all negatively regulate NMJ transmission.

Two-electrode voltage-clamp recordings of synaptic function comparing genetic background control (w^{1118}) with *dfmr1* ($dfmr1^{50M}$), *staufen* ($stau^{HL}$) and *coracle* ($cora^{14}$) mutants. (A) Example motor nerve-stimulated evoked excitatory junctional current (EJC) traces (1.0 mM Ca2+) showing ten superimposed responses in control (leftmost) versus *dfmr1*, *staufen* and *coracle* mutants. (B) Quantification of EJC amplitudes in all four genotypes. **P<0.01 and ***P<0.001. (C) Example miniature EJC (mEJC) recordings showing spontaneous synaptic vesicle fusion events. (D,E) Quantification of the overall mEJC frequency (D) and mEJC amplitude (E). There is no significant (ns) difference compared with the control for either measurement.

2.3.7 FMRP, Staufen and Coracle all negatively regulate trans-synaptic pMad signaling

Functional GluRIIA accumulation in the *dfmr1* mutant induces presynaptic bouton development via a non-canonical BMP trans-synaptic signaling pathway (Kamimura et al., 2019; Sulkowski et al., 2016). This may not involve a BMP ligand, but rather a direct interaction between postsynaptic GluRIIA and presynaptic BMP receptor (Sulkowski et al., 2016). Intercellular signaling triggers synaptic phosphorylation of pMad to induce bouton formation (Kamimura et al., 2019; Sulkowski et al., 2016; Upadhyay et al., 2017). As *dfmr1*, *staufen* and *coracle* mutants all showed increased GluRIIA levels and bouton formation, we hypothesized that all mutants activate GluRIIA-dependent signaling of presynaptic pMad. To test this idea, we triple labeled all three mutants with anti-HRP (to mark neuronal presynaptic membrane), anti-Bruchpilot (Brp; to mark presynaptic active zones) and anti-pMad (Kamimura et al., 2019). The Brp-positive active zones and pMad levels were assayed within anti-HRP thresholded boutons using laser-scanning confocal microscopy (LSM). However, this approach has restricted X-Y resolution to visualize the small, closely spaced active zones (~500-600 nm diameter; (Guggenheim et al., 2016; Pielage et al., 2006; Wegel et al., 2016)). Therefore, to better resolve pMad around Brp puncta, we also used higher resolution structured illumination microscopy (SIM) (Guggenheim et al., 2016).

In LSM imaging, Brp-positive active zone numbers in *dfmr1*, *staufen* and *coracle* mutant NMJs were all comparable to those in control NMJs, whereas the surrounding pMad labeling was consistently elevated in all three mutants (Figure 2.13A). Note that Brp did not colocalize with pMad, indicating that pMad surrounds the presynaptic active zones but is not present within each synapse. Compared with genetic control (w^{1118}) normalized pMad levels (intensity: 1.00±0.061), fluorescence quantification showed that presynaptic pMad was significantly elevated in *dfmr1* (1.52±0.14; P=0.005), *staufen* (1.64±0.14; P=0.001) and *coracle* (1.78±0.14; P<0.0001) mutants

(Figure 2.13C). At higher resolution, SIM imaging clearly revealed elevated pMad levels surrounding presynaptic active zones in all *dfmr1, staufen* and *coracle* mutants compared with controls (Figure 2.13B). Note in single NMJ boutons that Brp and pMad labeling were non-overlapping, but adjacent. In all three of the mutants, presynaptic pMad aberrantly accumulated around Brp-positive active zones. Importantly, quantification of the active zones compared with matched control (Brp puncta density/µm2: 1.44±0.07) showed no significant change in the *coracle* (1.54±0.05; P=0.54), *staufen* (1.46±0.02; P=0.99) or *dfmr1* (1.63±0.11; P=0.11) mutants (Figure 2.13D). These findings suggest that elevated pMad levels in all three mutants correlate with increased GluRIIA-dependent retrograde trans-synaptic signaling from the postsynaptic domain, rather than presynaptic active zone density.

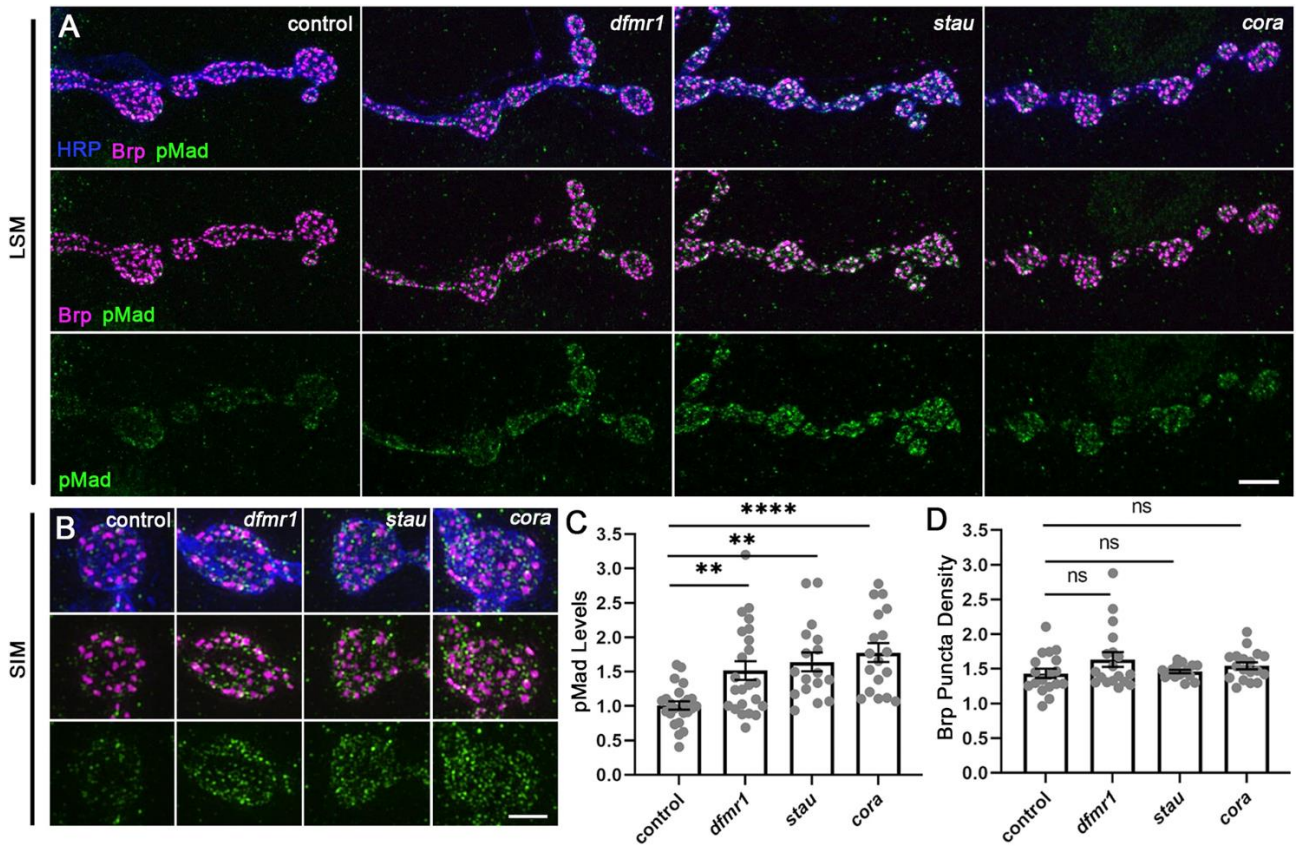

Figure 2.13 FMRP, Staufen and Coracle all negatively regulate NMJ pMad signaling.

Larval NMJs labeled for phosphorylated Mothers against decapentaplegic (pMad) at presynaptic active zones comparing genetic background control (w^{1118}) with *dfmr1* ($dfmr1^{50M}$), *staufen* ($stau^{HL}$) and *coracle* (*cora*14) mutants. (A) Laser scanning confocal microscope triple labeling for HRP (blue), active zone Bruchpilot (Brp; magenta) and pMad (green), with overlap shown in white. (B) Higher-resolution structured illumination microscope imaging of single synaptic boutons. (C) Quantification of pMad fluorescence intensity normalized to the background control. **P<0.01 and ****P<0.0001. (D) Quantification of synapse density (Brp puncta active zone number per μm2). There is no significant (ns) difference compared with the control for any of the mutants. Scale bars: 5 μm (A); 2 μm (B).

To directly test the postsynaptic to presynaptic signaling mechanism, all three genes were knocked down with muscle-targeted RNAi (Figure 2.14). Compared with the driver control (24B-Gal4/+), postsynaptic *dfmr1* RNAi caused a clear and consistent increase in presynaptic pMad levels (Figure 2.14A). Quantification normalized to the control showed a significant elevation in the knockdown (control 1.00±0.086, *dfmr1* RNAi 1.40±0.12; P=0.0098), with no change in BRP-marked active zone density (P=0.85; Figure 2.14B). Similarly, targeted knockdown of postsynaptic *staufen* resulted in an obvious elevation in pMad levels (Figure 2.14C). Quantification again indicated a significant increase in pMad fluorescence (control 1.00±0.085, *stau* RNAi 1.44±0.13; P=0.0072), with no change in synapse number (P=0.78; Figure 2.14D). Finally, muscle-targeted *coracle* RNAi also drove heightened presynaptic pMad levels (Figure 2.14E). Quantification likewise showed that there is a significant increase in pMad in the presynaptic boutons (control 1.00±0.084, *cora* RNAi 1.28±0.10, P=0.049), with no change in BRP-marked active zone density (Figure 2.14F). These findings indicate that targeted loss of all three genes in the postsynaptic muscle causes trans-synaptic elevation of pMad surrounding neuronal presynaptic active zones. Taken together, these results suggest that accumulated postsynaptic GluRIIA in *dfmr1*, *staufen* and *coracle* mutants activates presynaptic pMad signaling, which in turn induces new bouton formation during NMJ synaptic development.

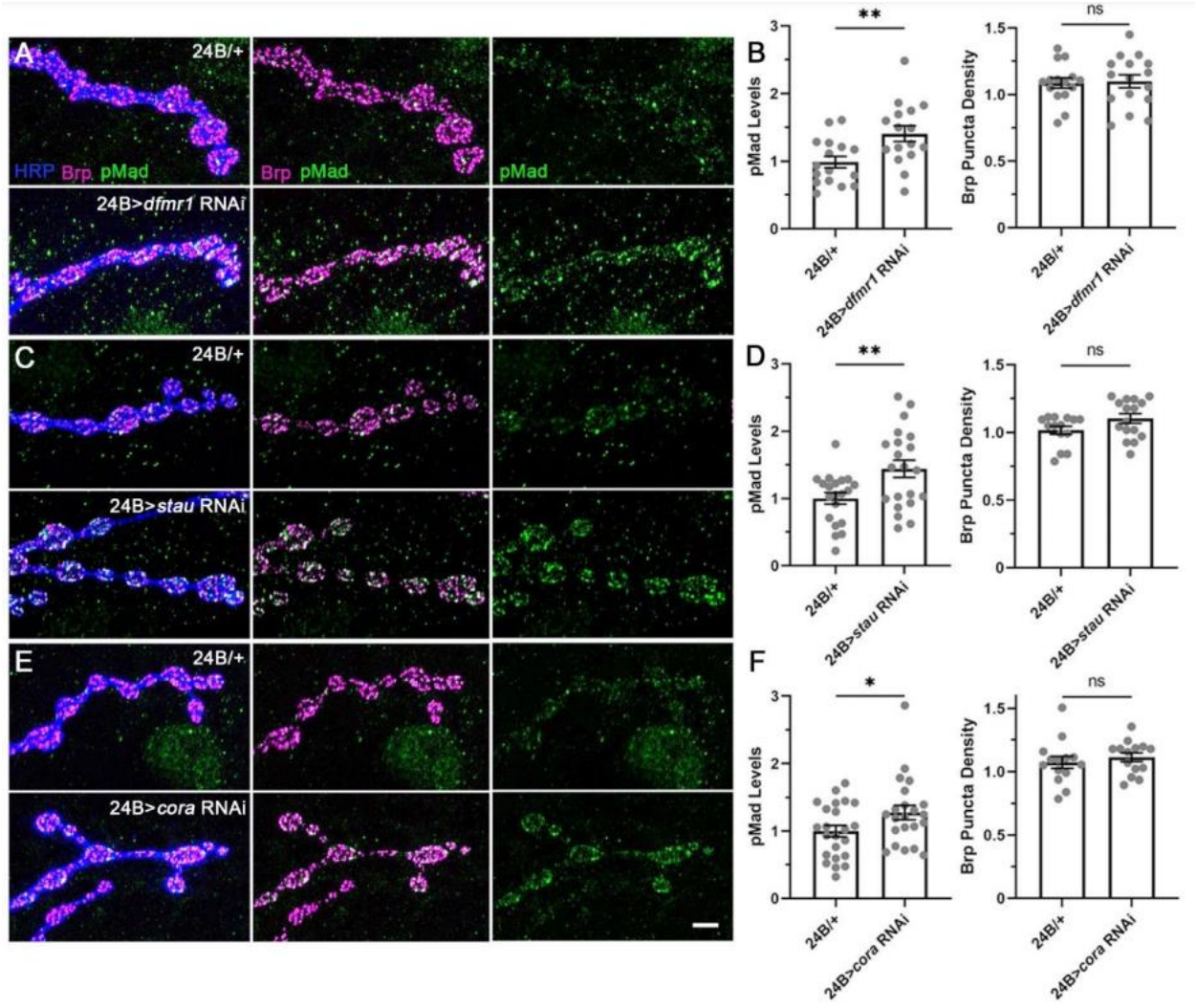

Figure 2.14 Postsynaptic FMRP, Staufen and Coracle all restrict pMad signaling.

Larval NMJs triple-labeled for HRP (blue), Brp (magenta) and pMad (green) in muscle driver controls (24B/+, top rows) and with *dfmr1* (24B>*dfmr1* RNAi), *staufen* (24B>*stau* RNAi) and *coracle* (24B>*cora* RNAi) knockdown. (A) Representative images of *dfmr1* postsynaptic RNAi. (B) Quantification of normalized pMad fluorescent intensity (left) and Brp active zone density (right). (C) Representative images of muscle-targeted *staufen* knockdown. (D) Quantification of pMad levels and Brp active zone density. (E) Images of *coracle* postsynaptic RNAi. Scale bar: 5 μm. (F) Quantification of presynaptic pMad levels and Brp active zone density. Significance is indicated at $p<0.05$ (*), $p<0.01$ (**) and $p>0.05$ (not significant; ns) based on student's t-tests.

2.4 Discussion

This study reveals the mechanism of the established FMRP negative regulation of postsynaptic GluRIIA receptors and presynaptic bouton formation in the *Drosophila* FXS disease model (Pan and Broadie, 2007; Zhang et al., 2001). Specifically, the mRNA-binding FMRP-positive translational regulator binds to *staufen* mRNA as predicted (D'Annessa et al., 2019), within the postsynaptic cell. Consequently, both *dfmr1* and *staufen* mutants share the elevated GluRIIA level and bouton number phenotypes based on a common postsynaptic pathway function, and genetically interact as trans-heterozygotes to reproduce these phenotypes. Staufen acts as a dsRBP (Banerjee and Barraud, 2014) to bind *coracle* mRNA as predicted (Laver et al., 2013); both *dfmr1* and *staufen* mutants exhibit elevated postsynaptic Coracle levels, and genetically interact as trans-heterozygotes to reproduce this phenotype. Coracle acts as a GluRIIA-binding anchoring scaffold within the postsynaptic domain to regulate local receptor accumulation (Chen et al., 2005). Consequently, *dfmr1, staufen* and *coracle* mutants all increase NMJ synaptic functional differentiation to elevate neurotransmission strength. Finally, the elevated postsynaptic GluRIIA levels mediate retrograde BMP receptor trans-synaptic signaling that induces pMad to drive new presynaptic bouton development (Kamimura et al., 2019; Sulkowski et al., 2016). *dfmr1, staufen* and *coracle* mutants all exhibit elevated presynaptic pMad levels, thereby linking the postsynaptic GluRIIA accumulation and presynaptic supernumerary bouton formation defects shared by all of these mutants.

The *staufen* mutant increased synaptic Coracle levels, GluRIIA levels and bouton number are all internally consistent. In a previous study (Gardiol and St Johnston, 2014), opposite phenotypes were measured in $staufen^{HL}/Df(2R)Pcl7B$, which reduces another 14 genes in heterozygous deficiency, including loci involved in neuronal development (e.g. grh, nopo;

(Almeida and Bray, 2005; Bakshi et al., 2020; Ketosugbo et al., 2017; Merkle et al., 2009)). Importantly, we similarly found reduced synaptic protein levels and bouton number in *staufen*^{HL}*/Df(2R)Pcl7B*, suggesting that heterozygosity of one or more of the neighboring genes impairs synaptic development (Mutsuddi et al., 2004; Tsou et al., 2015; Yilmazer et al., 2016). However, we showed that a *staufen* RNAi that reduces transcript levels by ~90% replicates the *staufen* mutant NMJ phenotypes of increased GluRIIA levels and synaptic bouton numbers. We also replicated this with a second, independent *staufen* RNAi line. Moreover, we showed that the effect is entirely restricted to postsynaptic muscle RNAi, with no effect from presynaptic neuron RNAi, consistent with restricted postsynaptic Staufen function (Gardiol and St Johnston, 2014). In addition, postsynaptic *staufen* rescue of the *staufen* mutant restored normal synaptic bouton formation, with OE reducing GluRIIA levels in *staufen* mutants and rescuing GluRIIA levels in *dfmr1* mutants. Both *staufen* mutants and postsynaptic *staufen* RNAi also share the arrested supernumerary satellite bouton development characterizing *dfmr1* null mutants (Friedman et al., 2013). These many independent lines of evidence confirm our results, and are consistent with the known parallel FMRP role in restricting GluRIIA levels and synaptic bouton formation (Pan and Broadie, 2007; Zhang et al., 2001).

To regulate *Staufen*, FMRP binds *staufen* mRNA and protects targeted *staufen* transcripts from degradation. FMRP contains at least three distinct RNA-binding domains (RBDs) (Kenny and Ceman, 2016), and *Staufen* has five RBDs (Laver et al., 2013). Staufen reportedly binds a specific RNA hairpin structure formed by long 3′ UTRs (Gardiol and St Johnston, 2014; Laver et al., 2013), but our RIP shows that Staufen also binds mRNAs that are not predicted to generate this secondary structure (Ramos et al., 2000). Although the decreased *staufen* mRNA levels in both *dfmr1* mutants and muscle-targeted *dfmr1* RNAi are predicted to be due to the lack of FMRP

binding, it is also possible that other unregulated interactors cause the downregulated *staufen* mRNA expression (Shah et al., 2020). Localized labeling with an anti-Staufen antibody has been reported in the postsynaptic NMJ (Gardiol and St Johnston, 2014), which we can confirm, but we could not reduce labeling in *staufen* hypomorphic mutants. We therefore have not shown Staufen labeling in the current study. Moreover, western blots have been reported with the same anti-Staufen antibody (St Johnston et al., 1991); however, our attempts were unsuccessful. We therefore used qPCR to measure *staufen* mRNA levels. Staufen binds to *coracle* mRNA, but does so in a non-selective manner. This result is consistent with Staufen acting as a very broad spectrum dsRBP (Heraud-Farlow and Kiebler, 2014; Laver et al., 2013), and suggests that Staufen likely acts with a translational regulator partner to generate specificity. FMRP is very well established to partner with other RBPs to mediate the translational regulation of its target transcripts (Bardoni et al., 1999; Bardoni et al., 2003; Didiot et al., 2009; Kenny et al., 2014).

The postsynaptic Coracle scaffold acts in a GluRIIA local anchoring mechanism, presumably to link the receptors to the underlying actin cytoskeleton (Chen et al., 2005). The jointly elevated Coracle and GluRIIA levels in both *dfmr1* and *staufen* mutants are consistent with this scaffold function. Because the *dfmr1/+; staufen/+* trans-heterozygotes share this correlated Coracle and GluRIIA upregulation in the postsynaptic domain, a single common signaling pathway is indicated. Coracle also restricts terminal branching development in peripheral sensory neurons (Jiang et al., 2019; Tenenbaum et al., 2017). Both *coracle* mutants and sensory neuron-targeted *coracle* RNAi also display increased dendritic branch and termini numbers. These phenotypes are similar to the expanded NMJ terminals and increased synaptic bouton development reported here. Importantly, both *coracle* loss of function (mutants and muscle-targeted RNAi) and gain of function (muscle-targeted OE) increase postsynaptic GluRIIA levels and generate

supernumerary boutons. Likewise, the knockdown and OE of many other similar scaffolds are known to cause phenocopying defects (McCarthy, 2010). Some examples include the muscle chaperone UNC-45 (Landsverk et al., 2007), the tight junction scaffold zonula occludens-1 (ZO-1) (Tokuda et al., 2014) and synaptic UNC-13 (Fulterer et al., 2018). Indeed, both *coracle* loss and OE similarly cause increased dendritic crossing in *Drosophila* sensory neurons (Tenenbaum et al., 2017), similar to the phenocopy of developmental defects reported here. Combining the roles of postsynaptic FMRP–Staufen–Coracle in GluRIIA clustering, we reasoned that this pathway must be a regulatory determinant of synaptic functional development.

Removing FMRP, Staufen and Coracle strongly enhances functional synaptic differentiation and NMJ neurotransmission strength. This is consistent with expectations from the postsynaptic GluRIIA accumulation in all of these mutants (Harris and Littleton, 2015). Elevated GluRIIA levels are well known to be associated with increased evoked functional responses and prolonged channel open times (DiAntonio et al., 1999; Schmid et al., 2008). A GluRIIA pore sequence (MQQ) critically required for the *Drosophila* channel Ca^{2+} permeability is conserved in mammalian receptors (Petersen et al., 1997). This selectivity allows Ca^{2+}-dependent participation in spontaneous (mEJC) and evoked (EJC) neurotransmission (Han et al., 2015). Although enhanced evoked EJC amplitudes are typically accompanied by mEJC alterations (Karunanithi et al., 2020; Sandstrom, 2011; Tsurudome et al., 2010), we find that mEJC amplitude and frequency are unchanged in both the *staufen* and *coracle* mutants, and show only minimal changes in the *dfmr1* mutants (Zhang et al., 2001). Classically, both evoked and spontaneous neurotransmission were thought to be mediated by the same vesicles (del Castillo and Katz, 1954; Groemer and Klingauf, 2007); however, more recent evidence has indicated that spontaneous and evoked neurotransmission have distinct machinery and vesicle pools (Groffen et al., 2010; Horvath et al.,

2020; Ramirez et al., 2012; Sara et al., 2005). Postsynaptic receptors can be segregated into different compartments that are activated by either spontaneous or evoked release (Atasoy et al., 2008). Our work supports this growing body of evidence for differential regulation. Importantly, GluRIIA has unique functions, modulating both presynaptic glutamate release and presynaptic bouton development (Bogdanik et al., 2004; Kamimura et al., 2019).

The *dfmr1*, *staufen* and *coracle* mutants all showed upregulated presynaptic pMad correlated with postsynaptic activated GluRIIA accumulation. GluRIIA activation triggers presynaptic pMad signaling via BMP receptors surrounding active zones, which, in turn, stabilizes GluRIIA receptors in the postsynaptic domains (Sulkowski et al., 2016). This trans-synaptic signaling mechanism induces new presynaptic bouton development. The targeted postsynaptic RNAi for all three genes confirms this intercellular link. Synaptic BMP signaling involves both the type I serine/threonine kinase receptors and the type II receptor Wit (Upadhyay et al., 2017). Although BMP ligand Glass bottom boat (Gbb) signaling via Wit presynaptic receptors is well established at the NMJ to modulate synaptogenesis (Ellis et al., 2010; Kim et al., 2019; McCabe et al., 2003), the mechanism of presynaptic bouton formation induced by activated GluRIIA signaling does not involve canonical BMP signaling via Gbb (Friedman et al., 2013; Kamimura et al., 2019). In the *dfmr1* mutants, we suggest that postsynaptic GluRIIA accumulation induces presynaptic bouton development via non-canonical GluRIIA-Wit trans-synaptic retrograde signaling (Sulkowski et al., 2016). Similarly, the muscle postsynaptic glypican Dally-like protein (Dlp) (Kamimura and Maeda, 2021) negatively regulates NMJ synaptic development by inhibiting this same non-canonical BMP pathway through decreased activated GluRIIA expression (Kamimura et al., 2019). Postsynaptic GluRIIA clustering can thus trigger presynaptic bouton formation, although supernumerary boutons do not always induce reciprocal GluRIIA changes

(Sulkowski et al., 2016). We conclude that an FMRP–Staufen–Coracle–GluRIIA–pMad pathway regulates intertwined structural and functional glutamatergic synapse development.

2.5 Materials and Methods

2.5.1 Drosophila genetics

All stocks were reared at 25°C on standard cornmeal/agar/molasses food. The genetic background control was w^{1118}. The viable *dfmr1* mutant was w; $dfmr1^{50M}$, in which the *dfmr1* locus has been completely removed via a P-element imprecise excision deletion (Zhang et al., 2001). The larval viable *staufen* mutant was w; $stau^{HL}$, which has a point mutation in the dsRNA-binding domain 5 specifically required for local mRNA translation (Figure 2.1A; St Johnston et al., 1991). The viable *coracle* mutant was w; $cora^{14}$, which has a nonsense mutation (Arg1607) reducing function (Lamb et al., 1998; Ward et al., 2001). Transgenic drivers were ubiquitous daughterless UH1-Gal4 (Rohrbough et al., 2004), neuronal elav-Gal4 (Kan et al., 2021) and muscle-specific 24B-Gal4 (Kim et al., 2021). All genetic crosses and recombinations to make double mutant lines were done using standard approaches. Transgenic UAS lines used in this study are listed in Table 2.2.

Line	Provider	Reference
UAS-*stau* RNAi	VDRC 106645	(Landskron et al. 2018)
UAS-*cora* RNAi	BDSC 51845	(Jiang et al., 2019)
UAS-*dfmr1* RNAi	BDSC 35200	(Flockhart et al., 2006)
UAS-myc-*cora*	Fehon Lab	(Ward IV et al., 1998)
UAS-*stau*-GFP	Ramaswami Lab	(Barbee et al., 2006)
UAS-YFP-*dfmr1*	Zarnescu Lab	(Cziko et al., 2009)

Table 2.2 Transgenic UAS lines used in this study.

2.5.2 Antibody labeling

Staged wandering third instars were dissected in phosphate-buffered saline (PBS). For FMRP, DLG, Brp and pMad labeling, tissues were fixed in 4% paraformaldehyde (PFA) diluted in PBS for 10 min at room temperature (RT). Coracle labeling was performed with 20 min fixation at RT. To label GluRIIA, larvae were fixed in 100% Bouin's fixative (Karr et al., 2009) for 5 min at RT. Fixed preparations were blocked for 1 h at RT in PBS with 0.2% Triton X-100 (PBST) plus 1% bovine serum albumin (BSA). Primary antibody incubation was done overnight at 4°C and secondary antibody incubation was done for 2.5 h at RT. Primary antibodies used were as follows: mouse anti-DLG [Developmental Studies Hybridoma Bank (DSHB), 4F3, 1:50], mouse anti-GluRIIA (DSHB, 8B4D2, 1:50), mouse anti-Coracle (DSHB, C566.9, 1:50), mouse anti-FMRP (Abcam, 10299, 1:250), mouse anti-Brp (DSHB, NC82, 1:100), rabbit anti-Smad3 (70hosphor S423+S425, Abcam 52903, 1:500), Cy5-conjuagted goat anti-HRP (Jackson ImmunoResearch, 147967, 1:250) and Cy3-conjugated goat anti-HRP (Jackson ImmunoResearch, 137589, 1:250). Secondary antibodies used were as follows: goat 488 anti-mouse (Invitrogen, A11001, 1:250), goat 488 anti-rabbit (Invitrogen, A11008, 1:250), donkey 555 anti-mouse (Invitrogen, A31570, 1:250) and donkey 488 anti-mouse (Invitrogen, A21202, 1:250).

2.5.3 Synaptic imaging

All confocal imaging was performed on a Zeiss LSM 510 META laser-scanning confocal microscope and projected in Zen software (Kopke et al., 2020). The NMJ areas and fluorescent intensities were analyzed via blinded z-stack sum projection in FIJI software (Guillen et al., 2020). GluRIIA levels were quantified in HRP-labeled NMJ areas with eliminated muscle intensity background, while Coracle levels were quantified in dilated 1 μm rings surrounding individual

NMJ boutons. For SIM, samples were imaged on a Nikon N-SIM microscope in 3D SIM mode (Kopke et al., 2020). Fluorophores were activated by 647 nm, 561 nm and 488 nm diode lasers. With a SR Apo TIRF 100× oil objective (1.49 NA WD 0.12) and an Andor iXon Ultra DU-897 EMCCD monochrome camera, samples were reconstructed through NIS-Elements (Nikon) with 0.12 μm step-size stacks. Stack reconstructions of the blinded raw data were done before image rendering and measurement analyses.

2.5.4 Quantitative real-time PCR

The total RNA from wandering third instars was isolated according to the instructions in the RNeasy Plus Mini Kit (Qiagen 74134). RNA (2 μg) measured by a Nanodrop 2000C was then reverse transcribed into complementary DNA (cDNA) with random hexamers using the High Capacity cDNA Reverse Transcription Kit (Applied Biosystems, 4368814). Resulting single-strand cDNA was then subjected to real-time PCR employing the SYBR Green Master Mix (Applied Biosystems, A25742) and using the CFX384 Touch Real-Time PCR system (Bio-Rad). Targeted transcripts were normalized to reference gene cDNA (GAPDH2). The cDNA primers used in this study are listed in Table 2.1.

2.5.5 RNA immunoprecipitation

Fifty wandering third instars of each genotype were homogenized in 500 μl RNase-free lysis buffer [20 mM HEPES, 100 mM NaCl, 2.5 mM EDTA, 0.05% (v/v) Triton X-100, 5% (v/v) glycerol] with 1% β-mercaptoethanol, 1× protease inhibitor cocktail (cOmplete mini EDTA-free Tablets, Sigma-Aldrich), and 400 U Rnase inhibitor (Applied Biosystems, N8080119). To preclear

the supernatant, the centrifuged lysates were incubated with 20 µl Protein G Dynabeads for 1 h at 4°C. In parallel, 200 µl Protein G Dynabeads were incubated in blocking buffer (1×PBS, 0.2% TWEEN 20, 0.1% tRNA and 5% BSA) for 1 h at 4°C, followed by coating with 10 µg of the primary antibody. Next, the precleared supernatant was incubated with antibody-bead conjugates overnight at 4°C. To reduce non-specific RNA binding in larval lysates, tRNA (Sigma-Aldrich, 10109541001) was added in lysis buffer as specified (e.g. 1 mg tRNA per 500 µl IP reaction). To purify bound RNAs, washed bead-protein-RNA complexes were incubated with a 500 µl TRIzole and chloroform mixture (Ambion, 15596026) for 10 min. Subsequently, 3 µl glycogen was applied to carry RNAs for the precipitation by mixing with 100 µl 2-propenol. The precipitated RNA was then reverse transcribed into single-strand cDNA and subjected to primer-specific PCR (Table S2). We used 2% agarose gels to analyze the PCR products. Primary antibodies used were mouse anti-Venus YFP (Sigma-Aldrich, MABE1906) and mouse anti-GFP (Sigma-Aldrich, G6539).

2.5.6 Synaptic electrophysiology

Wandering third instars were dissected along the dorsal midline, internal organs were removed, and body walls were glued down (Vetbond, 3 M). Next, all peripheral motor nerves were cut at the base of the ventral nerve cord. TEVC recordings were performed at 18°C in physiological saline (128 mM NaCl, 2 mM KCl, 4 mM MgCl2, 1 mM CaCl2, 70 mM sucrose and 5 mM HEPES, pH 7.2). Synaptic currents were recorded from ventral longitudinal muscle 6 of abdominal segments 3/4 under a Zeiss Axioskop microscope using a 40× water-immersion objective (Kopke et al., 2020). Muscles were impaled with two microelectrodes (1 mm outer diameter borosilicate capabilities; World Precision Instruments) of ∼15 MΩ resistance filled with 3 m KCl, and then clamped at a command voltage of −60 mV employing an Axoclamp-2B amplifier (Axon

Instruments; Kopke et al., 2020). To make the EJC recordings, the motor nerve was stimulated using a fire-polished glass suction electrode with 0.5 ms suprathreshold voltage stimuli at 0.2 Hz (Grass S88 stimulator). Data were filtered at 2 kHz. To quantify EJC amplitude, ten consecutive traces were recorded and averaged, with the average peak amplitude being reported. Spontaneous mEJC events were recorded in continuous 2 min sessions at 10 kHz, and analyzed using a 200 Hz low-pass filter (Kopke et al., 2020). Clampex 9.0 was used for data acquisition, and Clampfit 9 was used for data analysis (Axon Instruments).

2.5.7 Statistical analyses

All statistics were performed using GraphPad Prism software (v8.0). All data sets were subject to ROUT outlier tests with Q set to 1%. All paired data comparisons (i.e. bouton numbers, GluRIIA levels, FMRP levels, Coracle levels and qPCR measurements) were assayed using unpaired two-tailed Student's t-tests for two-way comparison with 95% confidence. All data sets of more than two comparisons (i.e. electrophysiology results, pMad levels and active zone numbers) were analyzed using one-way ANOVA. Dunnett's multiple comparison tests were performed to compare the mean of each experimental data set with the control mean. All figures show mean±s.e.m., with $P \leqslant 0.05$ considered significant.

2.6 Acknowledgements

We are grateful to the BDSC (Indiana University, Bloomington, IN, USA) and the VDRC (Vienna, Austria) for essential genetic lines, and the DSHB (University of Iowa, Iowa City, IA, USA) for essential antibodies. We thank Daniel St Johnston (The Gurdon Institute, University of

Cambridge, Cambridge, UK) and Richard Fehon (University of Chicago, Chicago, IL, USA) for *staufen* and *coracle* stocks, respectively. We thank Julian Hillyer, He Huang and Jim Patton (Vanderbilt University, Nashville, TN, USA) for qPCR equipment use, qPCR advice and RIP advice, respectively. We thank the Broadie Laboratory for extensive input.

2.7 Author contributions

Conceptualization: C.S., K.B.; Methodology: C.S., E.M.R.; Validation: C.S., K.B.; Formal analysis: C.S.; Investigation: C.S., S.N.L., E.M.R.; Resources: K.B.; Data curation: C.S.; Writing - original draft: C.S.; Writing - review & editing: C.S., S.N.L., K.B.; Visualization: C.S.; Supervision: K.B.; Project administration: K.B.; Funding acquisition: K.B.

2.8 Funding

This work was supported by funding from the National Institute of Mental Health (R01 grant MH084989 to K.B.). Deposited in PMC for release after 12 months.

CHAPTER III

Fragile X Mental Retardation Protein Coordinates Neuron-to-Glia Communication for Clearance of Developmentally Transient Brain Neurons

Chunzhu Song[1] and Kendal Broadie[1,2,3,4*]

Department of Biological Sciences[1], Department of Cell and Developmental Biology[2], Kennedy Center for Research on Human Development[3], and Vanderbilt Brain Institute[4], Vanderbilt University and Medical Center, Nashville, Tennessee, 37235, USA

This research is published in the *Proceedings of the National Academy of Sciences*.

PMID: 36920921

3.1 Abstract

In the developmental remodeling of brain circuits, neurons are removed by glial phagocytosis to optimize adult behavior. Fragile X mental retardation protein (FMRP) regulates neuron-to-glia signaling to drive glial phagocytosis for targeted neuron pruning. We find that FMRP acts in a mothers against decapentaplegic (Mad)-insulin receptor (InR)-protein kinase B (Akt) pathway to regulate pretaporter (Prtp) and amyloid precursor protein-like (APPL) signals directing this glial clearance. Neuronal RNAi of *Drosophila fragile X mental retardation 1* (*dfmr1*) elevates *mad* transcript levels and increases pMad signaling. Neuronal *dfmr1* and *mad* RNAi both elevate phospho–protein kinase B (pAkt) and delay neuron removal but cause opposite effects on InR expression. Genetically correcting pAkt levels in the *mad* RNAi background restores normal remodeling. Consistently, neuronal *dfmr1* and *mad* RNAi both decrease Prtp levels, whereas neuronal *InR* and *akt* RNAi increase Prtp levels, indicating FMRP works with pMad and insulin signaling to tightly regulate Prtp signaling and thus control glial phagocytosis for correct circuit remodeling. Neuronal *dfmr1* and *mad* and *akt* RNAi all decrease APPL levels, with the pathway signaling higher glial endolysosome activity for phagocytosis. These findings reveal a FMRP-dependent control pathway for neuron-to-glia communication in neuronal pruning, identifying potential molecular mechanisms for devising fragile X syndrome treatments.

Keywords: glia, phagocytosis, insulin, PDF-Tri clock neurons, *Drosophila*

3.2 Significance

Brain circuits are remodeled by the removal of neurons via glial engulfment and phagocytosis. The mechanism requires neuron-to-glia signaling to identify the targeted neuron, recruit glia, and trigger phagocytosis. This normal optimization process goes awry in neurological disease states such as fragile X syndrome (FXS), a leading heritable cause of intellectual disability and autism spectrum disorders. Epigenetic silencing of the Mrna-binding translational regulator fragile X mental retardation protein (FMRP) elevates mothers against decapentaplegic (Mad) transcript levels to increase 77hosphor-Mad (pMad) signaling and prevent brain circuit remodeling. In neurons, this FMRP-dependent regulatory network interacts with insulin receptor (InR) 77hosphor–protein kinase B (pAkt) control of two neuron-to-glia signals driving phagocytosis. This mechanism is critical for normal and diseased brain circuit remodeling.

3.3 Introduction

Neuron-to-glia communication has critical roles in controlling brain circuit remodeling (Boulanger and Dura, 2022; del Puerto et al., 2013; Raiders et al., 2021). Neuronal signaling induces glial phagocytosis from synapses to whole neurons, crucial in normal brains and in neurodevelopmental disorder conditions (Lee and Chung, 2019; Lieberman et al., 2019; Neniskyte and Gross, 2017; Raiders et al., 2021). Disruption of neuron-to-glia communication causes aberrant neuronal pruning, resulting in defects ranging from defective synaptic transmission (Marinelli et al., 2019; Stogsdill and Eroglu, 2017) to impaired circuit wiring (Fields et al., 2015) to transient neuroinflammation (Bernaus et al., 2020; Juliani et al., 2021). A key case is fragile X syndrome (FXS), a leading intellectual disability and autism spectrum disorder (Hagerman et al., 2017; Richter and Zhao, 2021), typically caused by the epigenetic loss of fragile X mental

retardation protein (FMRP) owing to expanded CGG repeats in the 5′-untranslated region of *fragile X mental retardation 1* (*fmr1*) (Richter and Zhao, 2021; Verkerk et al., 1991). In neurons, FMRP binds to specific transcripts to regulate protein translation during brain circuit development and later plasticity, including synaptic connectivity remodeling (Gatto and Broadie, 2011) and intercellular signaling mechanisms (Donnard et al., 2022; Friedman et al., 2013). In the *Drosophila* FXS disease model, FMRP loss blocks removal of the developmentally transient pigment-dispersing factor (PDF)-Tri peptidergic neurons from the juvenile brain (Gatto and Broadie, 2011). Cell-specific RNAi studies show that FMRP is required only in neurons, not glia, to transcellularly activate glial phagocytosis driving PDF-Tri neuron clearance (Vita et al., 2021). Thus, FMRP-dependent neuron-to-glia communication drives targeted neuron pruning, but the molecular mechanisms remain largely unknown.

FMRP regulates bone morphogenic protein (BMP) and insulin-like peptide (ILP) signaling (Song and Broadie, 2022). Activated *Drosophila* BMP receptors phosphorylate mothers against decapentaplegic (pMad) to control gene transcription, including the insulin receptor (InR) (Deignan et al., 2016; Gallagher and LeRoith, 2013). InRs phosphorylate protein kinase B (pAkt) (Ascano et al., 2012; Wong et al., 2013) to suppress dendrite pruning (Wong et al., 2013). Importantly, mouse FMRP binds *smad* messenger ribonucleic acid (mRNA) (*Drosophila mad* homologue) (Song et al., 2022), and *Drosophila* FMRP regulates pMad signaling levels in neurons (Song et al., 2022). Moreover, FMRP loss elevates InR-dependent signaling (Bu and Zhang, 2017). In neuron-to-glia communication, pretaporter (Prtp) and amyloid precursor protein like (APPL) from neurons both activate glial phagocytosis (Kessissoglou et al., 2020; Kuraishi et al., 2009). *Drosophila* Prtp traffics to the neuron surface to bind the glial phagocytotic receptor draper (Drpr) (Kuraishi et al., 2009; Nakano et al., 2019). Loss of neuronal FMRP decreases glial Drpr

expression (Vita et al., 2021), consistent with FMRP-dependent Prtp signaling. *Drosophila* APPL has a cleavable N terminus, and APPL release from neurons activates glial phagocytosis (Kessissoglou et al., 2020). Glia take up secreted APPL to maintain Drpr expression and up-regulate Rab GTPases, activating the glial endolysosomal network for the neuron clearance mechanism (Kessissoglou et al., 2020). Taken together, these studies suggest that neuronal FMRP interacts with neuronal InR, pMad, and pAkt signaling cascades to tightly regulate Prtp and APPL neuron-to-glia communication controlling the glial phagocytosis of target neurons during circuit remodeling in the juvenile brain.

Here, we use *Drosophila* brain PDF-Tri neuron removal via glial phagocytosis to study the neuron-to-glia communication remodeling mechanism, assaying both the early pruning steps at 1 day post-eclosion (dpe) and end-stage clearance (5 dpe) (Vita et al., 2021). We discover that neuronal FMRP binds *mad* mRNA to restrict pMad signaling in neurons. Surprisingly, however, we find that both neuronal *Drosophila fragile X mental retardation 1* (*dfmr1*) and *mad* RNAi similarly block PDF-Tri neuron removal, indicating a more complex regulatory mechanism. Consistently, we find pMad is a positive transcription factor for InRs driving downstream pAkt signaling but that pMad also indirectly inhibits pAkt, inducing the phenocopy between neuronal *dfmr1* and *mad* RNAi conditions. We find both neuronal *dfmr1* and *mad* RNAi similarly decrease Prtp neuron-to-glia signaling, resulting in reduced glial phagocytic activity and a block of PDF-Tri neuron clearance, whereas loss of neuronal InR and pAkt has that opposite phenotype of elevating Prtp to accelerate neuronal removal. We also discover that the FMRP-pMad-InR-pAkt pathway positively regulates neuronal APPL signaling to induce glial Rab7-driven endolysomal activation for PDF-Tri neuron clearance. Taken together, we conclude that neuronal FMRP-pMad and InR-pAkt cascades coordinate an integrated regulatory decision network governing neuron-

to-glia communication via neuronal Prtp and APPL signaling ligands that drive glial phagocytosis for targeted neuron pruning from brain circuits.

3.4 Results

3.4.1 Neuronal FMRP regulates pMad signaling to mediate PDF-Tri neuron clearance.

Previous genetic studies have shown that PDF-Tri neuron removal over the first 5 d in the early juvenile brain requires phagocytosis clearance by two cooperating glial subclasses (Friedman et al., 2013; Song and Broadie, 2022). To begin to dissect this mechanism further, we imaged interactions between glia and neurons early and late in this clearance process at 1 day posteclosion (dpe) and 5 dpe. To image neuron–glia interactions, we first used projected confocal microscopy to visualize glial localization relative to PDF-Tri neurons at 1 dpe during the early stages of the phagocytic removal (Figure 3.1A). In 2D projections, the glia-specific reversed polarity (Repo) nuclear marker shows glial cells closely surrounding the PDF-Tri neurons, with multiple glia in direct contact along the entire length of the neuronal processes (Figure 3.1 B, Top). In magnified three-dimensional (3D) reconstructed views, multiple glia (arrows) contact the PDF-Tri neuron, converging on the remodeling neurons from multiple directions (Figure 3.1 B Bottom, and Movie S1 that published in https://doi.org/10.1073/pnas.2216887120). To label the glial membrane, we expressed UAS-mCD8::GFP with repo-Gal4 to show the PDF-Tri neuronal cell body covered by glial projections (Movie S2 that published in https://doi.org/10.1073/pnas.2216887120), further demonstrating close interaction between glia and PDF-Tri neurons. Previous studies have shown neuronal FMRP signals glial phagocytosis for PDF-Tri neuron removal (Vita et al., 2021). To test this mechanism over the time course of clearance, we assayed the PDF-Tri neuron area at 1 dpe (early in the removal process) and 5 dpe (at the end of the removal process) in neuronal driver

controls (elav-Gal4/+) and with *dfmr1* RNAi (Figure 3.1C). At 1 dpe, controls (elav/+) already show dramatically reduced PDF-Tri neuron area compared to *dfmr1* RNAi (elav>*dfmr1* RNAi) animals (Figure 3.1D). Two-way ANOVA indicates that neuronal FMRP loss causes retention of significantly more PDF-Tri neuron area at 1 dpe. By the end of the removal process (5 dpe), controls show near-complete PDF-Tri neuron loss, whereas *dfmr1* RNAi results in neuron maintenance (Figure 3.1C). The control PDF-Tri neuron area is enormously reduced compared to neuron retention with *dfmr1* RNAi, a highly significant difference by two-way ANOVA (Figure 3.1D). To specifically test FMRP in PDF-Tri neurons, we assayed PDF driver controls (PDF-Gal4/+) alone and with targeted *dfmr1* RNAi (Figure 3.2A). FMRP loss in PDF neurons significantly lowers PDF-Tri neuron clearance at 1 dpe (Figure 3.2B). Taken together, these findings indicate that neuronal FMRP plays critical roles in driving normal PDF-Tri neuron clearance in the early juvenile brain.

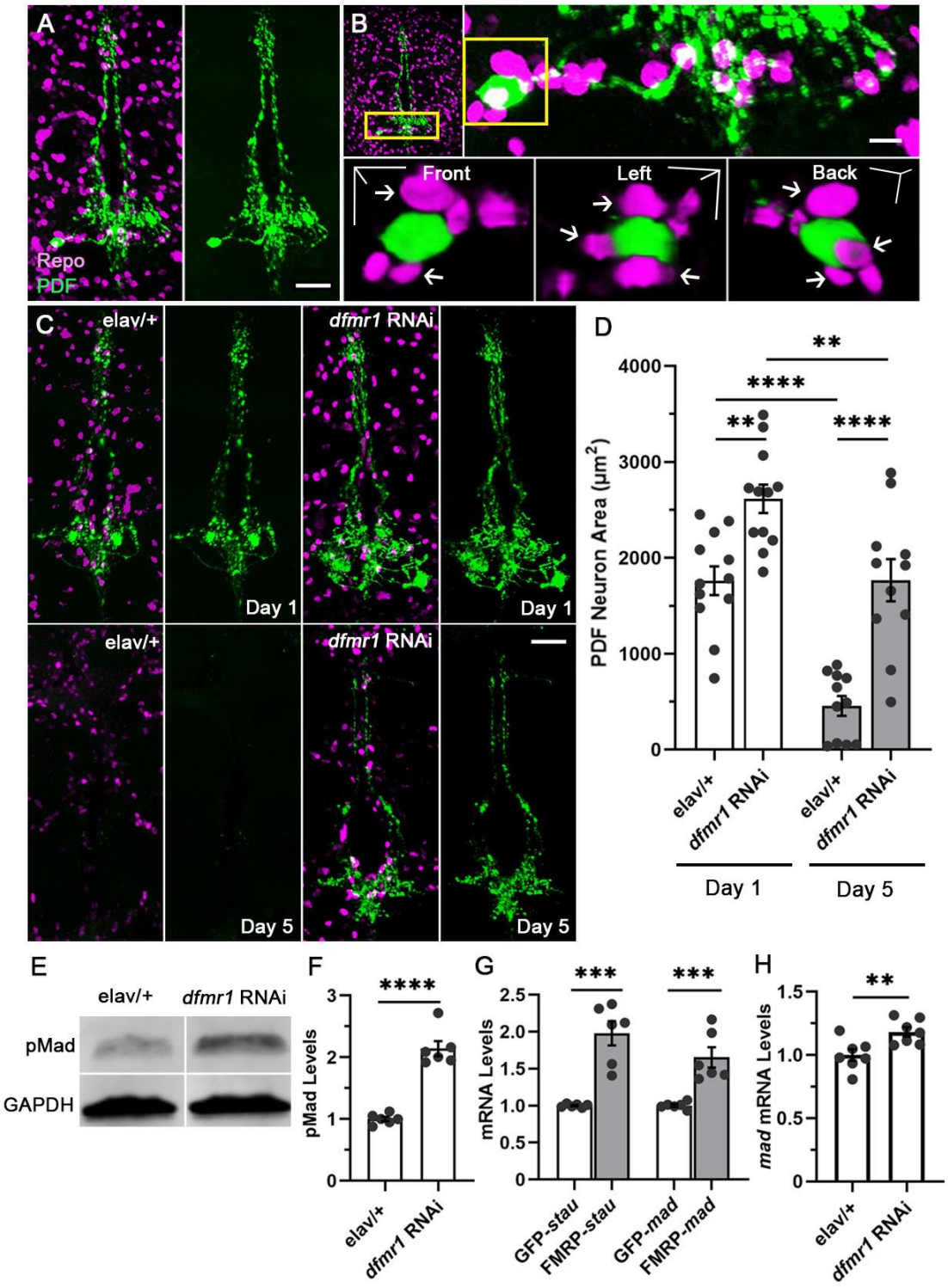
A
Repo
PDF
B
Front
Left
Back
C
elav/+
dfmr1 RNAi
Day 1
Day 5
D
PDF Neuron Area (µm²)
4000
3000
2000
1000
0
**
****
elav/+
dfmr1 RNAi
Day 1
Day 5
E
elav/+
dfmr1 RNAi
pMad
GAPDH
F
pMad Levels
****
G
mRNA Levels
***
GFP-stau
FMRP-stau
GFP-mad
FMRP-mad
H
mad mRNA Levels
**

Figure 3.1 Glial phagocytic removal of PDF-Tri neurons requires FMRP regulation of pMad.

A, PDF-Tri neuron (anti-PDF, green) and glial cells (anti-Repo, magenta) in the central brain at the beginning of the glial phagocytic removal (0 dpe). Scale bar: 20μm; B, Progressively higher magnified views of PDF-Tri neuron and glia interaction. Scale bar: magnified 2D (right top), 5μm; magnified 3D (right bottom), 5μm on X, Y and Z axes. C, Double labeling of the neuronal driver control (*elav*/+, left) and with *dfmr1* RNAi (right) at day 1 (top) and day 5 (bottom) post-eclosion. Scale bar, 20μm. D, Two-way ANOVA analysis of PDF-Tri neuron area quantification at both time points (data shown as mean ± sem. 1 dpe: control 1761.0 ± 149.80 vs. *dfmr1* RNAi 2615.0 ± 148.30, p=0.0047; 5 dpe: control 455.9 ± 104.10 vs. *dfmr1* RNAi 1767.0 ± 219.90, p<0.0001). There is no significant difference in glia density between *elav*/+ and *elav*>*dfmr1* RNAi (p=0.121). E, Representative anti-pMad Western blot of neuronal *elav*/+ control and with *dfmr1* RNAi. GAPDH is the loading control. F, Normalized pMad levels from the Western blots (control 1.00 ± 0.034 vs. *dfmr1* RNAi 2.14 ± 0.121; student's t-test, p<0.0001). G, RNA immunoprecipitation and normalized quantification of FMRP-bound transcripts. GFP-trap beads pull down neuronal YFP::FMRP together with negative control GFP (GFP-*stau* 1.00 ± 0.009 vs. FMRP-*stau* 1.979 ± 0.163, student's t-test, p=0.0001; GFP-*mad* 1.00 ± 0.019 vs. FMRP-*mad* 1.653 ± 0.137, student's t-test, p=0.0008). H, Normalized *mad* mRNA levels in *elav*/+ control and with *dfmr1* RNAi (control 1.00 ± 0.045 vs. *dfmr1* RNAi 1.182 ± 0.037, student's t-test, p=0.009). Dot plots show all data points. Statistical significance indicated as **p<0.01, ***p<0.001 and ****p<0.0001.

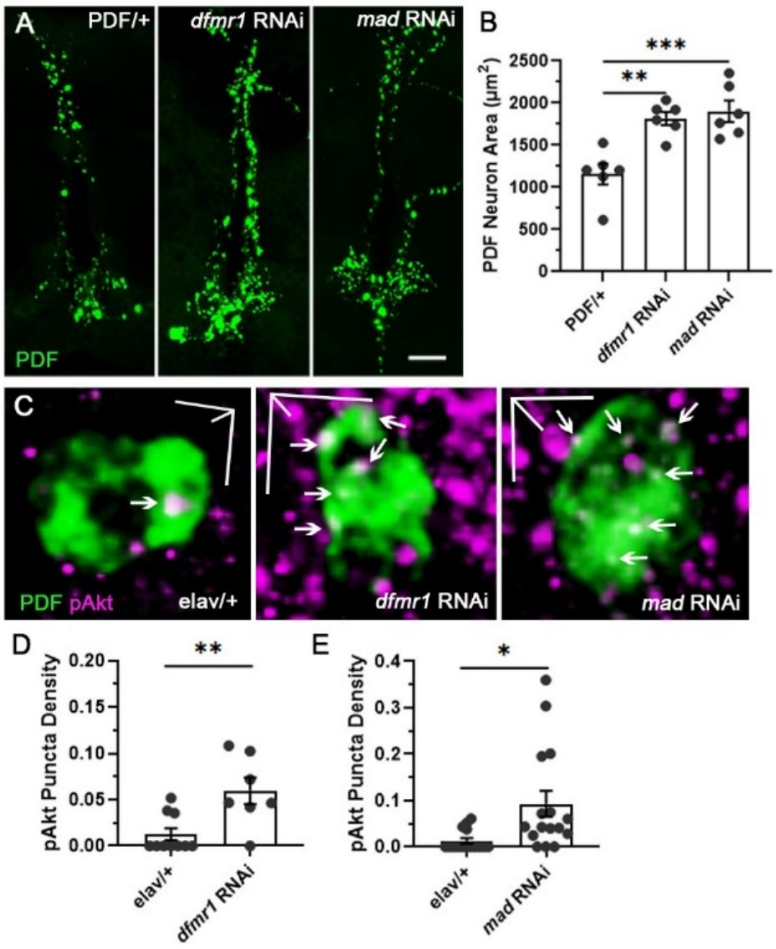

Figure 3.2 FMRP and Mad regulate pAkt signaling driving PDF-Tri neuron clearance by glia

A, PDF neurons (anti-PDF, green) in the PDF driver control (PDF-Gal4/+, left) and with *dfmr1* (middle) and *mad* RNAi (right) at 1 dpe. Scale bar: 20 μm. B, Quantification of PDF-Tri neuron area with one-way ANOVA (PDF-Gal4/+ 1156.0 ± 122.30 vs. *dfmr1* RNAi 1816.0 ± 78.26, p=0.0015; PDF/+ vs. *mad* RNAi 1902.0 ± 126.90, p=0.0005). C, PDF-Tri neuron (anti-PDF, green) and pAkt (anti-pAkt, magenta) double labeling in driver control (elav-Gal4/+, left) and with *dfmr1* (middle) and *mad* RNAi (right) at 1 dpe. pAkt puncta within PDF-Tri neurons highlighted with white arrows. Scale bar: 2.5 μm on X, Y and Z axes. D, Quantification of the pAkt puncta density in PDF-Tri neurons in driver control (elav/+) and with *dfmr1* RNAi (elav/+ 0.0125 ± 0.00651 vs. *dfmr1* RNAi 0.0596 ± 0.0143, p=0.005, student's t-test). E, Quantification of the pAkt puncta density in PDF-Tri neurons in driver control (elav/+) and with *mad* RNAi (elav/+ 0.0129 ± 0.00585 vs. *mad* RNAi 0.09284 ± 0.02775, p=0.0106; student's t-test).

We recently discovered that *dfmr1* null neurons accumulate high levels of phosphorylated mothers against decapentaplegic (pMad), indicating FMRP limits neuronal pMad signaling (Song et al., 2022). To study this mechanism of FMRP-pMad regulation in the context of PDF-Tri neuron removal from the developing brain, we first tested pMad levels with neuronal *dfmr1* RNAi in staged brain western blot analyses (Figure 3.1E). Comparisons with the neuronal driver controls (elav/+) show that *dfmr1* RNAi results in a consistently elevated pMad level. Quantified analyses indicate that neuronal *dfmr1* RNAi causes a significantly higher pMad signaling level, greater than twofold increase over the matched control (Figure 3.1F). Since mouse RNA immunoprecipitation (RIP) sequencing has shown that FMRP binds *smad* mRNA (*Drosophila mad* homologue) (Ascano et al., 2012), we next assayed for an RNA-binding interaction. To analyze FMRP-bound transcript levels, we used GFP-trap beads to pull down a FMRP::YFP fusion compared with a GFP-negative control from brain neurons (Song et al., 2022). As FMRP has been shown to bind *staufen* (*stau*) mRNA (Song et al., 2022), we use *stau* as the immunoprecipitation positive control (Figure 3.1G). With quantitative real-time PCR (qPCR) measurements, we found a >1.5-fold immunoprecipitation enrichment for *mad* mRNA occurs with FMRP::YFP pull-down as normalized compared to the GFP-negative control (Figure 3.1G). This is comparable to the approximately twofold immunoprecipitation for the *stau* positive control. These results show FMRP binds *mad* mRNA in brain neurons, so we next tested possible FMRP-dependent effects on *mad* transcription levels (Figure 3.1H). Compared with the driver control (elav/+), reducing neuronal FMRP (elav>*dfmr1* RNAi) causes a significant increase in *mad* mRNA levels (Figure 3.1H). This suggests that neuronal FMRP destabilizes bound *mad* transcripts to reduce the amount of protein produced. Taken together, these findings indicate that FMRP binds *mad* mRNA and reduces *mad* transcript levels, thereby presumably restricting pMad intracellular signaling.

During intracellular signaling, the phosphorylation of Mad (pMad) generates an active transcription factor that translocates into the nucleus to directly regulate gene expression (Deignan et al., 2016). We therefore next wanted to determine whether knockdown of neuronal *mad* mRNA impairs pMad signaling and whether neuronal pMad signaling regulates targeted PDF-Tri neuron removal. To test the first question, we compared driver controls (elav/+) to neuronal *mad* RNAi (elav>*mad* RNAi) to find a significant reduction in pMad protein levels. To test whether neuronal pMad regulates PDF-Tri neuron clearance, we therefore reduced pMad in neurons by neuronal *mad* RNAi (Figure 3.3A). Surprisingly, this knockdown results in impaired PDF-Tri neuron clearance similar to the *dfmr1* RNAi condition (compare to Figure 3.1 C and D). Starting early in the glial clearance process (1 dpe), and particularly at the end of the removal mechanism when PDF-Tri neurons are normally absent (5 dpe), neuronal *mad* RNAi results in a striking retention of most of the neuronal architecture (Figure 3.3A). Statistical analyses indicate that neuronal *mad* RNAi causes significantly reduced PDF-Tri neuron removal compared to driver controls (elav/+) at 1 dpe and an even stronger significant maintenance at 5 dpe (Figure 3.3B). To specifically test FMRP in PDF-Tri neurons, we assayed PDF driver controls (PDF-Gal4/+) alone and with *mad* RNAi (PDF>*mad* RNAi; Figure 3.2A). Loss of pMad signaling in PDF neurons very significantly lowers PDF-Tri neuron clearance at 1 dpe (Figure 3.2B). Since this conclusion is opposite to expectations, a second FMRP-pMad interactive pathway was suspected to result in the *dfmr1* RNAi phenocopy. As both FMRP and pMad interact with insulin receptor (InR) signaling (Deignan et al., 2016; Gross and Bassell, 2012; Song and Broadie, 2022), we therefore next focused on testing InR dysregulation in neuronal *dfmr1* and *mad* RNAi conditions. With qPCR assays, InR expression is oppositely modulated by neuronal *dfmr1* and *mad* RNAi (Figure 3.3C

and D), which fits the inhibitory regulation from FMRP to pMad. However, this fails to explain the phenocopy result. We therefore next explored interactions downstream of InR signaling.

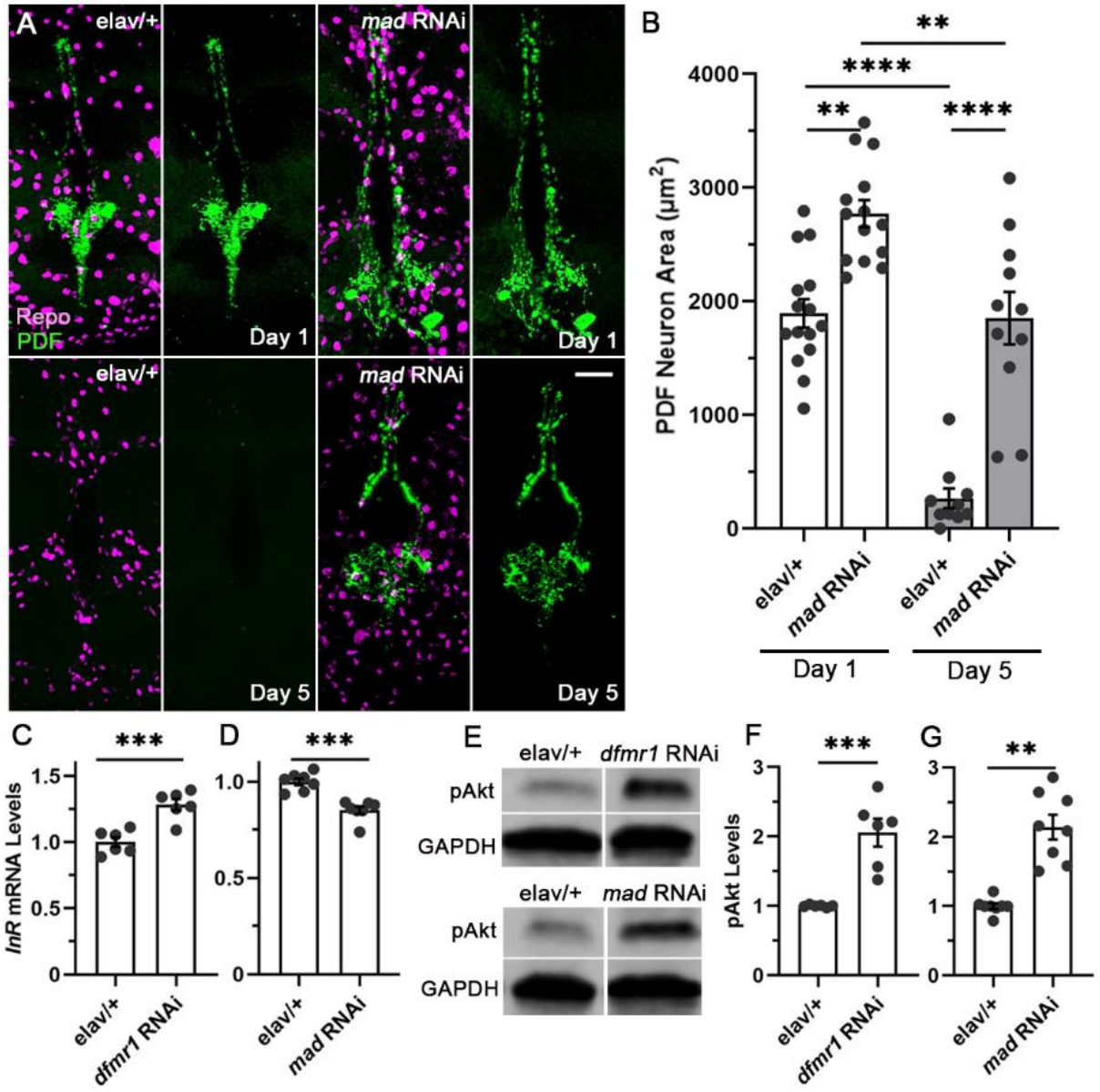

Figure 3.3 PDF-Tri neuron clearance through FMRP-pMad signaling upregulates pAkt level.

A, PDF-Tri neuron (green) and glia (magenta) labeling in the neuronal driver control only (*elav*/+, left) and with neuronally-driven *mad* RNAi (right) at day 1 (top) and day 5 (bottom) post-eclosion. PDF-Tri neuron alone is shown to the right for each image. Scale bar, 20μm. B, PDF-Tri neuron area quantification for both genotypes at both time points (1 dpe: control 1894.0 ± 125.10 vs. *mad* RNAi 2771.0 ± 118.60, two-way ANOVA, p=0.0020; 5 dpe: control 265.20 ± 86.97 vs. *mad* RNAi 1852.0 ± 230.80, two-way ANOVA, p<0.0001). There is no significant difference in glia density (anti-Repo) between *elav*/+ and *elav>mad* RNAi (p=0.642). C-D, Normalized *InR* mRNA levels with the neuronal *elav*/+ driver control compared to *dfmr1* RNAi (C, *elav*/+ 1.00 ± 0.036 vs. *dfmr1* RNAi 1.283 ± 0.0441, student's t-test, p=0.0006) and *mad* RNAi (D, *elav*/+ 1.00 ± 0.018 vs. *mad* RNAi 0.851 ± 0.020, student's t-test, p=0.0001). E, Representative anti-pAkt Western blots with the neuronal *elav*/+ driver control compared to both neuronal *dfmr1* RNAi (top) and neuronal *mad* RNAi (bottom) conditions. GAPDH is the loading control. F-G, Western blot quantification for both conditions compared to *elav*/+ driver control (F, *elav*/+ 1.00 ± 0.007 vs. *dfmr1* RNAi 2.06 ± 0.203, student's t-test, p=0.0004; G, *elav*/+ 1.00 ± 0.041 vs. *mad* RNAi 2.14 ± 0.178, student's t-test, p<0.0001). Dot plots show all data points. Statistical significance indicated as **p<0.01, ***p<0.001 and ****p<0.0001.

Activated InR phosphorylates protein kinase B (pAkt) (Armstrong and Drummond-Barbosa, 2018; Gil-Ranedo et al., 2019), and FMRP loss elevates pAkt in neurons (Gross and Bassell, 2012). To test whether pAkt is the dysregulated player in the FMRP-pMad signaling, we first used western blots to measure pAkt levels in driver controls (elav/+) compared with *dfmr1* and *mad* RNAi (Figure 3.3E). Quantification shows pAkt up-regulated by both neuronal *dfmr1* and *mad* RNAi, with a significantly approximately twofold enrichment in both cases (Figure 3.3F and G). To test pAkt in PDF-Tri neurons, we colabeled with anti-PDF and anti-pAkt. Both *dfmr1* and *mad* RNAi increase pAkt in PDF-Tri neurons at 1 dpe (Figure 3.2 C–E). These findings suggest pAkt upregulation generates the neuronal *dfmr1* and *mad* RNAi phenocopy blocking PDF-Tri neuron removal. Consistently, neuronal pAkt RNAi dramatically increases the rate of PDF-Tri neuron clearance (Figure 3.4A). Due to the complete neuron loss at 5 dpe in controls, we only measured the PDF-Tri neuron area at 1 dpe to show significantly accelerated neuronal removal early in the process (Figure 3.4B). As decreasing neuronal pMad results in aberrant pAkt elevation, we hypothesized that correcting neuronal pAkt levels in the reduced pMad background should restore normal clearance. With *mad* and *akt* double RNAi, PDF-Tri neuron clearance is restored to control levels (Figure 3.4 C and D), supporting this hypothesis. To test possible Gal4 dilution with double UAS constructs, we also expressed *akt* RNAi with control *gfp* RNAi. This double RNAi still significantly promotes neuron loss (Figure 3.5 A and B). We also overexpressed *akt* (elav>*akt* OE) to find slower PDF-Tri neuron loss at 1 dpe (Figure 3.5 C and D). PDF-Tri neuron clearance defects from InR knockdown (Figure 3.4 E and F) and constitutive activation (InR CA; Figure 3.5 C and D) are also consistent with InR acting as a positive regulator to pAkt (31). Importantly, *InR* and *akt* RNAi cause no significant effect on PDF-Tri neurons in pre-eclosion pharate adults (Figure 3.6 A–D), supporting a specific role for InR-pAkt signaling in PDF-Tri

neuron clearance. We finally tested InR-pAkt signaling within PDF-Tri neurons. Consistent with pan-neuronal RNAi, both PDF-Gal4-driven *InR* and *akt* RNAi promote PDF-Tri neuron clearance, while targeted *akt* and *mad* double RNAi correct the *akt* phenotype (Figure 3.7 A and B). These results show FMRP-pMad cross talk to InR-pAkt signaling regulates PDF-Tri neuron removal. However, this intracellular neuronal network must act to control intercellular signaling to drive glial phagocytosis, so we next turned to testing the neuron-to-glia communication mechanism.

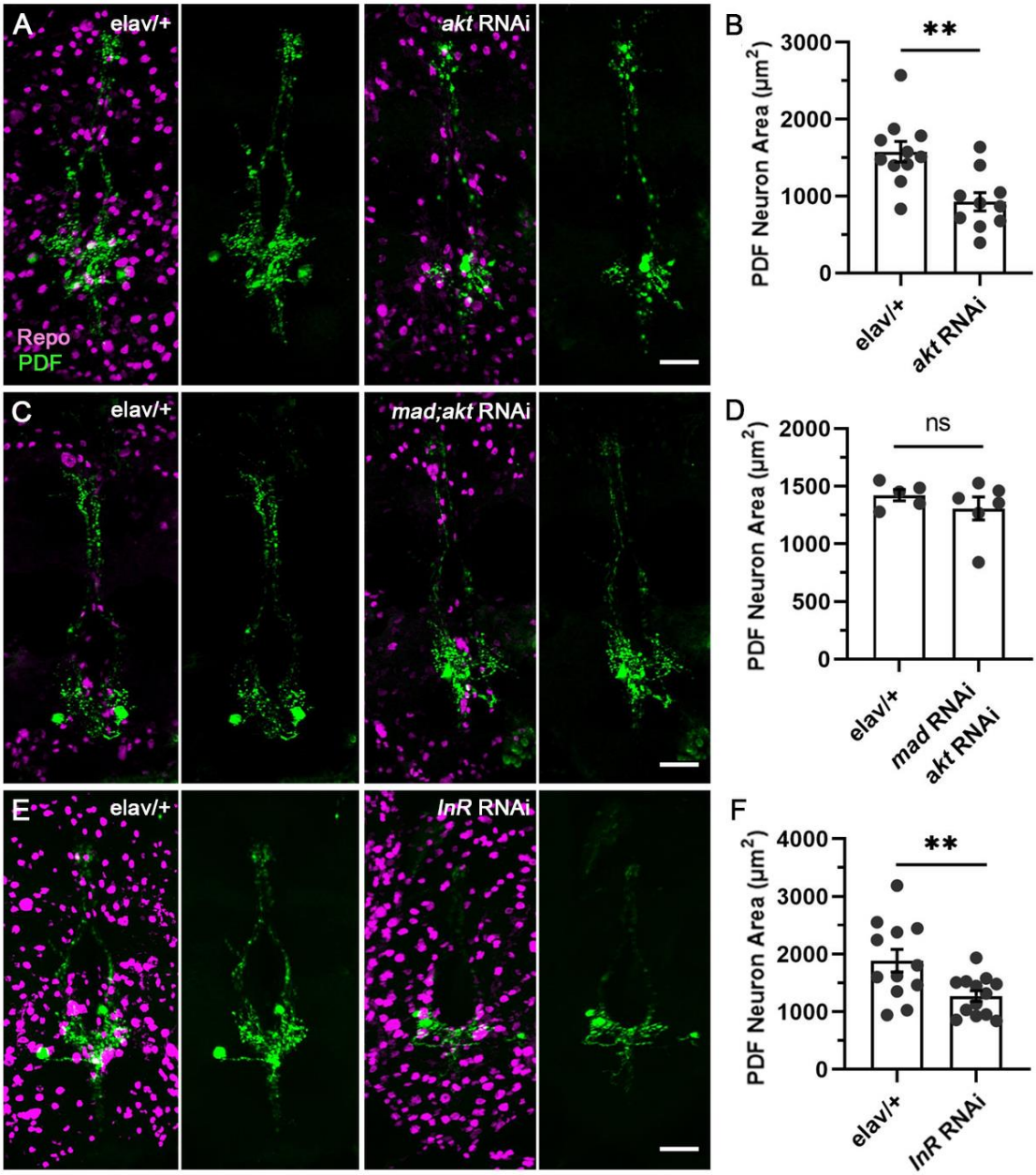
A
elav/+
akt RNAi
Repo
PDF
B
**
PDF Neuron Area (μm²)
3000
2000
1000
0
elav/+
akt RNAi
C
elav/+
mad;akt RNAi
D
ns
PDF Neuron Area (μm²)
2000
1500
1000
500
0
elav/+
mad RNAi
akt RNAi
E
elav/+
lnR RNAi
F
**
PDF Neuron Area (μm²)
4000
3000
2000
1000
0
elav/+
lnR RNAi

Figure 3.4 Neuronal knockdown of both InR and Akt accelerates PDF-Tri neuron clearance.

A, PDF-Tri neuron (anti-PDF, green) and glia (anti-Repo, magenta) double labeling in the neuronal driver control (*elav*/+, left) and *akt* RNAi (right) at day 1 post-eclosion during the early stages of the glial phagocytic removal process. Scale bar: 20μm. B, Quantification of PDF-Tri neuron area in the two conditions (*elav*/+ 1578.0 ± 132.0 vs. *akt* RNAi 927.10 ± 117.70, students' t-test, p=0.0017). There is no significant difference in glia density between *elav*/+ and *elav>akt* RNAi at 1 dpe (p=0.778). C, The same co-labeling with neuronal *mad* and *akt* RNAi driven in double knockdown combination at day 1. Scale bar: 20μm. D, Quantification of PDF-Tri neuron area in the two conditions (*elav*/+ 1424.0 ± 48.69 vs. *mad*; *akt* double RNAi 1308.0 ± 100.10, students' t-test, p=0.357). E, PDF-Tri neuron and glia double labeling in the neuronal driver control (*elav*/+, left) and with *InR* RNAi (right) at day 1. F, Quantification of PDF-Tri neuron area in the two conditions (*elav*/+ 1886.0 ± 196.10 vs. *InR* RNAi 1273.0 ± 94.27, students' t-test, p=0.008). There is no significant difference in glia density between *elav*/+ and *elav>InR* RNAi at 1 dpe (p=0.464). Dot plots show all data points. Statistical significance indicated as **p<0.01 and not significant (ns; p>0.05). Scale bar in all images: 20 μm.

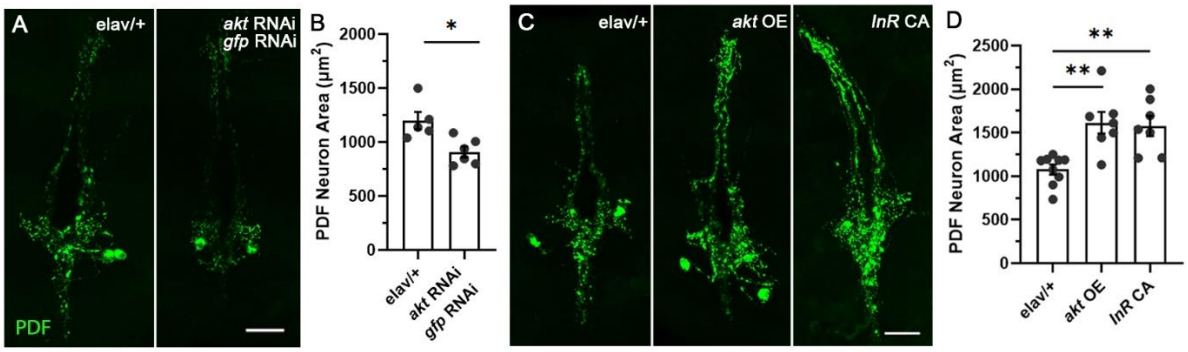

Figure 3.5 Neuronal insulin receptor and pAkt signaling inhibit PDF-Tri neuron clearance.

A, PDF-Tri neuron (anti-PDF, green) in neuronal driver control (elav-Gal4/+) and with combined *akt* + gfp RNAi at 1 dpe. Scale bar: 20 µm. B, Quantification of the PDF-Tri neuron area with student's t-test (elav-Gal4/+ control 1198.0 ± 80.25 vs. *akt* + gfp RNAi 909.50 ± 49.63, p=0.0112). C, PDF-Tri neuron in driver control (elav-Gal4/+, left) and with *akt* overexpression (OE, middle) and InR constitutive activation (CA, right) at 1 dpe. Scale bar: 20 µm. D. Quantification of the PDF-Tri neuron area with one-way ANOVA (elav-Gal4/+ 1078.0 ± 57.09 vs. *akt* OE 1614.0 ± 124.2, p=0.0015; elav-Gal4/+ vs. InR CA 1578.0 ± 116.0, p=0.003).

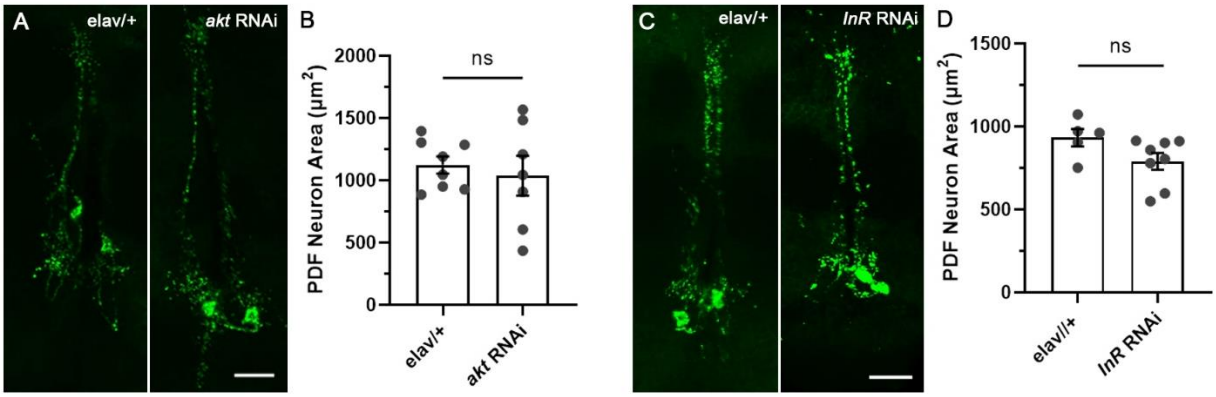

Figure 3.6 Neuronal pAkt and InR RNAi have no effect on pupal PDF-Tri neuron formation.

A, Pupal PDF-Tri neuron labeling (anti-PDF, green) in neuronal driver control (*elav*-Gal4/+) and with *akt* RNAi in pre-eclosion pharate adults. Scale bar: 20 µm. B, Quantification of the PDF-Tri neuron area with student's t-test (*elav*/+ 1123.0 ± 69.23 vs. *akt* RNAi 1037.0 ± 159.80, p=0.61). C, Pupal PDF-Tri neuron labeling in in driver control (*elav*/+) and with *InR* RNAi in pre-eclosion pharate adults. Scale bar: 20 µm. D, Quantification of PDF-Tri neuron area with student's t-test (*elav*/+ 933.0 ± 52.66 vs. *InR* RNAi 789.60 ± 50.58, p= 0.088).

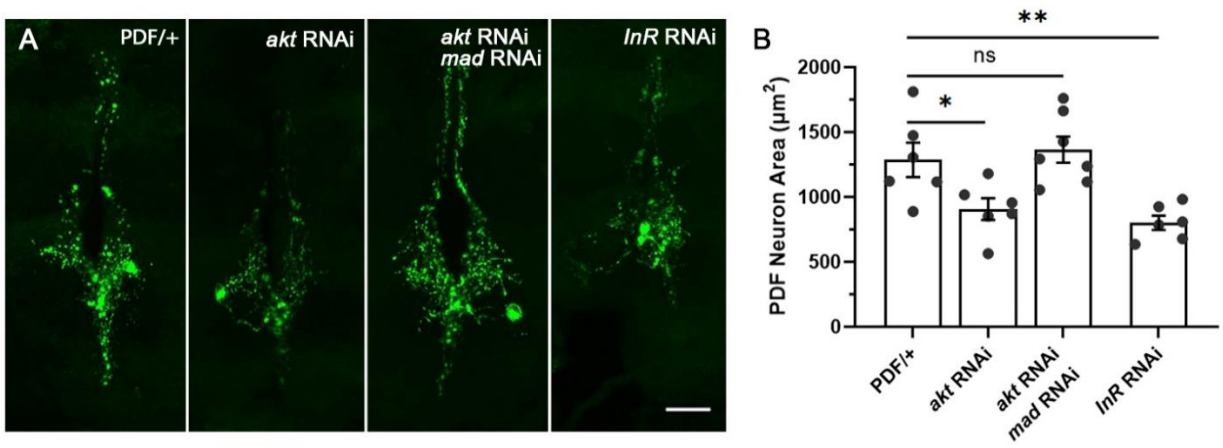

Figure 3.7 InR and pAkt signaling in PDF-Tri neurons mediates PDF-Tri neuron removal.

A, PDF-Tri neurons (anti-PDF, green) in the PDF neuronal driver control (*PDF*-Gal4/+) and with *InR* RNAi, *akt* RNAi, and double *mad* + *akt* RNAi at 1 dpe. Scale bar: 20 μm. B, Quantification of the PDF-tri neuron area with one-way ANOVA (*PDF*/+ control 1286.0 ± 132.40 vs. *akt* RNAi 803.10 ± 83.78, p=0.0361; *PDF*/+ vs. *akt* + *mad* RNAi 1365.0 ± 101.20, p=0.88; *PDF*/+ vs. *InR* RNAi 803.1 ± 55.15, p=0.007).

3.4.2 Neuronal FMRP-pMad-InR network regulates Pretaporter signaling for glial phagocytosis.

Neuronal pretaporter (Prtp) binds the glial draper engulfment receptor to drive the glial phagocytosis of neurons (Kuraishi et al., 2009). Neurons traffic Prtp from the endoplasmic reticulum (ER) to the plasma membrane cell surface to activate targeted glial phagocytosis (Kuraishi et al., 2009). We therefore next tested neuronal Prtp knockdown (elav>*prtp* RNAi) compared to the driver control (elav/+) to test whether PDF-Tri neuron removal involves Prtp signaling (Figure 3.8A). In assaying the full time course of the glial phagocytosis mechanism, we find strongly reduced PDF-Tri neuron clearance at both 1 dpe (early) and 5 dpe (late) with neuronal Prtp knockdown (Figure 3.8A). As usual, the aberrant retention is more obvious at 5 dpe, although the PDF-Tri neuron maintenance here is reduced relative to both the *dfmr1* and *mad* RNAi conditions (compare to Figs. 1 and 2), suggesting the combinatorial action of parallel neuron-to-glia signals (see below). Two-way ANOVAs show the PDF-Tri neuron area with neuronal *prtp* RNAi is significantly greater early in the glial removal process (1 dpe) and also at the end of clearance (5 dpe) when neurons are normally eliminated in the elav/+ driver controls (Figure 3.8B). These results suggest neuronal Prtp is involved in PDF-Tri neuron clearance by inducing glial phagocytosis. We therefore next tested whether the above neuronal FMRP-pMad and InR-pAkt network modulates Prtp signaling. With qPCR assays, both neuronal *dfmr1* and *mad* RNAi reduce prtp levels (Figure 3.8 C and D), consistent with the inhibition of PDF-Tri neuron clearance. Moreover, both neuronal *InR* and *akt* RNAi elevate prtp levels (Figure 3.8 E and F), consistent with accelerated PDF-Tri neuron clearance. These combined interactions provide a mechanism to explain the bidirectional change in PDF-Tri neuron removal in these two pathway conditions downstream of the linked neuronal regulation. Taken together, these findings show the neuronal

FMRP-pMad and InR-pAkt network controls Prtp signaling to regulate the glial phagocytic clearance of PDF-Tri neurons. However, another neuron-to-glia intercellular signaling mechanism seemed to be acting in parallel.

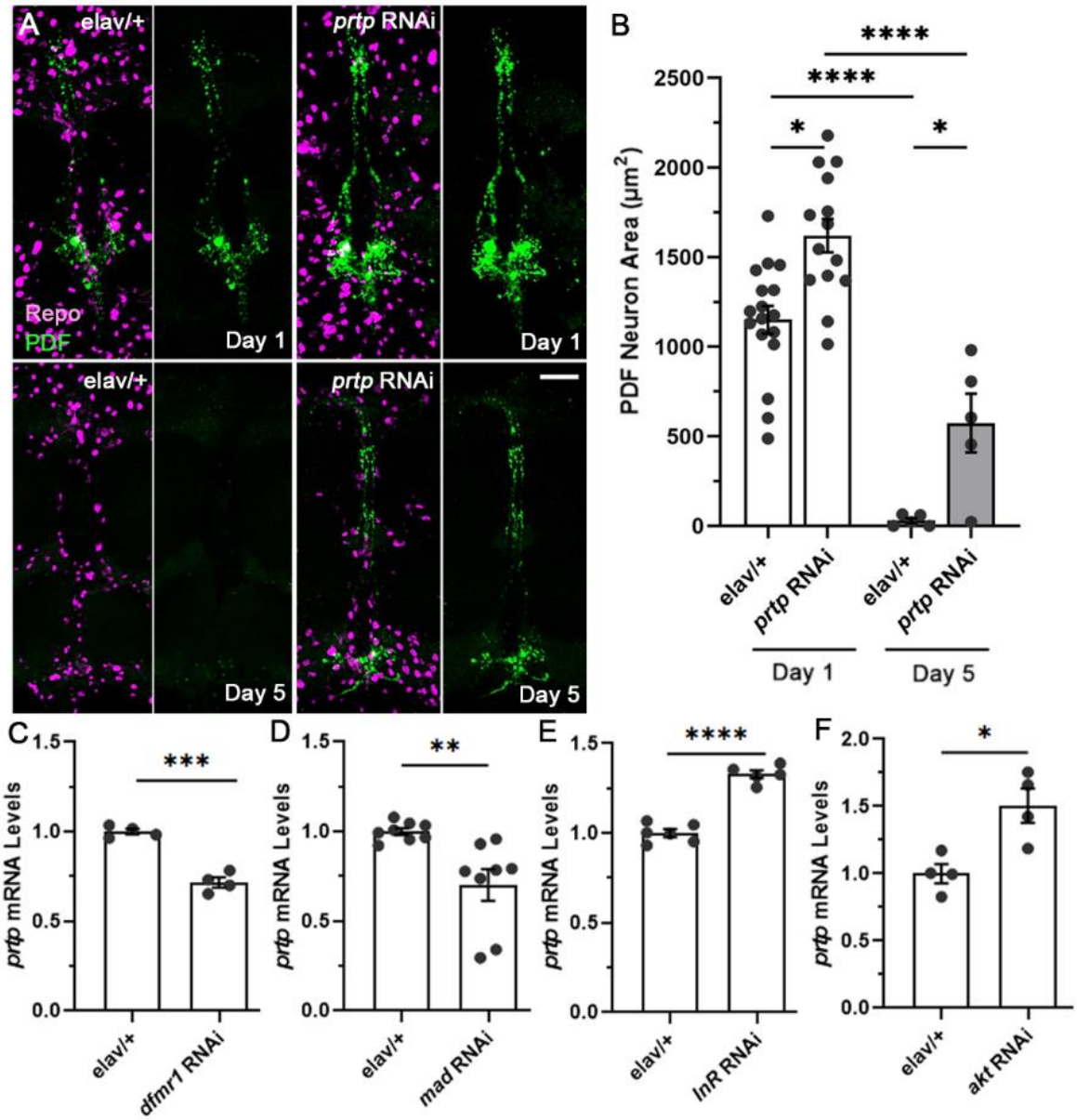

Figure 3.8 Neuron-to-glia Pretaporter signaling acts downstream of FMRP, pMad and InR.

A, PDF-Tri neuron (green) and glia (magenta) co-labeling with the neuronal driver control (*elav*/+, left) and neuronal *pretaporter* RNAi (*prtp*, right) at both day 1 (top) and day 5 (bottom). Scale bar: 20μm. B, Quantification of the PDF-Tri neuron area for both of the genotypes at both early and late time points (1 dpe: *elav*/+ 1151.0 ± 77.48 vs. *prtp* RNAi 1620.0 ± 93.28, two-way ANOVA, p=0.0148; 5 dpe: *elav*/+ 29.51 ± 14.21 vs. *prpt* RNAi 574.0 ± 164.10, two-way ANOVA, p=0.0432). There is no significant difference in glia density between *elav*/+ and *elav>prtp* RNAi (p=0.571). C, Normalized quantification of *prtp* mRNA levels in the neuronal driver control (*elav*/+, left) and with neuronal *dfmr1* RNAi (right) (*elav*/+ 1.00 ± 0.016 vs. *dfmr1* RNAi 0.717 ± 0.027, students' t-test, p=0.0001). D, Normalized quantification of *prtp* mRNA levels in the neuronal driver control (*elav*/+, left) and with neuronally-targeted *mad* RNAi (right) (*elav*/+ 1.00 ± 0.018 vs. *mad* RNAi 0.702 ± 0.089, students' t-test, p=0.0051). E, Normalized quantification of *prtp* mRNA levels in the neuronal driver control (*elav*/+, left) and with neuronal *InR* RNAi (right) (*elav*/+ 1.00 ± 0.021 vs. *InR* RNAi 1.329 ± 0.022, students' t-test, p<0.0001). F, Normalized quantification of *prtp* mRNA levels in the neuronal driver control (*elav*/+, left) and with neuronal *akt* RNAi (right) (*elav*/+ 1.00 ± 0.07045 vs. *InR* RNAi 1.507 ± 0.127, students' t-test, p=0.0130). Dot plots show all data points. Statistical significance indicated as *p<0.05, **p<0.01, ***p<0.001 and ****p<0.0001.

3.4.3 Neuronal FMRP-pMad and InR-pAkt network regulates amyloid precursor protein signaling.

In the mouse FXS model, FMRP restricts neuronal amyloid precursor protein (APP) levels (Westmark and Malter, 2007; Westmark et al., 2016). In *Drosophila*, the amyloid precursor protein-like (APPL) homologue cleaved N terminus released from brain neurons is engulfed by glia to activate their phagocytic function during brain neuron removal (Kessissoglou et al., 2020). To test whether neuronal APPL is required for PDF-Tri neuron clearance, we next compared driver controls (elav/+) with neuronal APPL knockdown (elav>*appl* RNAi) at 1 dpe (early) and 5 dpe (late) in the glial phagocytosis clearance process (Figure 3.9A). Brain imaging shows more PDF-Tri neuron retention with neuronal appl RNAi compared to driver controls at 1 dpe and 5 dpe, with the difference more obvious late in glial removal (Figure 3.9A). Quantification shows the removal of PDF-Tri neurons is significantly reduced with neuronal appl RNAi at both the 1 dpe and 5 dpe time points (Figure 3.9B). These results are consistent with recently reported APPL requirements in glia-mediated neuronal removal (Kessissoglou et al., 2020). We next tested if FMRP and APPL interact to regulate PDF-Tri neuron removal. Single *dfmr1*/+ and $appl^{d}$/+ heterozygotes have no significant impact on PDF-Tri neuron clearance compared to the genetic background control w^{1118}, whereas the *dfmr1*/+; $appl^{d}$/+ trans-heterozygote significantly increases PDF-Tri neuron retention (Figure 3.10 A and B). To investigate how neuronal FMRP-pMad and InR-pAkt signaling might regulate this APPL function, we next combined qPCR and western blots to measure APPL expression in targeted RNAi studies for neuronal *dfmr1*, *mad*, and *InR* RNAi (Figure 3.9 C–E). Quantified analyses show a similar significant reduction in appl transcript levels with both *dfmr1* and *mad* RNAi compared to the elav/+ driver controls (Figure 3.9 C and D), consistent with the PDF-Tri neuron persistence in both these conditions. Likewise, neuronal InR knockdown results

in an even more significant ~50% reduction in appl mRNA levels (Figure 3.9E). Moreover, neuronal *dfmr1, mad, InR,* and *akt* RNAi also decrease APPL protein levels (Figure 3.9F). The *dfmr1* and *mad* results are again consistent with the delayed neuronal removal, but the decreased APPL with *InR* and *akt* RNAi opposes the phenotype of accelerated PDF-Tri neuron removal. Taken together, neuronal FMRP-pMad and InR-pAkt cascades similarly regulate neuronal APPL levels. However, we still wished to test the role of neuronal signaling in glial activation for PDF-Tri neuron removal.

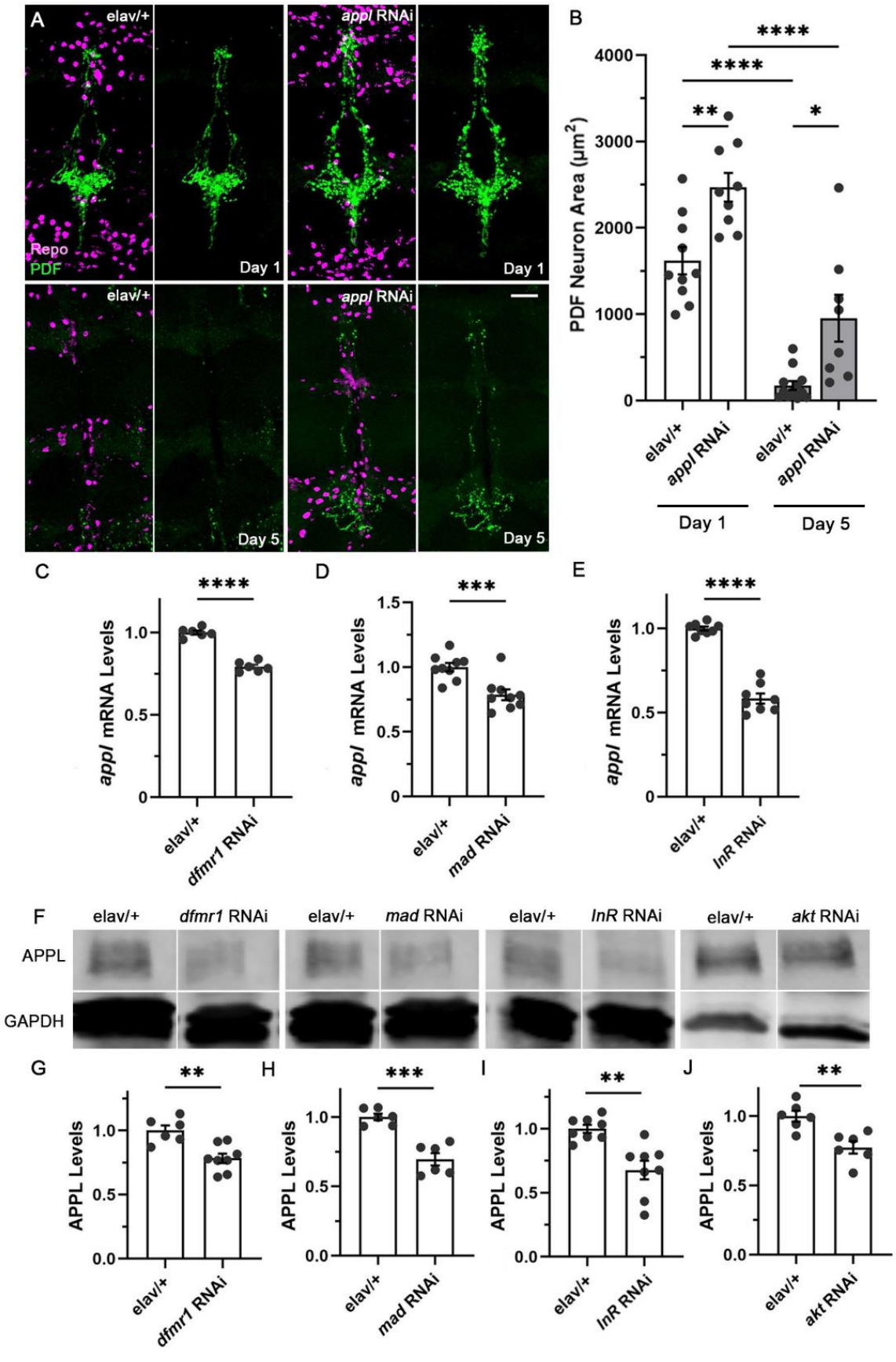
A
elav/+
appl RNAi
Repo
PDF
Day 1
Day 5
B
PDF Neuron Area (μm²)
4000
3000
2000
1000
0
****
****
**
*
elav/+
appl RNAi
elav/+
appl RNAi
Day 1
Day 5
C
appl mRNA Levels
1.0
0.5
0
****
elav/+
dfmr1 RNAi
D
appl mRNA Levels
1.5
1.0
0.5
0
***
elav/+
mad RNAi
E
appl mRNA Levels
1.0
0.5
0
****
elav/+
InR RNAi
F
elav/+
dfmr1 RNAi
elav/+
mad RNAi
elav/+
InR RNAi
elav/+
akt RNAi
APPL
GAPDH
G
APPL Levels
1.0
0.5
0.0
**
elav/+
dfmr1 RNAi
H
APPL Levels
1.0
0.5
0.0
***
elav/+
mad RNAi
I
APPL Levels
1.0
0.5
0.0
**
elav/+
InR RNAi
J
APPL Levels
1.0
0.5
0.0
**
elav/+
akt RNAi

Figure 3. 9 Neuronal APPL acts in the same pathway to facilitate PDF-Tri neuron clearance

A, PDF-Tri neuron (anti-PDF, green) and glial cell (anti-Repo, magenta) double labeling in the neuronal driver control (*elav*/+, left) and *appl* RNAi (right) at both day 1 (top) and day 5 (bottom). The PDF-Tri neuron alone (green) is shown to the right. Scale bar: 20μm. B, Quantification of PDF-Tri neuron area for both genotypes at both early and late time points (1 dpe: *elav*/+ 1620.0 ± 158.70 vs. *appl* RNAi 2469.0 ± 165.40, two-way ANOVA, p=0.0072; 5 dpe: *elav*/+ 175.0 ± 51.34 vs. *appl* RNAi 954.0 ± 272.50, two-way ANOVA, p=0.0195). There is no significant difference in glia density between *elav*/+ and *elav>appl* RNAi (p=0.746). C-E, Normalized quantification of *appl* mRNA levels in neuronal driver controls (*elav*/+, left) compared with neuronal *dfmr1* RNAi (C, *elav*/+ 1.00 ± 0.012 vs. *dfmr1* RNAi 0.79 ± 0.013, students' t-test, p<0.0001), *mad* RNAi (D, *elav*/+ 1.00 ± 0.032 vs. *mad* RNAi 0.70 ± 0.042, students' t-test, p=0.0009) and *InR* RNAi (E, *elav*/+ 1.00 ± 0.011 vs. *InR* RNAi 0.58 ± 0.030, students' t-test, p<0.0001). F, Representative anti-APPL Western blots with the neuronal *elav*/+ controls (left in each pairing) and neuronal *dfmr1* RNAi (left), *mad* RNAi (second from left), *InR* RNAi (second from right) and *akt* RNAi (right). G-J, Western blot quantification normalized to neuronal *elav*/+ controls (left in each pairing) for *dfmr1* RNAi (G, *elav*/+ 1.00 ± 0.039 vs. *dfmr1* RNAi 0.78 ± 0.037, students' t-test, p=0.0018), *mad* RNAi (H, *elav*/+ 1.00 ± 0.024 vs. *mad* RNAi 0.69 ± 0.045, students' t-test, p=0.0001), *InR* RNAi (I, *elav*/+ 1.00 ± 0.031 vs. *InR* RNAi 0.68 ± 0.073, students' t-test, p=0.0011) and *akt* RNAi (J, *elav*/+ 1.00 ± 0.040 vs. *akt* RNAi 0.77 ± 0.045, students' t-test, p=0.0037). Dot plots show all data points. Statistical significance indicated as *p<0.05, **p<0.01, ***p<0.001 and ****p<0.0001.

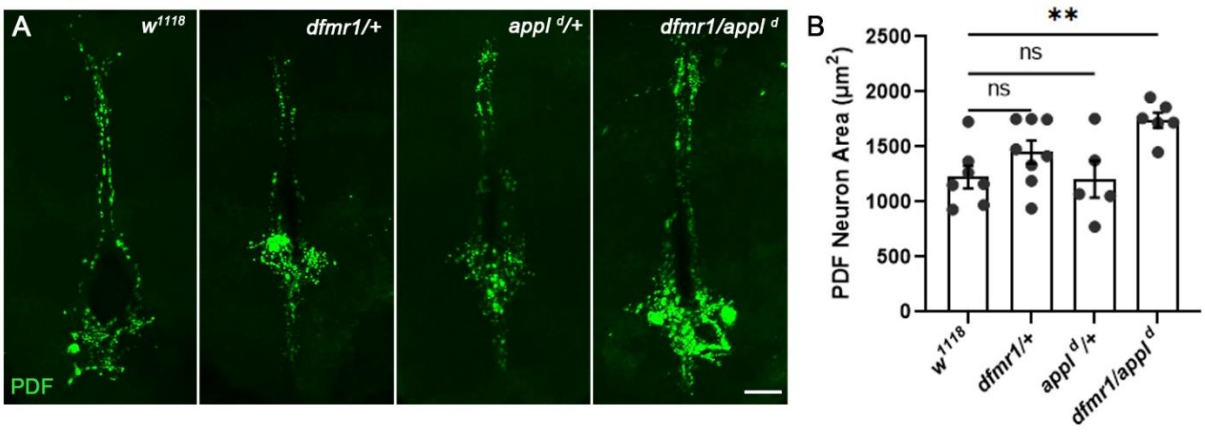

Figure 3.10 FMRP and APPL *trans*-heterozygous removal blocks PDF-Tri neuron clearance.

A, PDF-Tri neurons (anti-PDF, green) in genetic background control (w^{1118}), *dfmr1* heterozygote (*dfmr1*/+), $appl^{d}$ heterozygote ($appl^{d}$/+), and the double *trans*-heterozygote *dfmr1*/+; $appl^{d}$/+ (*dfmr1*/ $appl^{d}$) at 1 dpe. Scale bar: 20 µm. B, Quantification of PDF-Tri neuron area with one-way ANOVA (w^{1118} 1225.0 ± 101.70 vs. *dfmr1*/+ 1452.0 ± 104.80, p=0.31; w^{1118} vs. $appl^{d}$/+ 1206.0 ± 166.80, p=0.99; w^{1118} vs. *dfmr1*/$appl^{d}$ *1743.0* ± 68.97, p=0.009).

3.4.4 Neuronal FMRP-pMad and InR-pAkt network up-regulates glial endolysosomal activity.

Neuronal InR signaling inhibits glial engulfment (Folch et al., 2018; Kurant et al., 2008), with reduced endolysosomal activation in glia (Damisah et al., 2020). The APPL N terminus released from brain neurons up-regulates the glial Rab GTPases endolysosomal network for glial phagocytosis (Kessissoglou et al., 2020). Thus, the InR-pAkt-APPL regulation of glial activation has been established. To test whether neuronal FMRP-dependent pMad and Prtp signaling plays roles in transcellularly regulating glial endolysosomal activation, two binary transgenic systems were used in parallel: 1) neuron-targeted RNAi lines driven with Gal4/UAS, and 2) glia-targeted mCD8::GFP plasma membrane labeling with LexA/LexAOP (Figure 3.11A). All assays were done on glia immediately adjacent to the PDF-Tri neuron cell bodies at 1 dpe to investigate early-stage activation in the pruning glial population. As endolysosomal sorting starts with the Rab5 GTPase in early endosomes (Kessissoglou et al., 2020; Skjeldal et al., 2021), we first tested anti-Rab5 labeling in glia. None of the neuronal RNAi manipulations cause any change in the glial Rab5 signal, indicating early endosomal activity is not affected. Late endolysosomal sorting employs the Rab7 GTPase on late endosomes and lysosomes (Kessissoglou et al., 2020), so we next tested anti-Rab7 labeling in glia. Neuronal *dfmr1, mad,* and *prtp* RNAi all dramatically depress glial Rab7 (Figure 3.11A). The driver controls (elav/+) consistently have larger, more numerous Rab7 puncta in glia adjacent to the PDF-Tri neurons, whereas all three neuronal knockdowns (*dfmr1*, *mad*, and prtp RNAi) have obviously smaller Rab7 puncta that are relatively difficult to detect (Figure 3.11A). Quantification of glial Rab7 volume shows the most significant reduction with neuronal *dfmr1* RNAi normalized to the elav/+ control (Figure 3.11B). Consistent with the above regulatory pathway, both neuronal *mad* and *prtp* RNAi also exhibit significantly reduced glial

Rab7 volume during PDF-Tri neuron removal (Figure 3.11 C and D). Together with established neuronal InR and APPL signaling of glial activation (Damisah et al., 2020; Folch et al., 2018; Gross and Bassell, 2012; Kurant et al., 2008), these findings show neuronal FMRP-pMad-Prtp signaling triggers glial endolysosomal phagocytosis activation for neuron clearance in the juvenile brain.

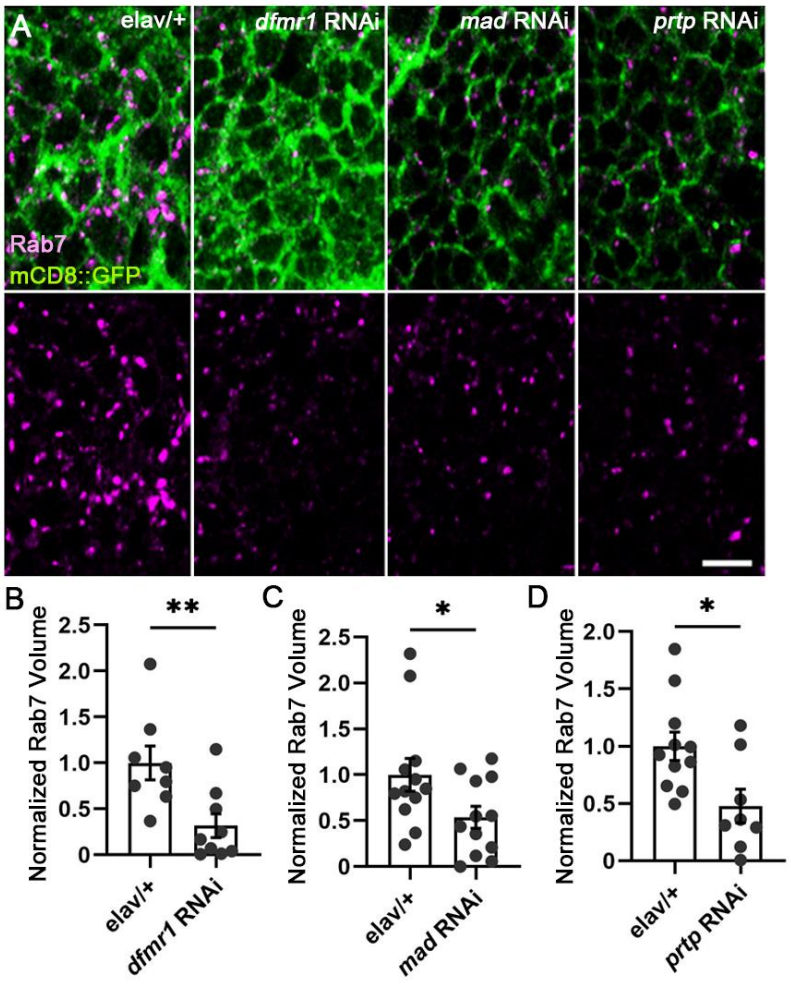

Figure 3.11 Neuronal FMRP-pMad-Prtp signaling activates the glial endolysosomal pathway.

A, Glial cells immediately adjacent to the PDF-Tri neurons in the central brain marked with membrane mCD8::GFP (green) and co-labeled with endolysosomal anti-Rab7 (magenta) at day 1 during the glial phagocytic removal process. The neuronal driver control alone (*elav*/+, left) is compared to driven *dfmr1* RNAi (second from left), *mad* RNAi (second from right), and *prtp* RNAi (right). The endolysosomal Rab7 is shown alone in the bottom row for all four genotypes. Scale bar: 20μm. B-D, Glial Rab7 volume normalized to the neuronal driver control (*elav*/+, left in each pairing) compared to neuronal *dfmr1* RNAi (B, *elav*/+ 1.00 ± 0.186 vs. *dfmr1* RNAi 0.318 ± 0.129, students' t-test, p= 0.0078), neuronal *mad* RNAi (C, *elav*/+ 1.00 ± 0.178 vs. *mad* RNAi 0.537 ± 0.119, students' t-test, p=0.041), and neuronal *prtp* RNAi (D, *elav*/+ 1.00 ± 0.123 vs. *prtp* RNAi 0.479 ± 0.147, students' t-test, p=0.014). Dot plots show all data points. Statistical significance indicated as *p<0.05 and **p<0.01.

3.5 Discussion

We have discovered an integrated mechanism of neuronal FMRP-dependent network signaling that regulates neuron-to-glia communication to drive the glial phagocytic removal of targeted neurons from an otherwise maintained brain circuit. Specifically, within the neurons, RNA-binding FMRP restricts the translation of bound *mad* transcripts to limit phosphorylated Mad (pMad) signaling, which, in turn, inhibits phosphorylated Akt (pAkt) to promote glial phagocytosis for neuron removal. In parallel, the neuronal insulin receptor (InR) regulates pAkt signaling in a second intersecting cascade controlling the neuronal clearance mechanism. This bone morphogenic protein (BMP) and insulin-like peptide (ILP) neural decision-making network (Song and Broadie, 2022) controls neuron-to-glia communication regulating glial phagocytosis function for targeted neuron removal. Neuronal pretaporter (Prtp) is a ligand for the draper (Drpr) engulfment receptor on glia (Kuraishi et al., 2009). The FMRP-pMad pathway promotes neuron-to-glia Prtp signaling to induce glial phagocytosis for neuron clearance, whereas the InR-pAkt pathway suppresses Prtp signaling to repress glia-mediated neuron removal. Neuronal amyloid precursor protein like (APPL) is released via a cleavable N terminus to activate Rab7 GTPase endolysomes in glia (Kessissoglou et al., 2020). The FMRP-pMad regulatory pathway promotes this neuron-to-glia APPL signaling, consistent with inducing glial phagocytosis for neuron clearance, and the intersecting InR-pAkt pathway also up-regulates this signaling, suggesting additional roles in neuron removal. Overall, these findings indicate neuronal FMRP coordinates signal transduction cascades to provide cross talk downstream of two signaling inputs (BMP and ILP), which provides output in the form of two neuron-to-glia signaling ligands (Prtp and APPL) that regulate glial phagocytosis for the clearance of targeted neurons from the juvenile brain.

3.5.1 From mRNA transcription to phosphorylated protein signaling.

We suggest RNA-binding FMRP limits pMad signaling levels by reducing the number of *mad* transcripts available for translation. FMRP is established to maintain protein translational homeostasis by modulating RNA target stability (Shu et al., 2020; Zhang et al., 2018). Ribosome profiling and transcriptome sequencing demonstrate imbalanced FMRP-targeted mRNA levels are common in the mouse FXS model brain due to reduced stabilization (Shu et al., 2020). In mouse RNA immunoprecipitation (RIP) sequencing, FMRP binds *smad* (*Drosophila mad* homologue) transcripts widely in the 5′-UTR, within the coding region, and in the 3′-UTR (Ascano et al., 2012). With both RIP and qPCR measurements, we find Drosophila FMRP likewise binds *mad* mRNA and that FMRP loss increases both *mad* transcripts and pMad protein levels within brain neurons. We therefore suggest a causal effect correlation, although other indirect regulatory mechanisms are also possible (Sardi et al., 2021; Urrutia et al., 2016). We find loss of neuronal pMad decreases InR levels but elevates InR-dependent pAkt signaling, suggesting cross talk inhibition from pMad to pAkt. The pMad transcription factor (Deignan et al., 2016) positively regulates InR expression. Downstream of the InR, pAkt regulates numerous targets, including target of rapamycin complexes (Saltykova et al., 2021) and the transcription factor forkhead box O (Das et al., 2016), to regulate cell fate decisions (Dutriaux et al., 2013; Jung and Suh, 2015). In the brain neuronal fate decision, we suggest pMad inhibits pAkt signaling as a major cross talk regulation within the neuron-to-glia signaling network. With western blot assays, we find reducing neuronal pMad levels causes no changes in Akt protein levels but a approximately twofold increase in pAkt signaling. Thus, FMRP-dependent pMad signaling modulates InR-pAkt signaling at two levels: as a positive transcription factor regulating InR expression and as an inhibitor of downstream pAkt

signaling. We conclude this cross talk provides critical regulation for targeted neuron pruning from the juvenile brain.

3.5.2 Brain circuit pruning in Fragile X Syndrome (FXS).

Neuron removal from brain circuits is a normal mechanism in neurodevelopment, often mediated by glial phagocytosis (Birge and Ucker, 2008; Fuchs and Steller, 2011; Riera Romo, 2021). During the clearance process, glia engulf neurons and degrade internalized debris in endolysosomes (McLaughlin et al., 2019; Xu et al., 2020). In glia, the engulfed neuronal debris is first sorted in Rab5 GTPase early endosomes (Kessissoglou et al., 2020), then trafficked from early-to-late endosomes with accompanying increased intravacuolar acidification, and finally delivered to Rab7 GTPase lysosomes where acid hydrolases complete the degradation process (Hu et al., 2015). In both rodent and *Drosophila* FXS disease models, this glial phagocytosis mechanism is severely impaired, resulting in a failure to prune neurons in brain circuits (Vandenberg et al., 2021; Vita et al., 2021). In the *Drosophila* FXS model, loss of neuronal FMRP decreases the glial Drpr engulfment receptor, and loss of glial Drpr blocks glial phagocytosis to prevent neuron removal (Vita et al., 2021). This previous study generated the hypothesis that the impaired brain circuit neuron removal in the FXS disease model is caused by the loss of neuron-to-glia communication driving glial phagocytosis (Gatto and Broadie, 2011). With neuron-specific RNAi trials, we find the neuronal FMRP-pMad pathway triggers Drpr ligand Prtp signaling from neurons to mediate glial engulfment and phagocytosis, whereas the neuronal InR-pAkt pathway represses Prtp to oppose the glial removal mechanism. Furthermore, we find targeted knockdown of neuronal FMRP, pMad, and Prtp impedes glial endolysosomal activation with reduced Rab7 expression, showing the neuronal FMRP-dependent network is required for glial phagocytosis

function. These findings are consistent with the impaired glia-mediated neuron pruning in FXS disease models (Vandenberg et al., 2021; Vita et al., 2021) and provide insight into the molecular mechanisms of this defect. Clearly, the decision to eliminate neurons by glial phagocytosis rests on multiple, distinct signaling inputs and is executed via parallel avenues of neuron-to-glia communication.

3.5.3 Neuronal Prtp vs. APPL regulation of glial phagocytosis.

We find that loss of either neuronal Prtp or APPL hampers glial phagocytosis neuron removal from the juvenile brain circuit but that loss of either signal alone causes a less severe impairment than blocking the neuronal FMRP-pMad pathway. These results suggest that Prtp and APPL act combinatorially downstream of FMRP-pMad, consistent with both neuronal Prtp and APPL driving the glial phagocytic clearance of targeted neurons (Kessissoglou et al., 2020; Kuraishi et al., 2009). Prtp is a transmembrane protein trafficked from the endoplasmic reticulum (ER) to the cell surface of a neuron thus marked for removal, where it binds the Drpr engulfment receptor on glia (Kuraishi et al., 2009). Through this mechanism, Prtp surface presentation downstream of the neuronal FMRP-pMad pathway is proposed to directly signal glial engulfment. In contrast, the cleaved extracellular domain of transmembrane APPL from neurons activates the glial endolysosomal network (Kessissoglou et al., 2020). This provides a separable function for APPL, suggesting why two signaling ligands mediate neuron removal by the glial phagocytosis mechanism. The Prtp signaling changes closely match the neuron clearance phenotypes of all neuronal *dfmr1*, *mad*, *InR*, and *akt* RNAi experiments. Likewise, the APPL signaling changes are consistent with FMRP-pMad regulation but not the InR-pAkt pathway. We therefore propose Prtp and APPL coregulate glial phagocytic activity with different strengths or independently participate

in glial phagocytosis via other regulatory mechanisms. To test the possibility that Prtp interacts with APPL in this clearance mechanism, we could test the putative cross talk interaction at molecular and/or genetic levels. Conversely, neuronal Prtp and APPL may be independent signals in neuron-to-glial communication linked predominantly or solely through upstream FMRP regulation. Future studies will dissect these combinatorial signals downstream of inputs targeting the clearance of neurons from the juvenile brain.

3.5.4 Neuronal InR vs. glial InR roles in glial phagocytosis.

The pigment-dispersing factor (PDF) brain circuit mediates circadian clock functions, with the developmentally transient central PDF-Tri neurons presumably driving eclosion timing (Gatto and Broadie, 2011). Multiple signals appear to coordinate the targeted clearance of PDF-Tri neurons from the juvenile brain, including insulin-like peptide (ILP) signaling (Vita et al., 2021). The insulin receptor (InR) is present in both neurons and glia, acting to coordinate intercellular communication and neuronal remodeling (Boulanger and Dura, 2022; Gu et al., 2013; Harrison et al., 2021; Musashe et al., 2016; Wong et al., 2013). For glial signaling, InRs are proposed to be activated by secreted ILPs from the remodeling neurons to stimulate transduction cascades promoting glial phagocytosis (Musashe et al., 2016; Vita et al., 2021). Glial InR phosphorylation triggers pAkt production, which, in turn, elevates Drpr engulfment receptor levels to drive glial phagocytosis (Musashe et al., 2016). Consistently, genetically increasing glial InR levels elevates glia-dependent neuron removal of the PDF-Tri neurons (Vita et al., 2021). In the *Drosophila* FXS disease model, loss of FMRP represses InR phosphorylation in glia, whereas glial InR activation restores PDF-Tri neuron pruning (Vita et al., 2021). For neuron signaling, we propose that InR-mediated pAkt signal transduction regulates neuron-to-glia communication in this same

remodeling process. Similarly, InR signaling in Drosophila dendrite arborization neurons inhibits their developmental pruning (Wong et al., 2013). Our work shows neuronal InR loss elevates Prtp signaling to drive glial phagocytosis, thus accelerating PDF-Tri neuron clearance from the juvenile brain. Neuronal InRs may be responding to autocrine ILP signaling from the remodeling neurons (Musashe et al., 2016; Vita et al., 2021) or ILPs from another source which is coordinating neuron and glia functions to properly regulate the glial phagocytosis neuron removal process. Future work will investigate how the different intercellular signals act on both neurons and glia to ensure the exact targeting and timing of the coordinated PDF-Tri neuron clearance from the juvenile brain.

3.6 Materials and Methods

3.6.1 *Drosophila* genetics

All Drosophila stocks were reared on cornmeal/agar/molasses food at 25 °C. Loss-of-function mutants used include $dfmr1^{50M}$ (Song et al., 2022) and appld Bloomington Drosophila Stock Center (BDSC# 43632) alleles (Kessissoglou et al., 2020). Transgenic drivers used include pan-neuronal elav-Gal4 (Song et al., 2022), PDF-Gal4 (BDSC# 6899) (Vita et al., 2021), and glial repo-LexA (BDSC# 67096) (Dong et al., 2021). The controls include the w^{1118} genetic background (Song et al., 2022) and the transgenic drivers alone. All genetic crosses and recombinations to make double transgenic insertions were performed with standard methods. Transgenic stocks were obtained from the Bloomington Drosophila Stock Center (BDSC) and are listed in Table 3.1. UAS lines alone have been tested to show no significant effect on the PDF-Tri neuron phenotype (Figure 3.12 A–C).

Transgenic Line	Insertion	BDSC#
UAS-*dfmr1* RNAi (Song et al., 2022)	$y^{[1]}\ sc^{[*]}\ v^{[1]}\ sev^{[21]}$;P{$y^{[+t7.7]}\ v^{[+t1.8]}$=TRiP.GL00075}attP2	35200
UAS-*mad* RNAi (Tracy Cai et al., 2019)	$y^{[1]}\ v^{[1]}$; P{$y^{[+t7.7]}\ v^{[+t1.8]}$=TRiP.JF01263}attP2	31315
UAS-*InR* RNAi (Nakamura et al., 2020)	$y^{[1]}\ sc^{[*]}\ v^{[1]}\ sev^{[21]}$;P{$y^{[+t7.7]}\ v^{[+t1.8]}$=TRiP.GL00139}attP2	35251
UAS-*akt* RNAi (Ni et al., 2009)	$y^{[1]}\ v^{[1]}$; P{$y^{[+t7.7]}\ v^{[+t1.8]}$=TRiP.HMS06047}attP40/CyO	82957
UAS-*akt* RNAi (Ito and Igaki, 2021)	$y^{[1]}\ v^{[1]}$; P{$y^{[+t7.7]}\ v^{[+t1.8]}$=TRiP.HM04007}attP2	31701
UAS-*appl* RNAi (Raza et al., 2019)	$y^{[1]}\ v^{[1]}$; P{$y^{[+t7.7]}\ v^{[+t1.8]}$=TRiP.JF02878}attP2	28043
UAS-*prtp* RNAi (Ni et al., 2011)	$y^{[1]}\ sc^{[*]}\ v^{[1]}\ sev^{[21]}$; P{$y^{[+t7.7]}\ v^{[+t1.8]}$=TRiP.HMC04406}attP40	56965
UAS-*gfp* RNAi (Lin et al., 2020)	$w^{[1118]}$; P{$w^{[+mC]}$=UAS-GFP.dsRNA.R}142	9330
UAS-*InR* CA (Vita et al., 2021)	$y^{[1]}\ w^{[1118]}$; P{$w^{[+mC]}$=UAS-InR.del}2	8248
UAS-*akt* OE (Li et al., 2022)	$y^{[1]}\ w^{[1118]}$; P{$w^{[+mC]}$=UAS-Akt.Exel}2	8191
LexAOP-mCD8::GFP (Chan et al., 2015)	$w^{[*]}$; P{$y^{[+t7.7]}\ w^{[+mC]}$= 13XLexAop2-mCD8::GFP} attP40 /CyO	32205

Table 3.1 Transgenic lines.

BDSC#, Bloomington *Drosophila* stock center number.

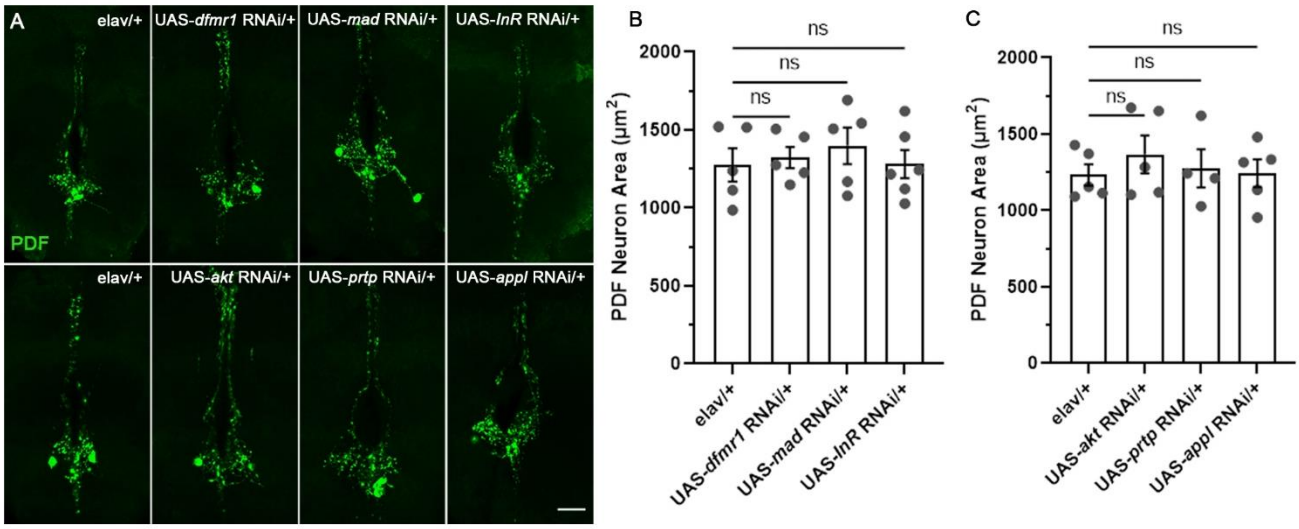

Figure 3.12 UAS-RNAi controls have no effect on the normal PDF-Tri neuron clearance

A, PDF-Tri neurons (anti-PDF, green) in driver control (*elav*/+) and matched UAS RNAi controls. Scale bar: 20 µm. B, Quantification of PDF-Tri neuron size in *dfmr1* RNAi, *mad* RNAi and *InR* RNAi controls with one-way ANOVA (*elav*/+ 1275.0 ±107.20 vs. UAS-*dfmr1* RNAi alone/+ 1322.0 ± 68.31, p=0.97; *elav*/+ vs. UAS-*mad* RNAi alone/+ 1397.0 ± 117.0, p=0.72; *elav*/+ vs. UAS-*InR* RNAi alone/+ 1281.0 ± 89.64, p>0.99). C, Quantification of PDF-Tri neuron size in *akt* RNAi, *prtp* RNAi and *appl* RNAi controls with one-way ANOVA (*elav*/+ 1232.0 ± 69.83 vs. UAS-*akt* RNAi alone/+ 1366.0 ± 124.80, p=0.68; *elav*/+ vs. UAS-*prtp* RNAi alone/+ 1276.0 ± 124.40, p=0.98; *elav*/+ vs. UAS-*appl* RNAi alone/+ 1244.0 ± 90.89, p>0.99).

3.6.2 Immunocytochemistry

Brains from synchronized, staged animals were dissected in phosphate-buffered saline (PBS), fixed in 4% paraformaldehyde in PBS for 30 min at room temperature (RT), and then blocked for 1 h at RT in PBS with 0.2% Triton X-100 (PBST) + 1% bovine serum albumin. Primary antibodies were diluted in the blocking buffer for incubation overnight at 4 °C, followed by washing 3X with PBST. Secondary antibodies were incubated for 3 h at RT and then washed 3X with PBST. Primary antibodies used were mouse anti-PDF [Developmental Studies Hybridoma Bank (DSHB), PDF C7,1:50], rabbit anti-Repo (gift from Dr. Benjamin Altenhein, University of Cologne, Germany, 1:1,000), chicken anti-GFP (Abcam, ab13970, 1:1,000), rabbit anti-Rab5 (Abcam, ab31261, 1:500), rabbit anti-pAkt (115hosphor S473, Cell Signaling, 4060S, 1:100), and mouse anti-Rab7 (DSHB, Rab7, 1:100). Secondary antibodies used were goat anti-mouse 488 (Invitrogen, A11001, 1:250), donkey anti-rabbit 555 (Invitrogen, A31572, 1:250), goat anti-chicken 488 (Invitrogen, A11039, 1:250), and goat anti-mouse 633 (Invitrogen, A21050, 1:250).

3.6.3 Confocal imaging

Brains were imaged on a Zeiss LSM 510 META laser scanning confocal microscope using 40X, 63X, and 100X oil immersion objectives (Song et al., 2022). All collected images were projected in Zen software. Identical microscope setting was used to collect and analyze all genotypes for all trials within any given experiment. For three-dimensional (3D) images, the cropped Z-stack was processed with the 3D viewer icon in FIJI software to visualize PDF-Tri neurons, Repo-positive glia, and pAkt puncta. PDF-Tri neurons with glia colabeling Z-stacks were maximum projected in FIJI software to quantify the outlined neuronal area. Glial Rab5/7-labeled

Z-stacks were sum projected to analyze total volumes. All Rab volumes were quantified only within labeled glia (repo-Gal4>mCD8::GFP membrane marker). The Rab volumes were divided by the imaged glial volume for normalization. The pAkt puncta within labeled PDF-Tri neurons were quantified based on 3D views. The number of pAkt puncta were divided by the PDF-Tri neuron area to quantify the pAkt puncta density.

3.6.4 Western blots

Staged heads (3 to 5 h after eclosion at 25 °C) were homogenized in lysis buffer (20 mM HEPES, 10 mM EDTA, 100 mM KCl, 1% (v/v) Triton X-100, and 5% (v/v) glycerol, pH 7.4) with 2X protease and phosphatase inhibitor cocktail (Thermo Scientific, WL334851). Homogenized lysate samples (50 μL lysis buffer/head) were incubated on a rotor for 15 min at 4 °C and then centrifuged at 14,000 rpm for 15 min at 4 °C. The supernatant was denatured with 1X NuPAGE LDS sample buffer (Invitrogen, NP0007) for 10 min at 100 °C. Protein samples were run in 4 to 15% Mini-PROTEAN TGX gels (Bio-Rad, 4568086) and then transferred onto PVDF membranes using the Trans-Blot Turbo Transfer System (Bio-Rad). PVDF membranes were blocked in TBS Intercept Blocking Buffer (Li-COR# 220121) for 1 h at RT, followed by incubating with primary and secondary antibodies. Primary antibodies used were rabbit anti-Smad3 (phospho S423+S425, Abcam, ab52903, 1:1,000), rabbit anti-pAkt (phospho S473, Cell Signaling, 4060S, 1:1,000), goat anti-GAPDH (glyceraldehyde 3-phosphate dehydrogenase) (Abcam, ab157156, 1:2,000), and chicken anti-APPL (a gift from Dr. Doris Kretzschmar, Oregon Health and Science University, USA; 1:1,000). Secondary antibodies used were goat anti-chicken 800 (Invitrogen, SA5-10076, 1:10,000), donkey anti-goat 680 (Invitrogen, A21084, 1:10,000), goat anti-mouse 800 (Invitrogen, SA535521, 1:10,000), and goat anti-rabbit 800 (Invitrogen, SA535571, 1:10,000). Blots were

scanned with an Odyssey CLx Imager (Li-COR). Fluorescent band intensities were quantified using Image Studio Lite software (Li-COR). To normalize protein levels, the fluorescent intensity of targeted proteins was divided by the loading control of glyceraldehyde 3-phosphate dehydrogenase (GAPDH).

3.6.5 Quantitative real-time PCR

RNA was extracted for ~30 heads at 1 day posteclosion (1 dpe). The RNA extraction procedure followed the instructions of the RNeasy Plus Micro Kit (Qiagen, 74034). RNA (2 μg) was reversely transcribed in 20-μL reaction mixture of SuperScript VILO Master Mix (Invitrogen, 11755-050), with cDNA (1 μL) then mixed with 19 μL diluted Power SYBR Green PCR Master Mix (Applied Biosystems, 4367659) for real-time PCR amplification using the Bio-Rad CFX96 system. The quantified PCR cycle number was normalized to the internal control GAPDH. All primers used in this study are listed in Table 3.2.

Gene	Forward	Reverse
GAPDH	CGTTCATGCCACCACCGCTA	CCACGTCCATCACGCCACAA
Mad	AACACACGCCGTCATATAGGCAAG	GGCCTCGAATCCATTGTTCACC
Stau	AAATGCTGCACAGGCTCTG	CAGTATTAAAATGCCTGGCATGGG
InR	ACTGTCACAAAATGTAAAACCTTGC	AACAGCTTGTTTCCCCTAATGA
Akt	CGTGGTCATGTACGAGATGATCT	CTAGATCTGTCCAGTTAATACTCGC
Prtp	GTGCAGTCATTGTCAGCGTTT	CTCGATCCAGAGAAGAGTGGG
Appl	GTCCCAAGCACTTCAAAACCGA	CCGCATTTATGTCATCCAAAGATCC

Table 3.2 PCR primers used in this study.

3.6.6 RNA immunoprecipitation

The procedure was done as in Song et al. (Song et al., 2022). Briefly; lysates were prepared from ~30 heads at 1 dpe with 500 μL RNase-free lysis buffer (20 mM HEPES, 100 mM NaCl, 2.5 mM EDTA, 0.05% (v/v) Triton X-100, 5% (v/v) glycerol, and 1% β-mercaptoethanol) with 1X protease inhibitor cocktail (cOmplete Mini EDTA-free tablets, Sigma-Aldrich) and 400 U RNase inhibitor (Applied Biosystems, N8080119). To precipitate RNA complexes, precleared lysates were incubated with 15 μL magnetic GFP-trap beads (ChromoTek) for 3 h at 4 °C, followed by washing 3X with lysis buffer. To purify bound RNAs, the washed beads were incubated with a 500 μL TRIzol and chloroform mixture (Ambion, 15596026) for 10 min. Subsequently, 1 μL glycogen was applied to carry RNAs for the precipitation by mixing with 100 μL 2-propenol. The above qPCR methods were performed to analyze the reverse-transcribed RNAs.

3.6.7 Statistical analyses

All statistical analyses were performed with GraphPad Prism software 9.0. All datasets were subject to ROUT outlier tests with Q set to 1%. Unpaired two-tailed Student's t tests with 95% confidence of comparisons were used for all two-way datasets (PDF-Tri neuron areas, Rab7 volumes, pAkt puncta density, western blot assays, and qPCR assays). All datasets with more than two comparisons (day 1 and day 5 PDF-Tri neuron areas with *dfmr1* RNAi, *mad* RNAi, prtp RNAi, and appl RNAi) were analyzed by two-way ANOVA tests with a 5% alpha significance level. The comparison with more than two datasets was analyzed using one-way ANOVA tests (PDF-Tri neuron area). Data are presented as the mean ± SEM. Significance is indicated by P value measurements shown as $P < 0.05$ (*), $P < 0.01$ (**), $P < 0.001$ (***), and $P < 0.0001$ (****). Values of $P > 0.05$ are deemed not significant (ns).

3.7 Data, materials, and software availability

All study data are included in this article.

3.8 Acknowledgments

We are particularly grateful to Dr. Benjamin Altenhein (University of Cologne, Germany) for the generous gift of the anti-Repo antibody and Dr. Doris Kretzschmar (Oregon Health and Science University, Portland, OR, USA) for the generous gift of the anti-APPL antibody. We thank the Bloomington Drosophila Stock Center (Indiana University, Bloomington, IN, USA) for essential genetic lines and the Developmental Studies Hybridoma Bank (University of Iowa, Iowa City, IA, USA) for essential antibodies. We are grateful to the Vanderbilt University Cell and Developmental Biology facility center and staff for help and the use of essential equipment. This work was entirely supported by funding from the National Institute of Mental Health R01 grant MH084989 to K.B.

3.9 Author contributions

C.S. designed research; C.S. performed research; C.S. contributed new reagents/analytic tools; C.S. analyzed data; K.B. editing, funding; and C.S. and K.B. wrote the paper.

CHAPTER IV

Discussion and Future Directions

In this dissertation, I report two independent but related research projects from my graduate training. With the powerful *Drosophila* genetic model, I focused on studying the dysregulation of intercellular signaling during 1) synapse formation and 2) circuit remodeling in a Fragile X syndrome (FXS) disease model. I used the larval neuromuscular junction (NMJ) for project 1, and the juvenile adult brain for project 2. Both projects tested FMRP-mediated molecular interactions, sequential signaling pathways, and neuronal responses based on synaptic and circuitry changes. In addition to FXS disease relevance, these mechanisms are important for normal neurodevelopment, and reflect processes highly conserved across species. My studies open the gate to avenues regarding the function of postsynaptic FMRP on presynaptic development, and neuronal FMRP directing neuron-to-glia crosstalk during brain circuit remodeling. In the future, I hope that this work will provide a foundation to map the core molecular cascades in these signaling networks as a means to design and implement new FXS treatments.

4.1 FMRP-dependent intercellular signaling in synapse formation

Biopsies of human FXS patients show overgrowth of immature dendritic spines, suggesting impaired/altered synaptic connectivity and neurotransmission (Huebschman et al., 2020; Pfeiffer and Huber, 2009). In both *Drosophila* and mouse FXS disease models, FMRP loss induces similar disordered synapses, with increased synaptic architecture, enhanced synaptic strength, and impaired synaptic plasticity (Repicky and Broadie, 2009; Suresh and Dunaevsky, 2017; Zhang et al., 2001). The Broadie Lab has also previously shown that the *Drosophila* FXS model exhibits altered postsynaptic glutamate receptor balance (GluRIIA/B; accumulated

GluRIIA) and enlarged presynaptic vesicle pools with elevated glutamate release (Pan and Broadie, 2007b; Pan et al., 2008). These defects likely explain the elevated NMJ transmission and hyperactivity in the FXS condition. However, the mechanism of GluRIIA accumulation remained largely unknown. In addressing this question, I revealed an FMRP-Staufen-Coracle signaling cascade regulating postsynaptic GluRIIA levels and, secondarily, presynaptic bouton formation (Song et al., 2022). Both FMRP and Staufen are RNA-binding proteins that sequentially regulate Coracle, a scaffold that anchors GluRIIA-containing receptors to the underlying cytoskeleton (Chen et al., 2005). In the FXS condition, the accumulated GluRIIA in turn activates *trans*-synaptic, non-canonical BMP signaling (Sulkowski et al., 2016) to induce presynaptic bouton formation and synaptic overgrowth (Song et al., 2022). While I thus built up a regulatory model for NMJ synaptic changes mediated by FMRP in the muscle, the study of related reverse signaling networks from postsynapse to presynapse more generally in glutamatergic synapses is just beginning. Future directions should concentrate on identifying ligands, receptors, synaptic endocytosis sorting mechanisms, and trafficking organelles.

4.1.1 The role of transcellular BMP signaling in NMJ synaptogenesis

Postsynaptic GluRIIA induces presynaptic pMad accumulation near active sites through noncanonical BMP receptor (BMPR) *trans*-synaptic signaling, which requires presynaptic BMPR Wishful thinking (Wit) but appears independent of BMP ligands (Sulkowski et al., 2016). In my NMJ study, I found reducing the muscle FMRP-Staufen-Coracle cascade results in elevated postsynaptic GluRIIA levels and promotes elevated presynaptic pMad levels, suggesting a *trans*-synaptic signaling mechanism regulated by FMRP (Song et al., 2022). In a follow-up test of bouton formation, I explored if loss of NMJ postsynaptic FMRP impairs presynaptic bouton formation.

With muscle-targeted *dfmr1* RNAi (24B-Gal4>*dfmr1* RNAi), the bouton number is significantly increased compared to matched driver control (24B/+) (Figure 4.1). This evidence suggests that postsynaptic FMRP is required to regulate presynaptic development via the above noncanonical BMP signaling mechanism. An important future direction is determining which signaling molecules from the postsynaptic muscle activate presynaptic Wit. It is possible that GluRIIA directly interacts with Wit through Neto, a transmembrane protein that conjuncts with receptors, to stabilize synaptic architecture (Han et al., 2020). To test this possibility, first of all, using co-IP to test the direct molecular interaction between Wit, Neto, and GluRIIA. Second, predicting binding motifs in Neto with GluRIIA and Wit, and testing the interaction by using yeast two-hybrid systems or using CRISPR to knockout predicted motifs on Neto with combined *in vivo* co-IP to confirm the interaction with Wit and GluRIIA. Lastly, measuring bouton formation with increased GluRIIA accumulation in the background of disrupted binding motifs in Neto. Another possibility of intercellular activated Wit may be unknown Wit ligands that are released from muscle with accumulated GluRIIA background. An unbiased way to test this possibility is mapping Wit immunoprecipitation products with overexpressed GluRIIA on muscles versus genetic controls.

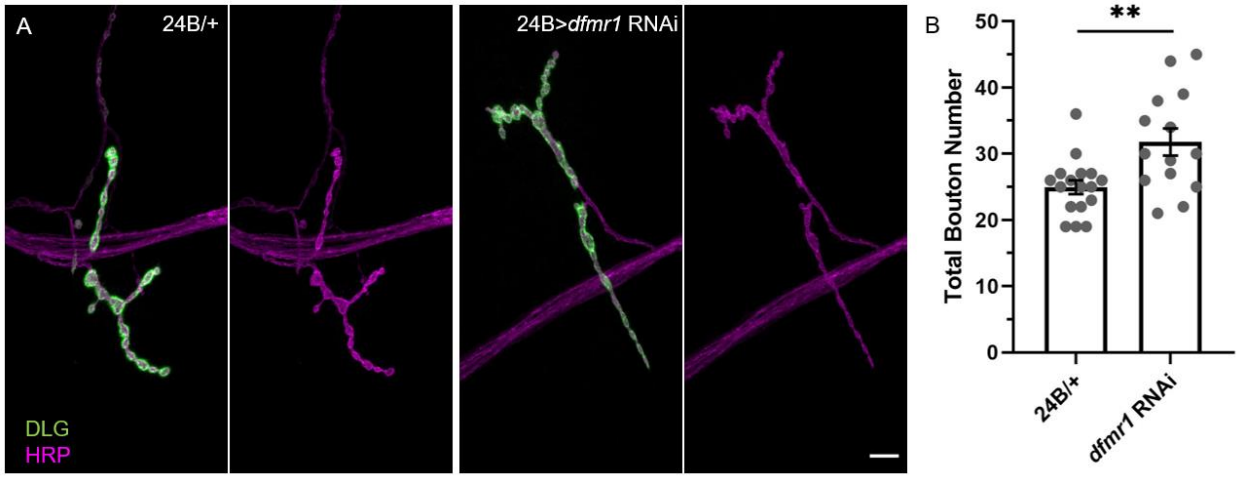

Figure 4.1 Postsynaptic FMRP is required to limit presynaptic bouton formation at NMJ.

A) Double labeling of *Drosophila* NMJ. HRP (magenta) labels axon terminals while DLG (green) targets postsynaptic SSR. Left double images show presynaptic bouton labeling in genetic control (24B/+) while the right images are muscle-targeted *dfmr1* RNAi (24B>*dfmr1* RNAi). Muscle-targeted *dfmr1* RNAi (24B-Gal4>*dfmr1* RNAi) causes the presynaptic bouton number to be elevated compared to the genetic control (24B-Gal4/+) **B)** Student's t-test indicates loss of FMRP in muscle significantly increases presynaptic bouton number (24B/+ 24.94±1.034 vs. *dfmr1* RNAi 31.79±2.041, p=0.0037; statistics shown in mean ± s.e.m.). Scale bar: 10 μm.

Another important future direction is to explore the mechanism of presynaptic pMad in regulating bouton formation. As a transcription factor, pMad has been identified to interact with several cofactors to form a complex regulating gene expression (Deignan et al., 2016; Newton et al., 2015; Sardi et al., 2021). In *Drosophila*, the reported pMad partners include Medea (Med) (Affolter and Basler, 2007; Li et al., 2020), Schnurri (Shn) (Gafner et al., 2013; Marty et al., 2000; Torres-Vazquez et al., 2000), Yorkie (Yki) (Huang et al., 2017; Sansores-Garcia et al., 2013), Moleskin (Msk) (Chen et al., 2010; Kimura and Imamoto, 2014) and Ultrabithorax (Ubx) (Li et al., 2016; Walsh and Carroll, 2007), among possible others. My NMJ immunofluorescence studies indicate pMad in the cytosol, but also concentrated in the muscle nucleus (Figure 4.2). Studies

indicate Mad is phosphorylated in cytosol via activated Wit (Moulton et al., 2020), then binds partners for nuclear translocation (Galbiati et al., 2020; Smith et al., 2012). So far, my research indicates postsynaptic FMRP intercellularly suppresses presynaptic pMad accumulation for the normal bouton formation, so future studies need to examine the neuronal nuclei. Morever, I have not tested if synaptic Med and other candidate partners are impacted via pMad binding, protein level, and/or subcellular localization. Furthermore, it will be important to test if pMad complexes regulate cytoskeleton assembly and protein trafficking mechanisms, which are known to be required for synaptic bouton development (Ho and Treisman, 2020; Hoover et al., 2019; Song et al., 2022).

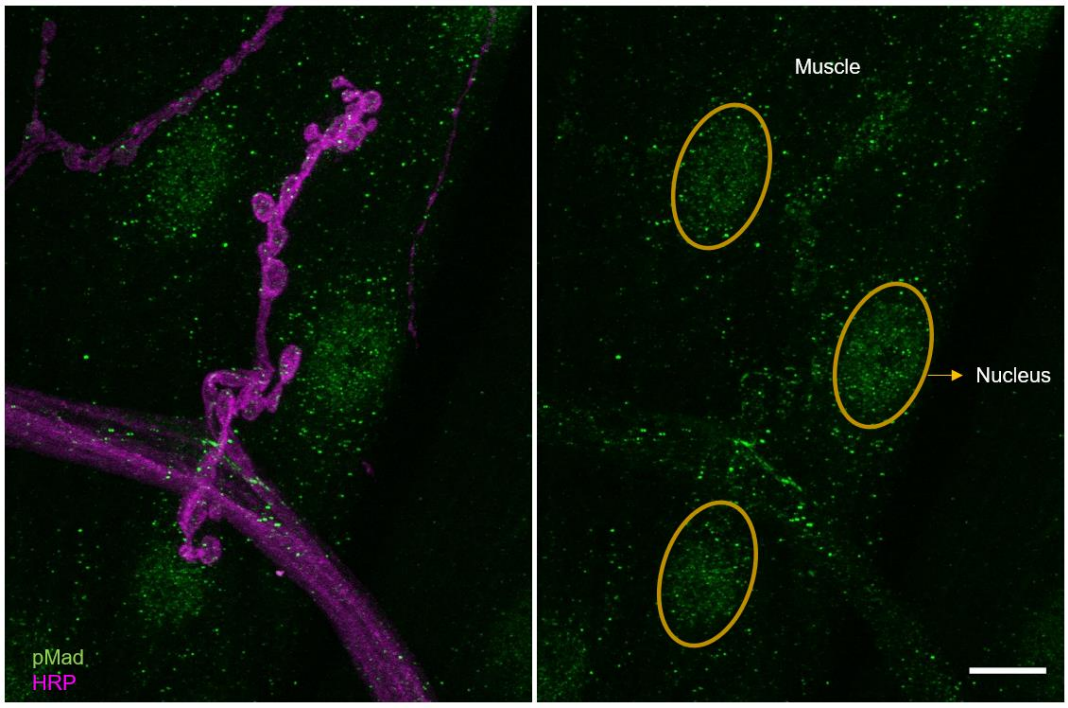

Figure 4.2 pMad localization at the NMJ.

Double labeling of pMad at the NMJ and muscle. HRP (magenta) labels axon terminals. pMad is labeled green in neurons and muscles. The left image shows merged channels of NMJ and muscle while the right is a single channel with pMad labeling. pMad is widely distributed in muscle cells and neurons at the *Drosophila* neuromuscular junction, but pMad is concentrated in the nuclei. Scale bar: 10 μm.

4.1.2 Other FMRP-dependent postsynaptic signaling networks

In addition to *trans*-synaptic BMPR signaling cascade, other signaling pathways also possibly play roles in postsynaptic FMRP-mediated muscle-to-neuron crosstalk (Song and Broadie, 2022). To explore these candidate mechanisms, it will be important to consider secreted Wnts, an acronym derives from *Drosophila* Wingless (Wg) whose developmental role was identified in the famous segment polarity screen (Nüsslein-Volhard and Wieschaus, 1980), and mouse INT-1, from a virus-induced breast tumorigenesis study (Nusse and Varmus, 1982). There are 7 Wnts in

Drosophila and 19 in mice. Cysteine-palmitoylated Wnts are secreted with the assistance of seven-pass transmembrane proteins Wntless (Wls) and evenness interrupted (Evi) (Bänziger et al., 2006; Bartscherer et al., 2006; Willert et al., 2003). Wnt receptors include the Frizzled (Fz) family, low-density lipoprotein receptor-related proteins-5/6 (LRP-5/6), receptor tyrosine kinase-like orphan receptor-1/2 (ROR1/2), and related to tyrosine (Y) kinase (Ryk) (Niehrs, 2012; Patel et al., 2019).

In the *Drosophila* FXS disease model, FMRP regulates *trans*-synaptic Wnt signaling to modulate NMJ synaptogenesis (Friedman et al., 2013), via the presynaptic Wg ligand and postsynaptic Fz2 receptor (Song and Broadie, 2022). Previous studies mostly focus on neuron-to-muscle signaling. For example, FMRP loss increases Wg secretion from presynaptic boutons to induce cleavage of the larval muscle Fz2 C-terminus (Fz2-C), which is translocated as a second messenger into postsynaptic nuclei (Friedman et al., 2013). Consistently, Wg overexpression within the presynaptic motor neuron activates Fz2-C accumulation within postsynaptic muscle nuclei (Mathew et al., 2005). However, Fz2 is also present in presynaptic membrane to direct presynaptic development (Wu et al., 2010). The activation of presynaptic Frizzled promotes presynaptic assembly through transducing signals to inhibit Shaggy/Gsk3β and MAP1B/Futsch (Franciscovich et al., 2008; Franco et al., 2004; Gögel et al., 2006; Roos et al., 2000). According to these reports, it would be interesting to test if postsynaptic FMRP regulates Wg secretion from muscles to mediate presynaptic congregation. One of the methods to measure it may tag muscle Wg with GFP by using CRISPR tissue-specific knock in, followed by detecting Wg::GFP signals at the NMJ with the postsynaptic *dfmr1* RNAi.

4.2.3 Glia participation in NMJ *trans*-synaptic signaling

Glia have multiples roles in modulating neuronal development, as well as synaptic assembly and pruning (Nave, 2010; Ou et al., 2014; White and Krämer-Albers, 2014). In mammals, several glial subtypes have been identified both in the central nervous system (CNS) and peripheral nervous system (PNS), included oligodendrocytes, astrocytes, ependymocytes, radial glia, Schwann cells, enteric glial cells, satellite cells, and microglia (Hanani and Spray, 2020; Jäkel and Dimou, 2017; Nazareth et al., 2021; Rasband, 2016). Based on differential tissue distribution, *Drosophila* glia are classified into surface glia (to form blood-brain barrier), neuropil glia (axon ensheathment and pruning) and cortex glia (gas and nutrition exchange) within the CNS, as well as multiple subtypes of peripheral glia in the PNS (Bittern et al., 2021; Kottmeier et al., 2020; Ou et al., 2014). The *Drosophila* NMJ has three glia subtypes (perineurial, subperineurial and wrapping glia), which regulate synapse formation and function (Figure 4.3) (Brink et al., 2012; Fuentes-Medel et al., 2012; Ou et al., 2014). In particular, studies have identified intercellular signaling pathways in glia essential to maintaining NMJ synaptic development and function. For example, NMJ glia secrete Wg to restrict GluRIIA clustering but also promote presynaptic glutamate release, although bouton formation is reportedly not impacted (Kerr et al., 2014). Moreover, Delta/Notch signaling in subperineurial glia suppresses c-Jun N-terminal kinase (JNK) activation to inhibit extracellular matrix metalloproteinase 1 (Mmp1) (Calderon et al., 2022), a major regulator of the synaptomatrix and NMJ *trans*-synaptic signaling. In the *Drosophila* FXS disease model, FMRP regulates Mmp1 secretion to modulate larval NMJ synaptic structure and function via control of secreted Wnt *trans*-synaptic signaling (Dear et al., 2016; Dear et al., 2017). However, it is unknown how FMRP links into this mechanism. It is therefore important to test this direction to further uncover the mechanism of peripheral glia-mediated NMJ synaptic modulation

in our FXS model. It would be interesting to detect NMJ morphology, neurotransmission, and secreted Wg levels by NMJ peripheral glia with glial- or muscle-targeted *dfmr1* RNAi.

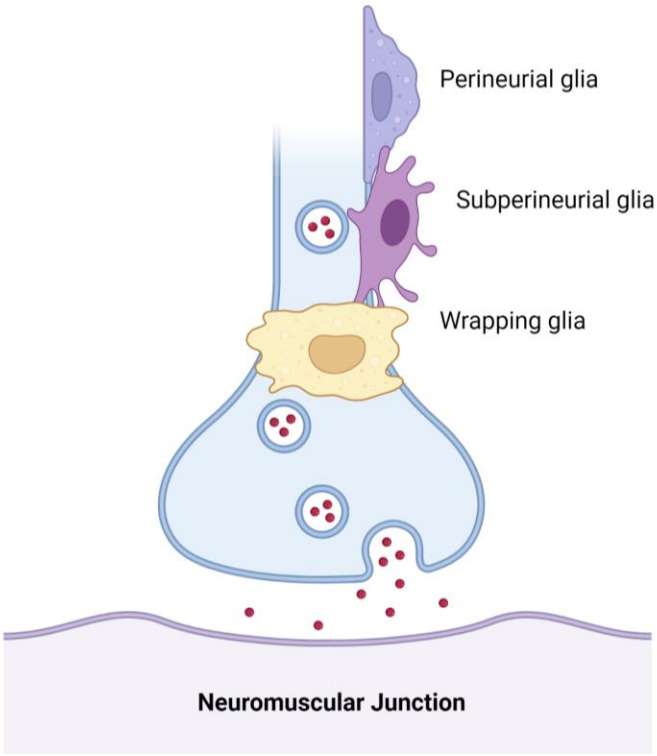

Figure 4.3 Different subtypes of peripheral glia at the *Drosophila* neuromuscular junction.

The perineurial glia, subperineurial glia and wrapping glia wrap around presynaptic axons to regulate synaptic structure and function. Perineurial glia functions in axon ensheathment (Ou et al., 2014). Subperineurial glia secretes Wg to restrict GluRIIA accumulation (Kerr et al., 2014). And wrapping glia guarantee neuronal signaling precision and axon growth to promote action potential conduction speed (Kottmeier et al., 2020).

4.3 FMRP-dependent neuron-to-glia communication in CNS remodeling

Loss of neuronal FMRP results in aberrant brain circuit remodeling due to downregulated glial phagocytosis activity (Song and Broadie, 2023). My study shows neuronal FMRP interacts with BMPR pMad and InR pAkt signaling to intercellularly direct glial endolysosome activity by mediating neuronal phagocytotic signals Prtp and APPL (Song and Broadie, 2023). The FMRP

translational regulator restricts bound *mad* transcripts to limit transcription factor pMad levels, which, in turn, controls InR-pAkt signaling for the expression of Prtp and APPL (Song and Broadie, 2023). I surprisingly discovered that reducing neuronal FMRP and pMad both lead to increased pAkt levels to result in a phenocopy of PDF-Tri neuron removal defects (Song and Broadie, 2023). Genetically correcting pAkt levels in neuronal *mad* RNAi background restores normal neuronal clearance. Finally, I found that reducing neuronal FMRP, pMad, and Prtp all cause an impaired glial endolysosome response, demonstrating a direct link between the neuronal FMRP-dependent signaling and glial phagocytosis function (Song and Broadie, 2023). However, numerous important questions in this research remain to be addressed in the future.

4.3.1 Mechanism of neuronal pMad inhibition of pAkt signaling

Based on previous chromatin immunoprecipitation (ChIP) sequencing results for pMad (Deignan et al., 2016), we tested whether pMad is a positive transcription factor for the InR signaling pathway. Previous sequencing shows pMad binds both InR and Akt DNA (Deignan et al., 2016), but I did not obtain significant differences in either Akt transcript or protein levels with neuronal *mad* RNAi, suggesting pMad may play no roles in Akt transcription and translation processes (Figure 4.4). However, I did demonstrate loss of neuronal pMad increases pAkt levels (Song and Broadie, 2023), suggesting pMad regulates Akt phosphorylation via an unknown mechanism. When exploring the mechanism of protein accumulation it is always critical to consider "how it is produced" and "how it is degraded". Thus, testing if pMad regulates the activity of Akt phosphorylation kinases and phosphatases, as well as Akt protein degradation, will be important directions for future studies. My studies indicate no change in Akt protein levels with pMad knockdown (Figure 4.4). However, downstream of InR signaling, 3-phosphoinositide-

dependent kinases (PDKs) and phosphatidylinositol 3-kinase (PI3K) reportedly phosphorylates different Akt residues to activate signal transduction (Cicenas, 2008; Hemmings and Restuccia, 2012; Yu and Cui, 2016), while numerous phosphatases, including Protein Phosphatase 2A (PP2A) (Kim et al., 2009) and PH domain leucine-rich repeat protein phosphatase (PHLPP) (Gao et al., 2005), can directly remove phosphates from pAkt to terminate signal transduction. Regarding Akt protein degradation, several E3 ubiquitin ligases (e.g. neural precursor cell expressed developmentally down-regulated protein 4; NEDD4) (Fan et al., 2013), directly attach ubiquitin to pAkt for proteasomal degradation. It is therefore important to test the direct/indirect pMad modulation of these pathways to determine the mechanism of pAkt inhibition.

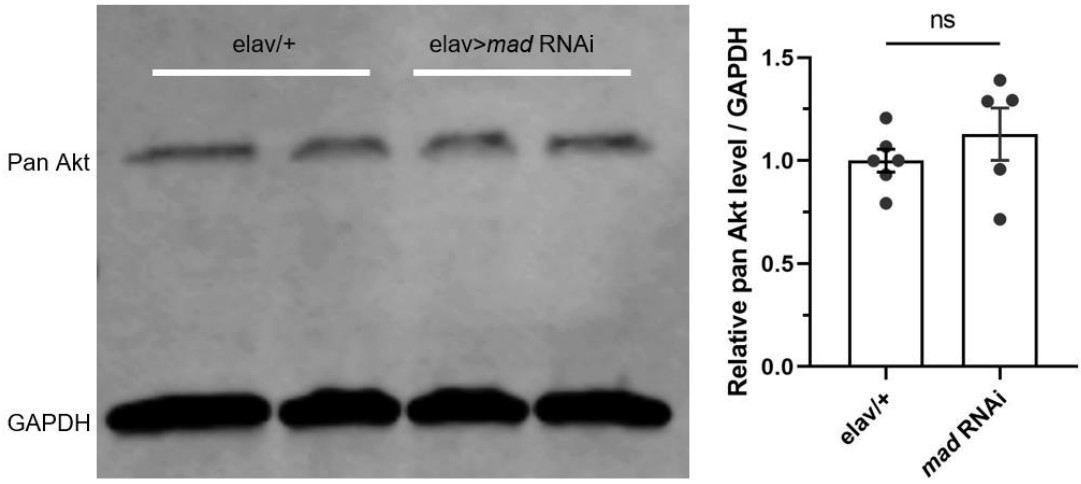

Figure 4.4 pMad plays no detectable roles in modulating Akt protein levels in the brain.

Western blot measurement indicates knockdown of neuronal pMad signaling does not significantly change pan Akt protein levels in whole brain lysates.

4.3.2 *Drosophila* APPL roles in glial engulfment in the FXS condition

Amyloid Precursor Protein (APP) is a type I single-transmembrane protein with a large extracellular N-terminus and a relatively short intracellular C-terminal domain (Coburger et al., 2013; Müller and Zheng, 2012). APP has three enzymatic cleavage sites that are processed by α-, β- and γ-secretases (Chow et al., 2010), which allow generation of multiple proteins with different cellular functions: secreted APPα (sAPPα), sAPPβ, amyloid-β (Aβ) oligomers, P3 domain, and APP intracellular domain (AICD) (Chow et al., 2010; De Strooper and Annaert, 2000). *Drosophila* has a single APP-like (APPL) homologue sharing just 30% homology at the amino acid level (Luo et al., 1990; Martin-Morris and White, 1990). In the *Drosophila* brain, an interesting recently defined function of the secreted APPL extracellular domain (sAPPL) is to intercellularly signal to glia for the guidance of neuronal clearance (Kessissoglou et al., 2020). In this study, sAPPL is engulfed by glia to maintain the expression of the Draper phagocytotic receptor during the clearance of injured olfactory neurons (Kessissoglou et al., 2020). Inspired by this report, we tested APPL expression with *dfmr1* null mutants and neuron-targeted *dfmr1* RNAi. Both exhibit delayed PDF-Tri neuron clearance in juvenile brains (Song and Broadie, 2023), and I predicted decreased APPL levels. With qPCR and Western blots, I found the APPL level is indeed reduced with neuronal *dfmr1* RNAi as hypothesized (Song and Broadie, 2023). Surprisingly, the global *dfmr1* mutant shows increased APPL transcript levels (Figure 4.5), suggesting FMRP-dependent APPL expression varies in different cells. Similar apparent conflicting results have been reported in the differently aged mouse FXS model and in cultured neurons (Westmark, 2019). Previous studies show APP levels substantially higher in juvenile mouse $Fmr1^{KO}$ cultured primary neurons versus controls (Westmark and Malter, 2007), but no significant changes in whole brain lysates (Pasciuto et al., 2015). In adult $Fmr1^{KO}$ mice, no significant difference in brain APP levels is apparent in the

hippocampus, cortex or cerebellum (Westmark et al., 2010). Another group of studies indicate decreased APP levels in cultured *Fmr1*^{KO} cortical neurons with antibody labeling and stable isotope labeling by amino acids in cell culture (SILAC) (Liao et al., 2008; Pasciuto et al., 2015). Taken together, it is important to continue exploring different functions of full-length APP and its cleaved segments in neuron-to-glia communication within different time windows and neuron types.

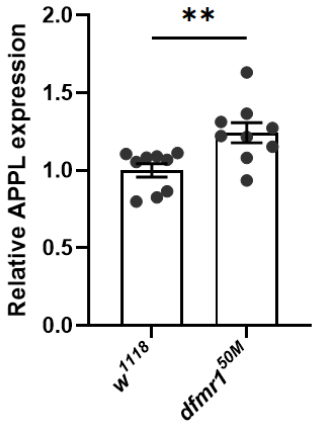

Figure 4.5 The *dfmr1* null mutant shows a significant increased *appl* mRNA level.

Statistics: unpaired Student's t-test shown in mean ± s.e.m. (*dfmr1*^{50M} 1.243±0.065 vs. *w*^{1118} 1.00±0.043, p=0.1919).

4.3.3 Other FMRP-dependent glial phagocytotic signals

To induce glia engulfment, released ligands bind phagocytotic receptors to activate glial intracellular signaling (MacDonald et al., 2006). The widely reported *Drosophila* phagocytotic receptor is Draper (MacDonald et al., 2006; Musashe et al., 2016) with two reported ligands, a protein Pretaporter (Kuraishi et al., 2009) and a phospholipid Phosphatidylserine (Kurematsu et al., 2022). However, Six-microns-under (SIMU) is reportedly another glial transmembrane

phagocytotic receptor that binds phosphatidylserine exposed on neuronal surfaces (Kurant et al., 2008). Both Draper and SIMU are expressed in multiple highly phagocytotic cell types, with conserved functional domains with Cell death abnormality protein 1 (CED-1), the first reported glial phagocytotic receptor in *C. elegans* (Zhou et al., 2001), as well as the human Scavenger Receptor from Endothelial Cells (SREC) (Adachi et al., 1997). Their extracellular N-termini contain Nimrod (NIM) repeats consisting of Elastin Microfibril Interfacer (EMI)-like domain that has a highly conserved CCxGY motif, and four Epidermal Growth Factor (EGF) domains with highly stereotyped spacing of Cys residues, which all have showed functions in phagocytosis (Kurant et al., 2008).

While numerous studies focus on the consequential signaling cascades of these identified receptors binding apoptotic signaling ligands, I am still curious if other type of ligands and glial receptors are involved in glial engulfment. In mice, an InR deficiency in astrocyte glia leads to aberrant neuronal circuit connectivity (Rhea and Banks, 2019). In *Drosophila*, glial *InR* RNAi blocks the clearance of PDF-Tri neurons and injured neuron removal is significantly delayed (Musashe et al., 2016; Vita et al., 2021). It has been suggested that neuronal insulin-like peptide (ILP) signaling to glial InRs is required to drive glial phagocytosis. However, it is not clear if the neuronal-secreted ILP signal belongs to a “find me” or “eat me” signal activating glial InRs. Other transcellular signaling pathways also possibly regulate glial activity. For example, Wnt/β-catenin signaling plays a central role in the response of astrocyte and microglia to neuroinflammation, neural mitochondrial dysfunction, dopaminergic neuroprotection, and oxidative stress (Marchetti, 2020). It will be important to test the function of glial Frizzled receptors for developmental neuron remodeling.

In the FXS condition, I have summarized recent evidence that FMRP interacts with insulin, BMP and Wnt signaling network to modulate synapse formation, neuron-to-glia communication, and neuronal circuit remodeling (Song and Broadie, 2022). Most of reported mechanisms regarding FMRP-dependent regulation heavily relys on protein-RNA interactions from the abundant FMRP candidate RNA targets. For example, this dissertation provides solid evidence that FMRP binds *mad* transcripts to restrict the level of pMad, a downstream molecule in BMP signaling pathway, which, in turn, controls insulin signaling for "eat me" Prtp expression (Song and Broadie, 2023). In mice, FMRP binds BMPR2 mRNA (*Drosophila* Wit homolog) to inhibit full-length isoform translation, thus causing accumulation of the noncanonical BMP pathway component Lin11/Isl1/Mec3 domain kinase 1 (LIMK1) within neurons (Kashima et al., 2016). It would be intriguing to map the full FMRP-RNA interaction network for BMP, insulin and Wnt signaling in the release of phagocytotic signals and synthesis of phagocytotic receptors. However, FMRP may also regulate the translation of proteins that are required for neuron-glia crosstalk via either direct or indirect protein-protein interactions. Many known FMRP-interacting proteins are RNA-binding proteins such as Caprin-1, NUFIP2, and FXRs (Bonaccorso et al., 2015). It will be important to profile phagocytotic signaling regulation targeted by FMRP RNA-binding partners with related mutants.

4.3.4 The role of mitochondria in neuron-to-glia crosstalk within FXS

Mitochondria play important roles in maintaining cellular function and tissue homeostasis during development. In developmental brains, mitochondria provide energy and metabolites to regulate survival and death for both neurons and glia, whose intercellular interaction is essential to prevent brain inflammation and aberrant circuitry remodeling (Song and Broadie, 2023). In the

FXS, loss of FMRP in the developmental murine forebrain induces futile proton cycling and deficiency in coenzyme Q (CoQ), a lipophilic molecule that carries electrons from mitochondrial Complexes I and II to Complexes III, thus causing aberrant density of dendritic spines in the young adult (Griffiths et al., 2020). This study suggests a possible hint that dysregulated mitochondria in either neurons or glia results in defects of neuronal pruning underlying FXS. However, it is not clear how this mitochondrial deficiency leads to abnormal dendritic pruning and if any transcellular signaling network fluctuates between neurons and glia. Studies also show partial of mitochondrial DNA (mtDNA)-encoded tRNAs and rRNAs are potentially transported into nucleus to coordinate nuclear gene transcription for cellular response (Amuthan et al., 2001; Gitschlag et al., 2016; Rashad et al., 2020). It is therefore possible that dysfunctional mitochondria in FXS intracellularly mis-regulate nuclear gene expression that is essential for neuronal morphology and neuron-glia crosstalk. Yet, researchers still lack solid proof to show these re-located mitochondrial small RNAs are physically delivered through mitochondrial membrane. It may be wise to focus on metabolism adaptation and lipid droplets accumulation that all related to mitochondrial reactive oxygen species (ROS) signaling for neuron-glia transcellular communication within a FXS picture.

References

Adachi, H., Tsujimoto, M., Arai, H. and Inoue, K. (1997). Expression Cloning of a Novel Scavenger Receptor from Human Endothelial Cells. *Journal of Biological Chemistry* **272**, 31217–31220.

Affolter, M. and Basler, K. (2007). The Decapentaplegic morphogen gradient: from pattern formation to growth regulation. *Nat Rev Genet* **8**, 663–674.

Almeida, M. S. and Bray, S. J. (2005). Regulation of post-embryonic neuroblasts by Drosophila Grainyhead. *Mechanisms of Development* **122**, 1282–1293.

Amuthan, G., Biswas, G., Zhang, S.-Y., Klein-Szanto, A., Vijayasarathy, C. and Avadhani, N. G. (2001). Mitochondria-to-nucleus stress signaling induces phenotypic changes, tumor progression and cell invasion. *EMBO J* **20**, 1910–1920.

Armstrong, A. R. and Drummond-Barbosa, D. (2018). Insulin signaling acts in adult adipocytes via GSK-3β and independently of FOXO to control Drosophila female germline stem cell numbers. *Dev Biol* **440**, 31–39.

Ascano, M., Mukherjee, N., Bandaru, P., Miller, J. B., Nusbaum, J. D., Corcoran, D. L., Langlois, C., Munschauer, M., Dewell, S., Hafner, M., et al. (2012). FMRP targets distinct mRNA sequence elements to regulate protein expression. *Nature* **492**, 382–386.

Ashley, C. T., Wilkinson, K. D., Reines, D. and Warren, S. T. (1993). FMR1 Protein: Conserved RNP Family Domains and Selective RNA Binding. *Science* **262**, 563–566.

Atasoy, D., Ertunc, M., Moulder, K. L., Blackwell, J., Chung, C., Su, J. and Kavalali, E. T. (2008). Spontaneous and Evoked Glutamate Release Activates Two Populations of NMDA Receptors with Limited Overlap. *J. Neurosci.* **28**, 10151–10166.

Atwood, H. L., Govind, C. K. and Wu, C.-F. (1993). Differential ultrastructure of synaptic terminals on ventral longitudinal abdominal muscles in Drosophila larvae. *Journal of Neurobiology* **24**, 1008–1024.

Awasaki, T., Huang, Y., O'Connor, M. B. and Lee, T. (2011). Glia instruct developmental neuronal remodeling through TGF-βsignaling. *Nat Neurosci* **14**, 821–823.

Bakshi, A., Sipani, R., Ghosh, N. and Joshi, R. (2020). Sequential activation of Notch and Grainyhead gives apoptotic competence to Abdominal-B expressing larval neuroblasts in Drosophila Central nervous system. *PLOS Genetics* **16**, e1008976.

Banerjee, S. and Barraud, P. (2014). Functions of double-stranded RNA-binding domains in nucleocytoplasmic transport. *RNA Biology* **11**, 1226–1232.

Bänziger, C., Soldini, D., Schütt, C., Zipperlen, P., Hausmann, G. and Basler, K. (2006). Wntless, a conserved membrane protein dedicated to the secretion of Wnt proteins from signaling cells. *Cell* **125**, 509–522.

Barbee, S. A., Estes, P. S., Cziko, A.-M., Hillebrand, J., Luedeman, R. A., Coller, J. M., Johnson, N., Howlett, I. C., Geng, C., Ueda, R., et al. (2006). Staufen- and FMRP-Containing Neuronal RNPs Are Structurally and Functionally Related to Somatic P Bodies. *Neuron* **52**, 997–1009.

Bardoni, B., Schenck, A. and Louis Mandel, J. (1999). A Novel RNA-binding Nuclear Protein That Interacts With the Fragile X Mental Retardation (FMR1) Protein. *Human Molecular Genetics* **8**, 2557–2566.

Bardoni, B., Castets, M., Huot, M.-E., Schenck, A., Adinolfi, S., Corbin, F., Pastore, A., Khandjian, E. W. and Mandel, J.-L. (2003). 82-FIP, a novel FMRP (Fragile X Mental Retardation Protein) interacting protein, shows a cell cycle-dependent intracellular localization. *Human Molecular Genetics* **12**, 1689–1698.

Bartscherer, K., Pelte, N., Ingelfinger, D. and Boutros, M. (2006). Secretion of Wnt Ligands Requires Evi, a Conserved Transmembrane Protein. *Cell* **125**, 523–533.

Bassell, G. J. and Warren, S. T. (2008). Fragile X Syndrome: Loss of Local mRNA Regulation Alters Synaptic Development and Function. *Neuron* **60**, 201–214.

Bernaus, A., Blanco, S. and Sevilla, A. (2020). Glia Crosstalk in Neuroinflammatory Diseases. *Frontiers in Cellular Neuroscience* **14**,.

Birge, R. B. and Ucker, D. S. (2008). Innate apoptotic immunity: the calming touch of death. *Cell Death Differ* **15**, 1096–1102.

Bittern, J., Pogodalla, N., Ohm, H., Brüser, L., Kottmeier, R., Schirmeier, S. and Klämbt, C. (2021). Neuron–glia interaction in the Drosophila nervous system. *Developmental Neurobiology* **81**, 438–452.

Blackwell, E. and Ceman, S. (2011). A new regulatory function of the region proximal to the RGG box in the Fragile X mental retardation protein. *Journal of Cell Science* **124**, 3060–3065.

Bogdanik, L., Mohrmann, R., Ramaekers, A., Bockaert, J., Grau, Y., Broadie, K. and Parmentier, M.-L. (2004). The Drosophila Metabotropic Glutamate Receptor DmGluRA Regulates Activity-Dependent Synaptic Facilitation and Fine Synaptic Morphology. *J. Neurosci.* **24**, 9105–9116.

Bolduc, F. V., Bell, K., Cox, H., Broadie, K. and Tully, T. (2008). Excess protein synthesis in Drosophila Fragile X mutants impairs long-term memory. *Nat Neurosci* **11**, 1143–1145.

Bonaccorso, C. m., Spatuzza, M., Di Marco, B., Gloria, A., Barrancotto, G., Cupo, A., Musumeci, S. a., D'Antoni, S., Bardoni, B. and Catania, M. v. (2015). Fragile X mental retardation protein (FMRP) interacting proteins exhibit different expression patterns during development. *International Journal of Developmental Neuroscience* **42**, 15–23.

Bonnet-Magnaval, F. (2016). Hypoxia and ER stress promote Staufen1 expression through an alternative translation mechanism. *Biochemical and Biophysical Research Communications* 7.

Boulanger, A. and Dura, J.-M. (2022). Neuron-glia crosstalk in neuronal remodeling and degeneration: Neuronal signals inducing glial cell phagocytic transformation in Drosophila. *BioEssays* **44**, 2100254.

Boulanger, A., Thinat, C., Züchner, S., Fradkin, L. G., Lortat-Jacob, H. and Dura, J.-M. (2021). Axonal chemokine-like Orion induces astrocyte infiltration and engulfment during mushroom body neuronal remodeling. *Nat Commun* **12**, 1849.

Brink, D. L., Gilbert, M., Xie, X., Petley-Ragan, L. and Auld, V. J. (2012). Glial Processes at the Drosophila Larval Neuromuscular Junction Match Synaptic Growth. *PLOS ONE* **7**, e37876.

Brown, W. T., Jenkins, E. C., Cohen, I. L., Fisch, G. S., Wolf-Schein, E. G., Gross, A., Waterhouse, L., Fein, D., Mason-Brothers, A. and Ritvo, E. (1986). Fragile X and autism: a multicenter survey. *Am J Med Genet* **23**, 341–352.

Bu, B. and Zhang, L. (2017). A New Link Between Insulin Signaling and Fragile X Syndrome. *Neurosci. Bull.* **33**, 118–120.

Calderon, M. R., Mori, M., Kauwe, G., Farnsworth, J., Ulian-Benitez, S., Maksoud, E., Shore, J. and Haghighi, A. P. (2022). Delta/Notch signaling in glia maintains motor nerve barrier function and synaptic transmission by controlling matrix metalloproteinase expression. *Proceedings of the National Academy of Sciences* **119**, e2110097119.

Cammarata, G. M., Bearce, E. A. and Lowery, L. A. (2016). Cytoskeletal social networking in the growth cone: How +TIPs mediate microtubule-actin cross-linking to drive axon outgrowth and guidance. *Cytoskeleton* **73**, 461–476.

Chan, Y.-B., Alekseyenko, O. V. and Kravitz, E. A. (2015). Optogenetic Control of Gene Expression in Drosophila. *PLOS ONE* **10**, e0138181.

Chan, J. C., Morgan, C. P., Adrian Leu, N., Shetty, A., Cisse, Y. M., Nugent, B. M., Morrison, K. E., Jašarević, E., Huang, W., Kanyuch, N., et al. (2020). Reproductive tract extracellular vesicles are sufficient to transmit intergenerational stress and program neurodevelopment. *Nat Commun* **11**, 1499.

Cheever, A., Blackwell, E. and Ceman, S. (2010). Fragile X protein family member FXR1P is regulated by microRNAs. *RNA* **16**, 1530–1539.

Chen, K., Merino, C., Sigrist, S. J. and Featherstone, D. E. (2005). The 4.1 Protein Coracle Mediates Subunit-Selective Anchoring of Drosophila Glutamate Receptors to the Postsynaptic Actin Cytoskeleton. *J. Neurosci.* **25**, 6667–6675.

Chen, S., Kaneko, S., Ma, X., Chen, X., Ip, Y. T., Xu, L. and Xie, T. (2010). Lissencephaly-1 controls germline stem cell self-renewal through modulating bone morphogenetic protein signaling and niche adhesion. *Proceedings of the National Academy of Sciences* **107**, 19939–19944.

Chou, V. T., Johnson, S. A. and Van Vactor, D. (2020). Synapse development and maturation at the drosophila neuromuscular junction. *Neural Development* **15**, 11.

Chow, V. W., Mattson, M. P., Wong, P. C. and Gleichmann, M. (2010). An Overview of APP Processing Enzymes and Products. *Neuromolecular Med* **12**, 1–12.

Chu, J.-F., Majumder, P., Chatterjee, B., Huang, S.-L. and Shen, C.-K. J. (2019). TDP-43 Regulates Coupled Dendritic mRNA Transport-Translation Processes in Co-operation with FMRP and Staufen1. *Cell Reports* **29**, 3118-3133.e6.

Cicenas, J. (2008). The Potential Role of Akt Phosphorylation in Human Cancers. *Int J Biol Markers* **23**, 1–9.

Clarke, G. L. 2, Chen, J. 2 and Nishimune, H. (2012). Presynaptic Active Zone Density during Development and Synaptic Plasticity. *Front. Mol. Neurosci.* **5**,.

Coburger, I., Dahms, S. O., Roeser, D., Gührs, K.-H., Hortschansky, P. and Than, M. E. (2013). Analysis of the Overall Structure of the Multi-Domain Amyloid Precursor Protein (APP). *PLOS ONE* **8**, e81926.

Coffee, R. L., Tessier, C. R., Woodruff, E. A. and Broadie, K. (2010). Fragile X mental retardation protein has a unique, evolutionarily conserved neuronal function not shared with FXR1P or FXR2P. *Dis Model Mech* **3**, 471–485.

Comery, T. A., Harris, J. B., Willems, P. J., Oostra, B. A., Irwin, S. A., Weiler, I. J. and Greenough, W. T. (1997). Abnormal dendritic spines in fragile X knockout mice: Maturation and pruning deficits. *PNAS* **94**, 5401–5404.

Connor, S. A., Hoeffer, C. A., Klann, E. and Nguyen, P. V. (2011). Fragile X mental retardation protein regulates heterosynaptic plasticity in the hippocampus. *Learn Mem* **18**, 207–220.

Courtney, N. A., Bao, H., Briguglio, J. S. and Chapman, E. R. (2019). Synaptotagmin 1 clamps synaptic vesicle fusion in mammalian neurons independent of complexin. *Nat Commun* **10**, 4076.

Crawford, D. C., Acuña, J. M. and Sherman, S. L. (2001). FMR1 and the fragile X syndrome: human genome epidemiology review. *Genet Med* **3**, 359–371.

Currie, D. A., Truman, J. W. and Burden, S. J. (1995). Drosophila glutamate receptor RNA expression in embryonic and larval muscle fibers. *Developmental Dynamics* **203**, 311–316.

Cziko, A.-M. J., McCann, C. T., Howlett, I. C., Barbee, S. A., Duncan, R. P., Luedemann, R., Zarnescu, D., Zinsmaier, K. E., Parker, R. R. and Ramaswami, M. (2009). Genetic Modifiers of dFMR1 Encode RNA Granule Components in Drosophila. *Genetics* **182**, 1051–1060.

Dalva, M. B. (2010). Remodeling of inhibitory synaptic connections in developing ferret visual cortex. *Neural Development* **5**, 5.

Damisah, E. C., Hill, R. A., Rai, A., Chen, F., Rothlin, C. V., Ghosh, S. and Grutzendler, J. (2020). Astrocytes and microglia play orchestrated roles and respect phagocytic territories during neuronal corpse removal in vivo. *Science Advances* **6**, eaba3239.

D'Annessa, I., Cicconardi, F. and Di Marino, D. (2019). Handling FMRP and its molecular partners: Structural insights into Fragile X Syndrome. *Progress in Biophysics and Molecular Biology* **141**, 3–14.

Das, J., Xu, S., Pany, S., Guillory, A., Shah, V. and Roman, G. W. (2013). The pre-synaptic Munc13-1 binds alcohol and modulates alcohol self-administration in Drosophila. *Journal of Neurochemistry* **126**, 715–726.

Das, T. P., Suman, S., Alatassi, H., Ankem, M. K. and Damodaran, C. (2016). Inhibition of AKT promotes FOXO3a-dependent apoptosis in prostate cancer. *Cell Death Dis* **7**, e2111–e2111.

De Strooper, B. and Annaert, W. (2000). Proteolytic processing and cell biological functions of the amyloid precursor protein. *Journal of Cell Science* **113**, 1857–1870.

Dear, M. L., Dani, N., Parkinson, W., Zhou, S. and Broadie, K. (2016). Two classes of matrix metalloproteinases reciprocally regulate synaptogenesis. *Development* **143**, 75–87.

Dear, M. L., Shilts, J. and Broadie, K. (2017). Neuronal activity drives FMRP- and HSPG-dependent matrix metalloproteinase function required for rapid synaptogenesis. *Sci Signal* **10**, eaan3181.

Deignan, L., Pinheiro, M. T., Sutcliffe, C., Saunders, A., Wilcockson, S. G., Zeef, L. A. H., Donaldson, I. J. and Ashe, H. L. (2016). Regulation of the BMP Signaling-Responsive Transcriptional Network in the Drosophila Embryo. *PLOS Genetics* **12**, e1006164.

Dejanovic, B., Wu, T., Tsai, M.-C., Graykowski, D., Gandham, V. D., Rose, C. M., Bakalarski, C. E., Ngu, H., Wang, Y., Pandey, S., et al. (2022). Complement C1q-dependent excitatory and inhibitory synapse elimination by astrocytes and microglia in Alzheimer's disease mouse models. *Nat Aging* **2**, 837–850.

del Castillo, J. and Katz, B. (1954). Quantal components of the end-plate potential. *J Physiol* **124**, 560–573.

del Puerto, A., Wandosell, F. and Garrido, J. J. (2013). Neuronal and glial purinergic receptors functions in neuron development and brain disease. *Frontiers in Cellular Neuroscience* **7**,.

Demarque, M., Represa, A., Becq, H., Khalilov, I., Ben-Ari, Y. and Aniksztejn, L. (2002). Paracrine Intercellular Communication by a Ca2+- and SNARE-Independent Release of GABA and Glutamate Prior to Synapse Formation. *Neuron* **36**, 1051–1061.

Dhara, M., Mantero Martinez, M., Makke, M., Schwarz, Y., Mohrmann, R. and Bruns, D. (2020). Synergistic actions of v-SNARE transmembrane domains and membrane-curvature modifying lipids in neurotransmitter release. *eLife* **9**, e55152.

DiAntonio, A., Petersen, S. A., Heckmann, M. and Goodman, C. S. (1999). Glutamate Receptor Expression Regulates Quantal Size and Quantal Content at the Drosophila Neuromuscular Junction. *J. Neurosci.* **19**, 3023–3032.

Didiot, M.-C., Subramanian, M., Flatter, E., Mandel, J.-L. and Moine, H. (2009). Cells Lacking the Fragile X Mental Retardation Protein (FMRP) have Normal RISC Activity but Exhibit Altered Stress Granule Assembly. *MBoC* **20**, 428–437.

Doll, C. A. and Broadie, K. (2015). Activity-dependent FMRP requirements in development of the neural circuitry of learning and memory. *Development* **142**, 1346–1356.

Doll, C. A., Vita, D. J. and Broadie, K. (2017). Fragile X Mental Retardation Protein Requirements in Activity-Dependent Critical Period Neural Circuit Refinement. *Curr Biol* **27**, 2318-2330.e3.

Dong, Q., Zavortink, M., Froldi, F., Golenkina, S., Lam, T. and Cheng, L. Y. (2021). Glial Hedgehog signalling and lipid metabolism regulate neural stem cell proliferation in Drosophila. *EMBO reports* **22**, e52130.

Donnard, E., Shu, H. and Garber, M. (2022). Single cell transcriptomics reveals dysregulated cellular and molecular networks in a fragile X syndrome model. *PLOS Genetics* **18**, e1010221.

Drozd, M., Bardoni, B. and Capovilla, M. (2018). Modeling Fragile X Syndrome in Drosophila. *Front Mol Neurosci* **11**, 124.

Dugré-Brisson, S., Elvira, G., Boulay, K., Chatel-Chaix, L., Mouland, A. J. and DesGroseillers, L. (2005). Interaction of Staufen1 with the 5′ end of mRNA facilitates translation of these RNAs. *Nucleic Acids Res* **33**, 4797–4812.

Dutriaux, A., Godart, A., Brachet, A. and Silber, J. (2013). The Insulin Receptor Is Required for the Development of the Drosophila Peripheral Nervous System. *PLOS ONE* **8**, e71857.

Ellis, J. E., Parker, L., Cho, J. and Arora, K. (2010). Activin signaling functions upstream of Gbb to regulate synaptic growth at the Drosophila neuromuscular junction. *Developmental Biology* **342**, 121–133.

Fan, C.-D., Lum, M. A., Xu, C., Black, J. D. and Wang, X. (2013). Ubiquitin-dependent Regulation of Phospho-AKT Dynamics by the Ubiquitin E3 Ligase, NEDD4-1, in the Insulin-like Growth Factor-1 Response *. *Journal of Biological Chemistry* **288**, 1674–1684.

Fazakerley, D. J., Krycer, J. R., Kearney, A. L., Hocking, S. L. and James, D. E. (2019). Muscle and adipose tissue insulin resistance: malady without mechanism? *Journal of Lipid Research* **60**, 1720–1732.

Featherstone, D. E., Rushton, E., Rohrbough, J., Liebl, F., Karr, J., Sheng, Q., Rodesch, C. K. and Broadie, K. (2005). An Essential Drosophila Glutamate Receptor Subunit That Functions in Both Central Neuropil and Neuromuscular Junction. *J. Neurosci.* **25**, 3199–3208.

Fernandez, M. P., Pettibone, H. L., Bogart, J. T., Roell, C. J., Davey, C. E., Pranevicius, A., Huynh, K. V., Lennox, S. M., Kostadinov, B. S. and Shafer, O. T. (2020). Sites of Circadian Clock Neuron Plasticity Mediate Sensory Integration and Entrainment. *Current Biology* **30**, 2225-2237.e5.

Fields, R. D., Woo, D. H. and Basser, P. J. (2015). Glial Regulation of the Neuronal Connectome through Local and Long-Distant Communication. *Neuron* **86**, 374–386.

Flockhart, I., Booker, M., Kiger, A., Boutros, M., Armknecht, S., Ramadan, N., Richardson, K., Xu, A., Perrimon, N. and Mathey-Prevot, B. (2006). FlyRNAi: the Drosophila RNAi screening center database. *Nucleic Acids Res* **34**, D489-494.

Folch, J., Ettcheto, M., Busquets, O., Sánchez-López, E., Castro-Torres, R. D., Verdaguer, E., Manzine, P. R., Poor, S. R., García, M. L., Olloquequi, J., et al. (2018). The Implication of the Brain Insulin Receptor in Late Onset Alzheimer's Disease Dementia. *Pharmaceuticals* **11**, 11.

Fouquet, W., Owald, D., Wichmann, C., Mertel, S., Depner, H., Dyba, M., Hallermann, S., Kittel, R. J., Eimer, S. and Sigrist, S. J. (2009). Maturation of active zone assembly by Drosophila Bruchpilot. *Journal of Cell Biology* **186**, 129–145.

Fox, M. E., Chandra, R., Menken, M. S., Larkin, E. J., Nam, H., Engeln, M., Francis, T. C. and Lobo, M. K. (2020). Dendritic remodeling of D1 neurons by RhoA/Rho-kinase mediates depression-like behavior. *Mol Psychiatry* **25**, 1022–1034.

Franciscovich, A. L., Mortimer, A. D. V., Freeman, A. A., Gu, J. and Sanyal, S. (2008). Overexpression Screen in Drosophila Identifies Neuronal Roles of GSK-3β/shaggy as a Regulator of AP-1-Dependent Developmental Plasticity. *Genetics* **180**, 2057–2071.

Franco, B., Bogdanik, L., Bobinnec, Y., Debec, A., Bockaert, J., Parmentier, M.-L. and Grau, Y. (2004). Shaggy, the Homolog of Glycogen Synthase Kinase 3, Controls Neuromuscular Junction Growth in Drosophila. *J. Neurosci.* **24**, 6573–6577.

Friedman, S. H., Dani, N., Rushton, E. and Broadie, K. (2013). Fragile X mental retardation protein regulates trans-synaptic signaling in Drosophila. *Dis Model Mech* **6**, 1400–1413.

Fuchs, Y. and Steller, H. (2011). Programmed Cell Death in Animal Development and Disease. *Cell* **147**, 742–758.

Fuentes-Medel, Y., Ashley, J., Barria, R., Maloney, R., Freeman, M. and Budnik, V. (2012). Integration of a Retrograde Signal during Synapse Formation by Glia-Secreted TGF-β Ligand. *Current Biology* **22**, 1831–1838.

Fulterer, A., Andlauer, T. F. M., Ender, A., Maglione, M., Eyring, K., Woitkuhn, J., Lehmann, M., Matkovic-Rachid, T., Geiger, J. R. P., Walter, A. M., et al. (2018). Active Zone Scaffold Protein Ratios Tune Functional Diversity across Brain Synapses. *Cell Rep* **23**, 1259–1274.

Furic, L., Maher-Laporte, M. and DesGroseillers, L. (2008). A genome-wide approach identifies distinct but overlapping subsets of cellular mRNAs associated with Staufen1- and Staufen2-containing ribonucleoprotein complexes. *RNA* **14**, 324–335.

Gafner, L., Dalessi, S., Escher, E., Pyrowolakis, G., Bergmann, S. and Basler, K. (2013). Manipulating the Sensitivity of Signal-Induced Repression: Quantification and Consequences of Altered Brinker Gradients. *PLOS ONE* **8**, e71224.

Galbiati, M., Crippa, V., Rusmini, P., Cristofani, R., Messi, E., Piccolella, M., Tedesco, B., Ferrari, V., Casarotto, E., Chierichetti, M., et al. (2020). Multiple Roles of Transforming Growth Factor Beta in Amyotrophic Lateral Sclerosis. *International Journal of Molecular Sciences* **21**, 4291.

Gallagher, E. J. and LeRoith, D. (2013). Insulin Mechanisms/Metabolic Actions. In *Encyclopedia of Biological Chemistry (Second Edition)* (ed. Lennarz, W. J.) and Lane, M. D.), pp. 602–607. Waltham: Academic Press.

Gao, T., Furnari, F. and Newton, A. C. (2005). PHLPP: a phosphatase that directly dephosphorylates Akt, promotes apoptosis, and suppresses tumor growth. *Mol Cell* **18**, 13–24.

Garber, K. B., Visootsak, J. and Warren, S. T. (2008). Fragile X syndrome. *Eur J Hum Genet* **16**, 666–672.

Gardiol, A. and St Johnston, D. (2014). Staufen targets coracle mRNA to Drosophila neuromuscular junctions and regulates GluRIIA synaptic accumulation and bouton number. *Dev Biol* **392**, 153–167.

Gatto, C. L. and Broadie, K. (2009). The Fragile X Mental Retardation Protein in Circadian Rhythmicity and Memory Consolidation. *Mol Neurobiol* **39**, 107–129.

Gatto, C. L. and Broadie, K. (2011). Fragile X mental retardation protein is required for programmed cell death and clearance of developmentally-transient peptidergic neurons. *Dev Biol* **356**, 291–307.

Gil-Ranedo, J., Gonzaga, E., Jaworek, K. J., Berger, C., Bossing, T. and Barros, C. S. (2019). STRIPAK Members Orchestrate Hippo and Insulin Receptor Signaling to Promote Neural Stem Cell Reactivation. *Cell Reports* **27**, 2921-2933.e5.

Gitschlag, B. L., Kirby, C. S., Samuels, D. C., Gangula, R. D., Mallal, S. A. and Patel, M. R. (2016). Homeostatic Responses Regulate Selfish Mitochondrial Genome Dynamics in C. elegans. *Cell Metab* **24**, 91–103.

Gögel, S., Wakefield, S., Tear, G., Klämbt, C. and Gordon-Weeks, P. R. (2006). The Drosophila microtubule associated protein Futsch is phosphorylated by Shaggy/Zeste-white 3 at an homologous GSK3beta phosphorylation site in MAP1B. *Mol Cell Neurosci* **33**, 188–199.

Golovin, R. M., Vest, J., Vita, D. J. and Broadie, K. (2019). Activity-Dependent Remodeling of Drosophila Olfactory Sensory Neuron Brain Innervation during an Early-Life Critical Period. *J. Neurosci.* **39**, 2995–3012.

Golovin, R. M., Vest, J. and Broadie, K. (2021). Neuron-Specific FMRP Roles in Experience-Dependent Remodeling of Olfactory Brain Innervation during an Early-Life Critical Period. *J. Neurosci.* **41**, 1218–1241.

Gomez, J. M., Wang, Y. and Riechmann, V. (2012). Tao controls epithelial morphogenesis by promoting Fasciclin 2 endocytosis. *J Cell Biol* **199**, 1131–1143.

Griffiths, K. K., Wang, A., Wang, L., Tracey, M., Kleiner, G., Quinzii, C. M., Sun, L., Yang, G., Perez-Zoghbi, J. F., Licznerski, P., et al. (2020). Inefficient thermogenic mitochondrial respiration due to futile proton leak in a mouse model of fragile X syndrome. *The FASEB Journal* **34**, 7404–7426.

Groemer, T. W. and Klingauf, J. (2007). Synaptic vesicles recycling spontaneously and during activity belong to the same vesicle pool. *Nat Neurosci* **10**, 145–147.

Groffen, A. J., Martens, S., Díez Arazola, R., Cornelisse, L. N., Lozovaya, N., de Jong, A. P. H., Goriounova, N. A., Habets, R. L. P., Takai, Y., Borst, J. G., et al. (2010). Doc2b is a high-affinity Ca2+ sensor for spontaneous neurotransmitter release. *Science* **327**, 1614–1618.

Gross, C. and Bassell, G. J. (2012). Excess Protein Synthesis in FXS Patient Lymphoblastoid Cells Can Be Rescued with a p110β-Selective Inhibitor. *Mol Med* **18**, 336–345.

Gu, T., Zhao, T. and Hewes, R. S. (2013). Insulin signaling regulates neurite growth during metamorphic neuronal remodeling. *Biology Open* **3**, 81–93.

Guangming, G., Junhua, G., Chenchen, Z., Yang, M. and Wei, X. (2020). Neurexin and Neuroligins Maintain the Balance of Ghost and Satellite Boutons at the Drosophila Neuromuscular Junction. *Frontiers in Neuroanatomy* **14**,.

Guggenheim, E. J., Khan, A., Pike, J., Chang, L., Lynch, I. and Rappoport, J. Z. (2016). Comparison of Confocal and Super-Resolution Reflectance Imaging of Metal Oxide Nanoparticles. *PLoS One* **11**, e0159980.

Guillen, R. X., Beckley, J. R., Chen, J.-S. and Gould, K. L. (2020). CRISPR-mediated gene targeting of CK1δ/ε leads to enhanced understanding of their role in endocytosis via phosphoregulation of GAPVD1. *Sci Rep* **10**, 6797.

Guy, A. T., Nagatsuka, Y., Ooashi, N., Inoue, M., Nakata, A., Greimel, P., Inoue, A., Nabetani, T., Murayama, A., Ohta, K., et al. (2015). Glycerophospholipid regulation of modality-specific sensory axon guidance in the spinal cord. *Science* **349**, 974–977.

Hagerman, R. J., Jackson III, A. W., Levitas, A., Rimland, B., Braden, M., Opitz, J. M. and Reynolds, J. F. (1986). An analysis of autism in fifty males with the fragile X syndrome. *American Journal of Medical Genetics* **23**, 359–374.

Hagerman, R. J., Berry-Kravis, E., Hazlett, H. C., Bailey, D. B., Moine, H., Kooy, R. F., Tassone, F., Gantois, I., Sonenberg, N., Mandel, J. L., et al. (2017). Fragile X syndrome. *Nat Rev Dis Primers* **3**, 1–19.

Hallam, S. J., Goncharov, A., McEwen, J., Baran, R. and Jin, Y. (2002). SYD-1, a presynaptic protein with PDZ, C2 and rhoGAP-like domains, specifies axon identity in C. elegans. *Nat Neurosci* **5**, 1137–1146.

Han, T. H., Dharkar, P., Mayer, M. L. and Serpe, M. (2015). Functional reconstitution of Drosophila melanogaster NMJ glutamate receptors. *PNAS* **112**, 6182–6187.

Han, T. H., Vicidomini, R., Ramos, C. I., Wang, Q., Nguyen, P., Jarnik, M., Lee, C.-H., Stawarski, M., Hernandez, R. X., Macleod, G. T., et al. (2020). Neto-α Controls Synapse Organization and Homeostasis at the Drosophila Neuromuscular Junction. *Cell Reports* **32**, 107866.

Hanani, M. and Spray, D. C. (2020). Emerging importance of satellite glia in nervous system function and dysfunction. *Nat Rev Neurosci* **21**, 485–498.

Hansen, R. S., Gartler, S. M., Scott, C. R., Chen, S. H. and Laird, C. D. (1992). Methylation analysis of CGG sites in the CpG island of the human FMR1 gene. *Hum Mol Genet* **1**, 571–578.

Harris, K. P. and Littleton, J. T. (2015). Transmission, Development, and Plasticity of Synapses. *Genetics* **201**, 345–375.

Harrison, N. J., Connolly, E., Gubieda, A. G., Yang, Z., Altenhein, B., Perez, M. L., Moreira, M., Sun, J. and Hidalgo, A. (2021). Regenerative neurogenic response from glia requires insulin-driven neuron-glia communication. *eLife*.

Hart, M. P. (2019). Stress-Induced Neuron Remodeling Reveals Differential Interplay Between Neurexin and Environmental Factors in Caenorhabditis elegans. *Genetics* **213**, 1415–1430.

Hemmings, B. A. and Restuccia, D. F. (2012). PI3K-PKB/Akt Pathway. *Cold Spring Harb Perspect Biol* **4**, a011189.

Heraud-Farlow, J. E. and Kiebler, M. A. (2014). The multifunctional Staufen proteins: conserved roles from neurogenesis to synaptic plasticity. *Trends in Neurosciences* **37**, 470–479.

Ho, C. H. and Treisman, J. E. (2020). Specific Isoforms of the Guanine-Nucleotide Exchange Factor dPix Couple Neuromuscular Synapse Growth to Muscle Growth. *Developmental Cell* **54**, 117-131.e5.

Hong, H., Zhao, K., Huang, S., Huang, S., Yao, A., Jiang, Y., Sigrist, S., Zhao, L. and Zhang, Y. Q. (2020). Structural Remodeling of Active Zones Is Associated with Synaptic Homeostasis. *J. Neurosci.* **40**, 2817–2827.

Hoover, K. M., Gratz, S. J., Qi, N., Herrmann, K. A., Liu, Y., Perry-Richardson, J. J., Vanderzalm, P. J., O'Connor-Giles, K. M. and Broihier, H. T. (2019). The calcium channel subunit α2δ-3 organizes synapses via an activity-dependent and autocrine BMP signaling pathway. *Nat Commun* **10**, 5575.

Horvath, P. M., Piazza, M. K., Monteggia, L. M. and Kavalali, E. T. (2020). Spontaneous and evoked neurotransmission are partially segregated at inhibitory synapses. *eLife* **9**, e52852.

Hu, Y.-B., Dammer, E. B., Ren, R.-J. and Wang, G. (2015). The endosomal-lysosomal system: from acidification and cargo sorting to neurodegeneration. *Translational Neurodegeneration* **4**, 18.

Huang, J., Reilein, A. and Kalderon, D. (2017). Yorkie and Hedgehog independently restrict BMP production in escort cells to permit germline differentiation in the Drosophila ovary. *Development* **144**, 2584–2594.

Huebschman, J. L., Corona, K. S., Guo, Y. and Smith, L. N. (2020). The Fragile X Mental Retardation Protein Regulates Striatal Medium Spiny Neuron Synapse Density and Dendritic Spine Morphology. *Frontiers in Molecular Neuroscience* **13**,.

Hutagalung, A. H. and Novick, P. J. (2011). Role of Rab GTPases in Membrane Traffic and Cell Physiology. *Physiological Reviews* **91**, 119–149.

Ikeno, T. and Nelson, R. J. (2015). Acute melatonin treatment alters dendritic morphology and circadian clock gene expression in the hippocampus of Siberian Hamsters. *Hippocampus* **25**, 142–148.

Ito, T. and Igaki, T. (2021). Yorkie drives Ras-induced tumor progression by microRNA-mediated inhibition of cellular senescence. *Science Signaling* **14**, eaaz3578.

Jäkel, S. and Dimou, L. (2017). Glial Cells and Their Function in the Adult Brain: A Journey through the History of Their Ablation. *Frontiers in Cellular Neuroscience* **11**,.

Jan, L. Y. and Jan, Y. N. (1982). Antibodies to horseradish peroxidase as specific neuronal markers in Drosophila and in grasshopper embryos. *Proc Natl Acad Sci U S A* **79**, 2700–2704.

Jiang, N., Rasmussen, J. P., Clanton, J. A., Rosenberg, M. F., Luedke, K. P., Cronan, M. R., Parker, E. D., Kim, H.-J., Vaughan, J. C., Sagasti, A., et al. (2019). A conserved morphogenetic mechanism for epidermal ensheathment of nociceptive sensory neurites. *eLife* **8**, e42455.

Juliani, J., Vassileff, N. and Spiers, J. G. (2021). Inflammatory-Mediated Neuron-Glia Communication Modulates ALS Pathophysiology. *J. Neurosci.* **41**, 1142–1144.

Jung, H. J. and Suh, Y. (2015). Regulation of IGF -1 signaling by microRNAs. *Frontiers in Genetics* **5**,.

Kaeser, P. S., Deng, L., Wang, Y., Dulubova, I., Liu, X., Rizo, J. and Südhof, T. C. (2011). RIM Proteins Tether Ca2+ Channels to Presynaptic Active Zones via a Direct PDZ-Domain Interaction. *Cell* **144**, 282–295.

Kamimura, K. and Maeda, N. (2021). Glypicans and Heparan Sulfate in Synaptic Development, Neural Plasticity, and Neurological Disorders. *Front. Neural Circuits* **15**,.

Kamimura, K., Odajima, A., Ikegawa, Y., Maru, C. and Maeda, N. (2019). The HSPG Glypican Regulates Experience-Dependent Synaptic and Behavioral Plasticity by Modulating the Non-Canonical BMP Pathway. *Cell Reports* **28**, 3144-3156.e4.

Kan, L., Ott, S., Joseph, B., Park, E. S., Dai, W., Kleiner, R. E., Claridge-Chang, A. and Lai, E. C. (2021). A neural m 6 A/Ythdf pathway is required for learning and memory in Drosophila. *Nat Commun* **12**, 1458.

Kang, D., Wang, D., Xu, J., Quan, C., Guo, X., Wang, H., Luo, J., Yang, Z., Chen, S. and Chen, J. (2018). The InR/Akt/TORC1 Growth-Promoting Signaling Negatively Regulates JAK/STAT Activity and Migratory Cell Fate during Morphogenesis. *Developmental Cell* **44**, 524-531.e5.

Karr, J., Vagin, V., Chen, K., Ganesan, S., Olenkina, O., Gvozdev, V. and Featherstone, D. E. (2009). Regulation of glutamate receptor subunit availability by microRNAs. *Journal of Cell Biology* **185**, 685–697.

Karunanithi, S., Cylinder, D., Ertekin, D., Zalucki, O. H., Marin, L., Lavidis, N. A., Atwood, H. L. and Swinderen, B. van (2020). Proportional Downscaling of Glutamatergic Release Sites by the General Anesthetic Propofol at Drosophila Motor Nerve Terminals. *eNeuro* **7**,.

Kashima, R., Roy, S., Ascano, M., Martinez-Cerdeno, V., Ariza-Torres, J., Kim, S., Louie, J., Lu, Y., Leyton, P., Bloch, K. D., et al. (2016). Augmented noncanonical BMP type II receptor signaling mediates the synaptic abnormality of fragile X syndrome. *Science Signaling*.

Kavalali, E. T. (2015). The mechanisms and functions of spontaneous neurotransmitter release. *Nat Rev Neurosci* **16**, 5–16.

Kenny, P. and Ceman, S. (2016). RNA Secondary Structure Modulates FMRP's Bi-Functional Role in the MicroRNA Pathway. *International Journal of Molecular Sciences* **17**, 985.

Kenny, P. J., Zhou, H., Kim, M., Skariah, G., Khetani, R. S., Drnevich, J., Arcila, M. L., Kosik, K. S. and Ceman, S. (2014). MOV10 and FMRP regulate AGO2 association with microRNA recognition elements. *Cell Rep* **9**, 1729–1741.

Kenny, P. J., Kim, M., Skariah, G., Nielsen, J., Lannom, M. C. and Ceman, S. (2020). The FMRP–MOV10 complex: a translational regulatory switch modulated by G-Quadruplexes. *Nucleic Acids Research* **48**, 862–878.

Kerr, K. S., Fuentes-Medel, Y., Brewer, C., Barria, R., Ashley, J., Abruzzi, K. C., Sheehan, A., Tasdemir-Yilmaz, O. E., Freeman, M. R. and Budnik, V. (2014). Glial Wingless/Wnt Regulates Glutamate Receptor Clustering and Synaptic Physiology at the Drosophila Neuromuscular Junction. *J Neurosci* **34**, 2910–2920.

Kessissoglou, I. A., Langui, D., Hasan, A., Maral, M., Dutta, S. B., Hiesinger, P. R. and Hassan, B. A. (2020). The Drosophila amyloid precursor protein homologue mediates neuronal survival and neuroglial interactions. *PLOS Biology* **18**, e3000703.

Ketosugbo, K. F., Bushnell, H. L. and Johnson, R. I. (2017). A screen for E3 ubiquitination ligases that genetically interact with the adaptor protein Cindr during Drosophila eye patterning. *PLOS ONE* **12**, e0187571.

Khadilkar, R. J., Vogl, W., Goodwin, K. and Tanentzapf, G. (2017). Modulation of occluding junctions alters the hematopoietic niche to trigger immune activation. *eLife* **6**, e28081.

Kidokoro, Y. (2003). Roles of SNARE Proteins and Synaptotagmin I in Synaptic Transmission: Studies at the Drosophila Neuromuscular Synapse. *NSG* **12**, 13–30.

Kim, K., Baek, A., Hwang, J.-E., Choi, Y. A., Jeong, J., Lee, M.-S., Cho, D. H., Lim, J.-S., Kim, K. I. and Yang, Y. (2009). Adiponectin-Activated AMPK Stimulates Dephosphorylation of AKT through Protein Phosphatase 2A Activation. *Cancer Research* **69**, 4018–4026.

Kim, N., Kim, S., Nahm, M., Kopke, D., Kim, J., Cho, E., Lee, M.-J., Lee, M., Kim, S. H., Broadie, K., et al. (2019). BMP-dependent synaptic development requires Abi-Abl-Rac signaling of BMP receptor macropinocytosis. *Nat Commun* **10**, 684.

Kim, J., Kim, S., Nahm, M., Li, T.-N., Lin, H.-C., Kim, Y. D., Lee, J., Yao, C.-K. and Lee, S. (2021). ALS2 regulates endosomal trafficking, postsynaptic development, and neuronal survival. *Journal of Cell Biology* **220**,.

Kimura, M. and Imamoto, N. (2014). Biological Significance of the Importin-β Family-Dependent Nucleocytoplasmic Transport Pathways. *Traffic* **15**, 727–748.

Kittel, R. J., Wichmann, C., Rasse, T. M., Fouquet, W., Schmidt, M., Schmid, A., Wagh, D. A., Pawlu, C., Kellner, R. R., Willig, K. I., et al. (2006). Bruchpilot Promotes Active Zone Assembly, Ca2+ Channel Clustering, and Vesicle Release. *Science* **312**, 1051–1054.

Kopke, D. L., Leahy, S. N., Vita, D. J., Lima, S. C., Newman, Z. L. and Broadie, K. (2020). Carrier of Wingless (Cow) Regulation of Drosophila Neuromuscular Junction Development. *eNeuro* **7**,.

Kottmeier, R., Bittern, J., Schoofs, A., Scheiwe, F., Matzat, T., Pankratz, M. and Klämbt, C. (2020). Wrapping glia regulates neuronal signaling speed and precision in the peripheral nervous system of Drosophila. *Nat Commun* **11**, 4491.

Kremer, M. C., Jung, C., Batelli, S., Rubin, G. M. and Gaul, U. (2017). The glia of the adult Drosophila nervous system. *Glia* **65**, 606–638.

Kuraishi, T., Nakagawa, Y., Nagaosa, K., Hashimoto, Y., Ishimoto, T., Moki, T., Fujita, Y., Nakayama, H., Dohmae, N., Shiratsuchi, A., et al. (2009). Pretaporter, a Drosophila protein serving as a ligand for Draper in the phagocytosis of apoptotic cells. *EMBO J* **28**, 3868–3878.

Kurant, E., Axelrod, S., Leaman, D. and Gaul, U. (2008). The novel engulfment receptor Six-microns-under acts upstream of Draper in the glial phagocytosis of apoptotic neurons. *Cell* **133**, 498–509.

Kurematsu, C., Sawada, M., Ohmuraya, M., Tanaka, M., Kuboyama, K., Ogino, T., Matsumoto, M., Oishi, H., Inada, H., Ishido, Y., et al. (2022). Synaptic pruning of murine adult-born neurons by microglia depends on phosphatidylserine. *Journal of Experimental Medicine* **219**, e20202304.

Lala, T., Doan, J. K., Takatsu, H., Hartzell, H. C., Shin, H.-W. and Hall, R. A. (2022). Phosphatidylserine exposure modulates adhesion GPCR BAI1 (ADGRB1) signaling activity. *Journal of Biological Chemistry* **298**, 102685.

Lamb, R. S., Ward, R. E., Schweizer, L. and Fehon, R. G. (1998). Drosophila coracle, a Member of the Protein 4.1 Superfamily, Has Essential Structural Functions in the Septate

Junctions and Developmental Functions in Embryonic and Adult Epithelial Cells. *Mol Biol Cell* **9**, 3505–3519.

Landskron, L., Steinmann, V., Bonnay, F., Burkard, T. R., Steinmann, J., Reichardt, I., Harzer, H., Laurenson, A.-S., Reichert, H. and Knoblich, J. A. The asymmetrically segregating lncRNA cherub is required for transforming stem cells into malignant cells. *eLife* **7**, e31347.

Landsverk, M. L., Li, S., Hutagalung, A. H., Najafov, A., Hoppe, T., Barral, J. M. and Epstein, H. F. (2007). The UNC-45 chaperone mediates sarcomere assembly through myosin degradation in Caenorhabditis elegans. *Journal of Cell Biology* **177**, 205–210.

Laver, J. D., Li, X., Ancevicius, K., Westwood, J. T., Smibert, C. A., Morris, Q. D. and Lipshitz, H. D. (2013). Genome-wide analysis of Staufen-associated mRNAs identifies secondary structures that confer target specificity. *Nucleic Acids Res* **41**, 9438–9460.

Lee, E. and Chung, W.-S. (2019). Glial Control of Synapse Number in Healthy and Diseased Brain. *Frontiers in Cellular Neuroscience* **13**,.

Li, H., Qi, Y. and Jasper, H. (2016). Ubx dynamically regulates Dpp signaling by repressing Dad expression during copper cell regeneration in the adult Drosophila midgut. *Developmental Biology* **419**, 373–381.

Li, Y., Zhang, F., Jiang, N., Liu, T., Shen, J. and Zhang, J. (2020). Decapentaplegic signaling regulates Wingless ligand production and target activation during Drosophila wing development. *FEBS Letters* **594**, 1176–1186.

Li, Y., Dong, P., Yang, Y., Guo, T., Zhao, Q., Miao, D., Li, H., Lu, T., Xia, F., Lyu, J., et al. (2022). Metabolic control of progenitor cell propagation during Drosophila tracheal remodeling. *Nat Commun* **13**, 2817.

Liao, L., Park, S. K., Xu, T., Vanderklish, P. and Yates, J. R. (2008). Quantitative proteomic analysis of primary neurons reveals diverse changes in synaptic protein content in fmr1 knockout mice. *Proceedings of the National Academy of Sciences* **105**, 15281–15286.

Licznerski, P. and Duman, R. S. (2013). Remodeling of axo-spinous synapses in the pathophysiology and treatment of depression. *Neuroscience* **251**, 33–50.

Lieberman, O. J., McGuirt, A. F., Tang, G. and Sulzer, D. (2019). Roles for neuronal and glial autophagy in synaptic pruning during development. *Neurobiology of Disease* **122**, 49–63.

Lin, K.-Y., Wang, W.-D., Lin, C.-H., Rastegari, E., Su, Y.-H., Chang, Y.-T., Liao, Y.-F., Chang, Y.-C., Pi, H., Yu, B.-Y., et al. (2020). Piwi reduction in the aged niche eliminates germline stem cells via Toll-GSK3 signaling. *Nat Commun* **11**, 3147.

Littleton, J. T., Stern, M., Schulze, K., Perin, M. and Bellen, H. J. (1993). Mutational analysis of Drosophila synaptotagmin demonstrates its essential role in Ca2+-activated neurotransmitter release. *Cell* **74**, 1125–1134.

Liu, B., Li, Y., Stackpole, E. E., Novak, A., Gao, Y., Zhao, Y., Zhao, X. and Richter, J. D. (2018). Regulatory discrimination of mRNAs by FMRP controls mouse adult neural stem cell differentiation. *PNAS* **115**, E11397–E11405.

Low, L. K. and Cheng, H.-J. (2006). Axon pruning: an essential step underlying the developmental plasticity of neuronal connections. *Philos Trans R Soc Lond B Biol Sci* **361**, 1531–1544.

Lowery, L. A. and Vactor, D. V. (2009). The trip of the tip: understanding the growth cone machinery. *Nat Rev Mol Cell Biol* **10**, 332–343.

Luo, L. Q., Martin-Morris, L. E. and White, K. (1990). Identification, secretion, and neural expression of APPL, a Drosophila protein similar to human amyloid protein precursor. *J. Neurosci.* **10**, 3849–3861.

MacDonald, J. M., Beach, M. G., Porpiglia, E., Sheehan, A. E., Watts, R. J. and Freeman, M. R. (2006). The Drosophila Cell Corpse Engulfment Receptor Draper Mediates Glial Clearance of Severed Axons. *Neuron* **50**, 869–881.

Marchetti, B. (2020). Nrf2/Wnt resilience orchestrates rejuvenation of glia-neuron dialogue in Parkinson's disease. *Redox Biology* **36**, 101664.

Marinelli, S., Basilico, B., Marrone, M. C. and Ragozzino, D. (2019). Microglia-neuron crosstalk: Signaling mechanism and control of synaptic transmission. *Seminars in Cell & Developmental Biology* **94**, 138–151.

Marrus, S. B. and DiAntonio, A. (2004). Preferential Localization of Glutamate Receptors Opposite Sites of High Presynaptic Release. *Current Biology* **14**, 924–931.

Martin-Morris, L. E. and White, K. (1990). The Drosophila transcript encoded by the beta-amyloid protein precursor-like gene is restricted to the nervous system. *Development* **110**, 185–195.

Marty, T., Müller, B., Basler, K. and Affolter, M. (2000). Schnurri mediates Dpp-dependent repression of brinker transcription. *Nat Cell Biol* **2**, 745–749.

Mathew, D., Ataman, B., Chen, J., Zhang, Y., Cumberledge, S. and Budnik, V. (2005). Wingless Signaling at Synapses Is Through Cleavage and Nuclear Import of Receptor DFrizzled2. *Science* **310**, 1344–1347.

McCabe, B. D., Marqués, G., Haghighi, A. P., Fetter, R. D., Crotty, M. L., Haerry, T. E., Goodman, C. S. and O'Connor, M. B. (2003). The BMP Homolog Gbb Provides a Retrograde Signal that Regulates Synaptic Growth at the Drosophila Neuromuscular Junction. *Neuron* **39**, 241–254.

McCarthy, N. (2010). Regulation and crosstalk. *Nat Rev Mol Cell Biol* **11**, 390–390.

McClatchey, A. I. (2012). ERM proteins. *Current Biology* **22**, R784–R785.

McClatchey, A. I. (2014). ERM proteins at a glance. *Journal of Cell Science* **127**, 3199–3204.

McLaughlin, C. N., Perry-Richardson, J. J., Coutinho-Budd, J. C. and Broihier, H. T. (2019). Dying Neurons Utilize Innate Immune Signaling to Prime Glia for Phagocytosis during Development. *Developmental Cell* **48**, 506-522.e6.

Menon, K. P., Carrillo, R. A. and Zinn, K. (2013). Development and plasticity of the Drosophila larval neuromuscular junction. *Wiley Interdiscip Rev Dev Biol* **2**, 647–670.

Merkle, J. A., Rickmyre, J. L., Garg, A., Loggins, E. B., Jodoin, J. N., Lee, E., Wu, L. P. and Lee, L. A. (2009). no poles encodes a predicted E3 ubiquitin ligase required for early embryonic development of Drosophila. *Development* **136**, 449–459.

Micklem, D. R., Adams, J., Grünert, S. and St Johnston, D. (2000). Distinct roles of two conserved Staufen domains in oskar mRNA localization and translation. *EMBO J* **19**, 1366–1377.

Mittelstaedt, T. and Schoch, S. (2007). Structure and evolution of RIM-BP genes: Identification of a novel family member. *Gene* **403**, 70–79.

Morizawa, Y. M., Matsumoto, M., Nakashima, Y., Endo, N., Aida, T., Ishikane, H., Beppu, K., Moritoh, S., Inada, H., Osumi, N., et al. (2022). Synaptic pruning through glial synapse engulfment upon motor learning. *Nat Neurosci* **25**, 1458–1469.

Moulton, M. J., Humphreys, G. B., Kim, A. and Letsou, A. (2020). O-GlcNAcylation Dampens Dpp/BMP Signaling to Ensure Proper Drosophila Embryonic Development. *Developmental Cell* **53**, 330-343.e3.

Müller, M. and Davis, G. W. (2012). Trans-Synaptic Control of Presynaptic Ca2+ Influx Achieves Homeostatic Potentiation of Neurotransmitter Release. *Curr Biol* **22**, 1102–1108.

Müller, U. C. and Zheng, H. (2012). Physiological Functions of APP Family Proteins. *Cold Spring Harb Perspect Med* **2**, a006288.

Musashe, D. T., Purice, M. D., Speese, S. D., Doherty, J. and Logan, M. A. (2016). Insulin-like Signaling Promotes Glial Phagocytic Clearance of Degenerating Axons through Regulation of Draper. *Cell Reports* **16**, 1838–1850.

Mutsuddi, M., Marshall, C. M., Benzow, K. A., Koob, M. D. and Rebay, I. (2004). The Spinocerebellar Ataxia 8 Noncoding RNA Causes Neurodegeneration and Associates with Staufen in Drosophila. *Current Biology* **14**, 302–308.

Myrick, L. K., Hashimoto, H., Cheng, X. and Warren, S. T. (2015). Human FMRP contains an integral tandem Agenet (Tudor) and KH motif in the amino terminal domain. *Hum Mol Genet* **24**, 1733–1740.

Nagai, T., Ibata, K., Park, E. S., Kubota, M., Mikoshiba, K. and Miyawaki, A. (2002). A variant of yellow fluorescent protein with fast and efficient maturation for cell-biological applications. *Nat Biotechnol* **20**, 87–90.

Nagata, S., Suzuki, J., Segawa, K. and Fujii, T. (2016). Exposure of phosphatidylserine on the cell surface. *Cell Death Differ* **23**, 952–961.

Nakamura, M., Verboon, J. M., Allen, T. E., Abreu-Blanco, M. T., Liu, R., Dominguez, A. N. M., Delrow, J. J. and Parkhurst, S. M. (2020). Autocrine insulin pathway signaling regulates actin dynamics in cell wound repair. *PLOS Genetics* **16**, e1009186.

Nakano, R., Iwamura, M., Obikawa, A., Togane, Y., Hara, Y., Fukuhara, T., Tomaru, M., Takano-Shimizu, T. and Tsujimura, H. (2019). Cortex glia clear dead young neurons via Drpr/dCed-6/Shark and Crk/Mbc/dCed-12 signaling pathways in the developing Drosophila optic lobe. *Developmental Biology* **453**, 68–85.

Nave, K.-A. (2010). Myelination and support of axonal integrity by glia. *Nature* **468**, 244–252.

Nazareth, L., St John, J., Murtaza, M. and Ekberg, J. (2021). Phagocytosis by Peripheral Glia: Importance for Nervous System Functions and Implications in Injury and Disease. *Frontiers in Cell and Developmental Biology* **9**,.

Nelson, Thomas. J., Sun, M.-K., Hongpaisan, J. and Alkon, D. L. (2008). Insulin, PKC signaling pathways and synaptic remodeling during memory storage and neuronal repair. *European Journal of Pharmacology* **585**, 76–87.

Neniskyte, U. and Gross, C. T. (2017). Errant gardeners: glial-cell-dependent synaptic pruning and neurodevelopmental disorders. *Nat Rev Neurosci* **18**, 658–670.

Newton, F. G., Harris, R. E., Sutcliffe, C. and Ashe, H. L. (2015). Coordinate post-transcriptional repression of Dpp-dependent transcription factors attenuates signal range during development. *Development* **142**, 3362–3373.

Ni, J.-Q., Liu, L.-P., Binari, R., Hardy, R., Shim, H.-S., Cavallaro, A., Booker, M., Pfeiffer, B. D., Markstein, M., Wang, H., et al. (2009). A Drosophila Resource of Transgenic RNAi Lines for Neurogenetics. *Genetics* **182**, 1089–1100.

Ni, J.-Q., Zhou, R., Czech, B., Liu, L.-P., Holderbaum, L., Yang-Zhou, D., Shim, H.-S., Tao, R., Handler, D., Karpowicz, P., et al. (2011). A genome-scale shRNA resource for transgenic RNAi in Drosophila. *Nat Methods* **8**, 405–407.

Niehrs, C. (2012). The complex world of WNT receptor signalling. *Nat Rev Mol Cell Biol* **13**, 767–779.

Nusse, R. and Varmus, H. E. (1982). Many tumors induced by the mouse mammary tumor virus contain a provirus integrated in the same region of the host genome. *Cell* **31**, 99–109.

Nüsslein-Volhard, C. and Wieschaus, E. (1980). Mutations affecting segment number and polarity in Drosophila. *Nature* **287**, 795–801.

Ou, J., He, Y., Xiao, X., Yu, T.-M., Chen, C., Gao, Z. and Ho, M. S. (2014). Glial cells in neuronal development: recent advances and insights from Drosophila melanogaster. *Neurosci. Bull.* **30**, 584–594.

Pan, L. and Broadie, K. S. (2007a). Drosophila Fragile X Mental Retardation Protein and Metabotropic Glutamate Receptor A Convergently Regulate the Synaptic Ratio of Ionotropic Glutamate Receptor Subclasses. *J Neurosci* **27**, 12378–12389.

Pan, L. and Broadie, K. S. (2007b). Drosophila Fragile X Mental Retardation Protein and Metabotropic Glutamate Receptor A Convergently Regulate the Synaptic Ratio of Ionotropic Glutamate Receptor Subclasses. *J. Neurosci.* **27**, 12378–12389.

Pan, L., Zhang, Y. Q., Woodruff, E. and Broadie, K. (2004). The Drosophila fragile X gene negatively regulates neuronal elaboration and synaptic differentiation. *Curr Biol* **14**, 1863–1870.

Pan, L., Woodruff, E., Liang, P. and Broadie, K. (2008). Mechanistic relationships between Drosophila fragile X mental retardation protein and metabotropic glutamate receptor A signaling. *Molecular and Cellular Neuroscience* **37**, 747–760.

Paolicelli, R. C., Bolasco, G., Pagani, F., Maggi, L., Scianni, M., Panzanelli, P., Giustetto, M., Ferreira, T. A., Guiducci, E., Dumas, L., et al. (2011). Synaptic Pruning by Microglia Is Necessary for Normal Brain Development. *Science* **333**, 1456–1458.

Park, E. and Maquat, L. E. (2013). Staufen-mediated mRNA decay. *WIREs RNA* **4**, 423–435.

Parnas, D., Haghighi, A. P., Fetter, R. D., Kim, S. W. and Goodman, C. S. (2001). Regulation of Postsynaptic Structure and Protein Localization by the Rho-Type Guanine Nucleotide Exchange Factor dPix. *Neuron* **32**, 415–424.

Pasciuto, E., Ahmed, T., Wahle, T., Gardoni, F., D'Andrea, L., Pacini, L., Jacquemont, S., Tassone, F., Balschun, D., Dotti, C. G., et al. (2015). Dysregulated ADAM10-Mediated Processing of APP during a Critical Time Window Leads to Synaptic Deficits in Fragile X Syndrome. *Neuron* **87**, 382–398.

Patel, S., Alam, A., Pant, R. and Chattopadhyay, S. (2019). Wnt Signaling and Its Significance Within the Tumor Microenvironment: Novel Therapeutic Insights. *Frontiers in Immunology* **10**,.

Peng, J.-J., Lin, S.-H., Liu, Y.-T., Lin, H.-C., Li, T.-N. and Yao, C.-K. (2019). A circuit-dependent ROS feedback loop mediates glutamate excitotoxicity to sculpt the Drosophila motor system. *eLife* **8**, e47372.

Petersen, S. A., Fetter, R. D., Noordermeer, J. N., Goodman, C. S. and DiAntonio, A. (1997). Genetic Analysis of Glutamate Receptors in Drosophila Reveals a Retrograde Signal Regulating Presynaptic Transmitter Release. *Neuron* **19**, 1237–1248.

Petzoldt, A. G., Lee, Y.-H., Khorramshahi, O., Reynolds, E., Plested, A. J. R., Herzel, H. and Sigrist, S. J. (2014). Gating Characteristics Control Glutamate Receptor Distribution and Trafficking In Vivo. *Current Biology* **24**, 2059–2065.

Pfeiffer, B. E. and Huber, K. M. (2009). The State of Synapses in Fragile X Syndrome. *Neuroscientist* **15**, 549–567.

Pielage, J., Fetter, R. D. and Davis, G. W. (2006). A postsynaptic Spectrin scaffold defines active zone size, spacing, and efficacy at the Drosophila neuromuscular junction. *J Cell Biol* **175**, 491–503.

Pieretti, M., Zhang, F., Fu, Y.-H., Warren, S. T., Oostra, B. A., Caskey, C. T. and Nelson, D. L. (1991). Absence of expression of the FMR-1 gene in fragile X syndrome. *Cell* **66**, 817–822.

PRICE, T. J., FLORES, C. M., CERVERO, F. and HARGREAVES, K. M. (2006). THE RNA BINDING AND TRANSPORT PROTEINS STAUFEN AND FRAGILE X MENTAL RETARDATION PROTEIN ARE EXPRESSED BY RAT PRIMARY AFFERENT NEURONS AND LOCALIZE TO PERIPHERAL AND CENTRAL AXONS. *Neuroscience* **141**, 2107–2116.

Qin, G., Schwarz, T., Kittel, R. J., Schmid, A., Rasse, T. M., Kappei, D., Ponimaskin, E., Heckmann, M. and Sigrist, S. J. (2005). Four Different Subunits Are Essential for Expressing the Synaptic Glutamate Receptor at Neuromuscular Junctions of Drosophila. *J. Neurosci.* **25**, 3209–3218.

Quiñones-Frías, M. C. and Littleton, J. T. (2021). Function of Drosophila Synaptotagmins in membrane trafficking at synapses. *Cell Mol Life Sci* **78**, 4335–4364.

Rahman, M. M., Islam, M. R., Yamin, M., Islam, M. M., Sarker, M. T., Meem, A. F. K., Akter, A., Emran, T. B., Cavalu, S. and Sharma, R. (2022). Emerging Role of Neuron-Glia in Neurological Disorders: At a Glance. *Oxidative Medicine and Cellular Longevity* **2022**, e3201644.

Raiders, S., Han, T., Scott-Hewitt, N., Kucenas, S., Lew, D., Logan, M. A. and Singhvi, A. (2021). Engulfed by Glia: Glial Pruning in Development, Function, and Injury across Species. *J. Neurosci.* **41**, 823–833.

Rajaratnam, A., Shergill, J., Salcedo-Arellano, M., Saldarriaga, W., Duan, X. and Hagerman, R. (2017). Fragile X syndrome and fragile X-associated disorders. *F1000Res* **6**, 2112.

Ramirez, D. M. O., Khvotchev, M., Trauterman, B. and Kavalali, E. T. (2012). Vti1a identifies a vesicle pool that preferentially recycles at rest and maintains spontaneous neurotransmission. *Neuron* **73**, 121–134.

Ramos, A., Grünert, S., Adams, J., Micklem, D. R., Proctor, M. R., Freund, S., Bycroft, M., St Johnston, D. and Varani, G. (2000). RNA recognition by a Staufen double-stranded RNA-binding domain. *The EMBO Journal* **19**, 997–1009.

RAMOS, A., HOLLINGWORTH, D. and PASTORE, A. (2003). G-quartet-dependent recognition between the FMRP RGG box and RNA. *RNA* **9**, 1198–1207.

Rana, M. S., Wang, X. and Banerjee, A. (2018). An improved strategy for fluorescent tagging of membrane proteins for overexpression and purification in mammalian cells. *Biochemistry* **57**, 6741–6751.

Rasband, M. N. (2016). Glial Contributions to Neural Function and Disease. *Mol Cell Proteomics* **15**, 355–361.

Rashad, S., Tominaga, T. and Niizuma, K. (2020). The cell and stress-specific canonical and non-canonical tRNA cleavage. 2020.02.04.934695.

Raza, Q., Choi, J. Y., Li, Y., O'Dowd, R. M., Watkins, S. C., Chikina, M., Hong, Y., Clark, N. L. and Kwiatkowski, A. V. (2019). Evolutionary rate covariation analysis of E-cadherin identifies Raskol as a regulator of cell adhesion and actin dynamics in Drosophila. *PLOS Genetics* **15**, e1007720.

Razak, K. A., Dominick, K. C. and Erickson, C. A. (2020). Developmental studies in fragile X syndrome. *Journal of Neurodevelopmental Disorders* **12**, 13.

Renden, R. B. and Broadie, K. (2003). Mutation and activation of Galpha s similarly alters pre- and postsynaptic mechanisms modulating neurotransmission. *J Neurophysiol* **89**, 2620–2638.

Repicky, S. and Broadie, K. (2009). Metabotropic Glutamate Receptor–Mediated Use–Dependent Down-Regulation of Synaptic Excitability Involves the Fragile X Mental Retardation Protein. *Journal of Neurophysiology* **101**, 672–687.

Rhea, E. M. and Banks, W. A. (2019). Role of the Blood-Brain Barrier in Central Nervous System Insulin Resistance. *Frontiers in Neuroscience* **13**,.

Richter, J. D. and Zhao, X. (2021). The molecular biology of FMRP: new insights into fragile X syndrome. *Nat Rev Neurosci* **22**, 209–222.

Riera Romo, M. (2021). Cell death as part of innate immunity: Cause or consequence? *Immunology* **163**, 399–415.

Rival, T., Soustelle, L., Cattaert, D., Strambi, C., Iché, M. and Birman, S. (2006). Physiological requirement for the glutamate transporter dEAAT1 at the adult Drosophila neuromuscular junction. *Journal of Neurobiology* **66**, 1061–1074.

Rohrbough, J., Rushton, E., Palanker, L., Woodruff, E., Matthies, H. J. G., Acharya, U., Acharya, J. K. and Broadie, K. (2004). Ceramidase Regulates Synaptic Vesicle Exocytosis and Trafficking. *J. Neurosci.* **24**, 7789–7803.

Roos, J., Hummel, T., Ng, N., Klämbt, C. and Davis, G. W. (2000). Drosophila Futsch Regulates Synaptic Microtubule Organization and Is Necessary for Synaptic Growth. *Neuron* **26**, 371–382.

Roth, M., Ronco, L., Cadavid, D., Durbin-Johnson, B., Hagerman, R. J. and Tassone, F. (2021). FMRP Levels in Human Peripheral Blood Leukocytes Correlates with Intellectual Disability. *Diagnostics* **11**, 1780.

Sakai, J. (2020). How synaptic pruning shapes neural wiring during development and, possibly, in disease. *Proceedings of the National Academy of Sciences* **117**, 16096–16099.

Saltykova, I. V., Elahi, A., Pitale, P. M., Gorbatyuk, O. S., Athar, M. and Gorbatyuk, M. S. (2021). Tribbles homolog 3-mediated targeting the AKT/mTOR axis in mice with retinal degeneration. *Cell Death Dis* **12**, 1–11.

Sandstrom, D. J. (2011). Extracellular Protons Reduce Quantal Content and Prolong Synaptic Currents at the *Drosophila* Larval Neuromuscular Junction. *Journal of Neurogenetics* **25**, 104–114.

Sansores-Garcia, L., Atkins, M., Moya, I. M., Shahmoradgoli, M., Tao, C., Mills, G. B. and Halder, G. (2013). Mask Is Required for the Activity of the Hippo Pathway Effector Yki/YAP. *Current Biology* **23**, 229–235.

Santos, E. and Noggle, C. A. (2011). Synaptic Pruning. In *Encyclopedia of Child Behavior and Development* (ed. Goldstein, S.) and Naglieri, J. A.), pp. 1464–1465. Boston, MA: Springer US.

Sara, Y., Virmani, T., Deák, F., Liu, X. and Kavalali, E. T. (2005). An isolated pool of vesicles recycles at rest and drives spontaneous neurotransmission. *Neuron* **45**, 563–573.

Sardi, J., Bener, M. B., Simao, T., Descoteaux, A. E., Slepchenko, B. M. and Inaba, M. (2021). Mad dephosphorylation at the nuclear pore is essential for asymmetric stem cell division. *PNAS* **118**,.

Sauvola, C. W. and Littleton, J. T. (2021). SNARE Regulatory Proteins in Synaptic Vesicle Fusion and Recycling. *Frontiers in Molecular Neuroscience* **14**,.

Schafer, D. P., Lehrman, E. K., Kautzman, A. G., Koyama, R., Mardinly, A. R., Yamasaki, R., Ransohoff, R. M., Greenberg, M. E., Barres, B. A. and Stevens, B. (2012). Microglia Sculpt Postnatal Neural Circuits in an Activity and Complement-Dependent Manner. *Neuron* **74**, 691–705.

Scheffer, L. K., Xu, C. S., Januszewski, M., Lu, Z., Takemura, S., Hayworth, K. J., Huang, G. B., Shinomiya, K., Maitlin-Shepard, J., Berg, S., et al. (2020). A connectome and analysis of the adult Drosophila central brain. *eLife* **9**, e57443.

Schmid, A., Hallermann, S., Kittel, R. J., Khorramshahi, O., Frölich, A. M. J., Quentin, C., Rasse, T. M., Mertel, S., Heckmann, M. and Sigrist, S. J. (2008). Activity-dependent site-specific changes of glutamate receptor composition in vivo. *Nat Neurosci* **11**, 659–666.

Scholze, A. R., Foo, L. C., Mulinyawe, S. and Barres, B. A. (2014). BMP Signaling in Astrocytes Downregulates EGFR to Modulate Survival and Maturation. *PLOS ONE* **9**, e110668.

Schuster, C. M., Ultsch, A., Schloss, P., Cox, J. A., Schmitt, B. and Betz, H. (1991). Molecular Cloning of an Invertebrate Glutamate Receptor Subunit Expressed in Drosophila Muscle. *Science* **254**, 112–114.

See, J., Mamontov, P., Ahn, K., Wine-Lee, L., Crenshaw, E. B. and Grinspan, J. B. (2007). BMP signaling mutant mice exhibit glial cell maturation defects. *Molecular and Cellular Neuroscience* **35**, 171–182.

Sekar, A., Bialas, A. R., de Rivera, H., Davis, A., Hammond, T. R., Kamitaki, N., Tooley, K., Presumey, J., Baum, M., Van Doren, V., et al. (2016). Schizophrenia risk from complex variation of complement component 4. *Nature* **530**, 177–183.

Shah, S., Molinaro, G., Liu, B., Wang, R., Huber, K. M. and Richter, J. D. (2020). FMRP Control of Ribosome Translocation Promotes Chromatin Modifications and Alternative Splicing of Neuronal Genes Linked to Autism. *Cell Reports* **30**, 4459-4472.e6.

Sharma, P., Mesci, P., Carromeu, C., McClatchy, D. R., Schiapparelli, L., Yates, J. R., Muotri, A. R. and Cline, H. T. (2019). Exosomes regulate neurogenesis and circuit assembly. *Proceedings of the National Academy of Sciences* **116**, 16086–16094.

Shu, H., Donnard, E., Liu, B., Jung, S., Wang, R. and Richter, J. D. (2020). FMRP links optimal codons to mRNA stability in neurons. *Proc Natl Acad Sci U S A* **117**, 30400–30411.

Siller, S. S. and Broadie, K. (2011). Neural circuit architecture defects in a Drosophila model of Fragile X syndrome are alleviated by minocycline treatment and genetic removal of matrix metalloproteinase. *Disease Models & Mechanisms* **4**, 673–685.

Sivachenko, A., Li, Y., Abruzzi, K. C. and Rosbash, M. (2013). The Transcription Factor Mef2 Links the Drosophila Core Clock to Fas2, Neuronal Morphology, and Circadian Behavior. *Neuron* **79**, 281–292.

Skjeldal, F. M., Haugen, L. H., Mateus, D., Frei, D. M., Rødseth, A. V., Hu, X. and Bakke, O. (2021). De novo formation of early endosomes during Rab5-to-Rab7a transition. *Journal of Cell Science* **134**, jcs254185.

Smith, M., Turki-Judeh, W. and Courey, A. J. (2012). SUMOylation in Drosophila Development. *Biomolecules* **2**, 331–349.

Sokolova, D., Childs, T. and Hong, S. (2021). Insight into the role of phosphatidylserine in complement-mediated synapse loss in Alzheimer's disease. *Fac Rev* **10**, 19.

Sone, M., Suzuki, E., Hoshino, M., Hou, D., Kuromi, H., Fukata, M., Kuroda, S., Kaibuchi, K., Nabeshima, Y. and Hama, C. (2000). Synaptic development is controlled in the periactive zones of Drosophila synapses. *Development* **127**, 4157–4168.

Song, C. and Broadie, K. (2022). Dysregulation of BMP, Wnt, and Insulin Signaling in Fragile X Syndrome. *Frontiers in Cell and Developmental Biology* **10**,.

Song, C. and Broadie, K. (2023). Fragile X mental retardation protein coordinates neuron-to-glia communication for clearance of developmentally transient brain neurons. *Proceedings of the National Academy of Sciences* **120**, e2216887120.

Song, C., Leahy, S. N., Rushton, E. M. and Broadie, K. (2022). RNA-binding FMRP and Staufen sequentially regulate the Coracle scaffold to control synaptic glutamate receptor and bouton development. *Development* **149**, dev200045.

Soto, E., Ortega-Ramírez, A. and Vega, R. (2018). Protons as Messengers of Intercellular Communication in the Nervous System. *Frontiers in Cellular Neuroscience* **12**,.

St Johnston, D., Beuchle, D. and Nüsslein-Volhard, C. (1991). Staufen, a gene required to localize maternal RNAs in the Drosophila egg. *Cell* **66**, 51–63.

Starke, E. L., Zius, K. and Barbee, S. A. (2022). FXS causing missense mutations disrupt FMRP granule formation, dynamics, and function. *PLOS Genetics* **18**, e1010084.

Stenmark, H. (2009). Rab GTPases as coordinators of vesicle traffic. *Nat Rev Mol Cell Biol* **10**, 513–525.

Stogsdill, J. A. and Eroglu, C. (2017). The interplay between neurons and glia in synapse development and plasticity. *Current Opinion in Neurobiology* **42**, 1–8.

Sulkowski, M., Kim, Y.-J. and Serpe, M. (2014). Postsynaptic glutamate receptors regulate local BMP signaling at the Drosophila neuromuscular junction. *Development* **141**, 436–447.

Sulkowski, M. J., Han, T. H., Ott, C., Wang, Q., Verheyen, E. M., Lippincott-Schwartz, J. and Serpe, M. (2016). A Novel, Noncanonical BMP Pathway Modulates Synapse Maturation at the Drosophila Neuromuscular Junction. *PLOS Genetics* **12**, e1005810.

Suresh, A. and Dunaevsky, A. (2017). Relationship Between Synaptic AMPAR and Spine Dynamics: Impairments in the FXS Mouse. *Cerebral Cortex* **27**, 4244–4256.

Tabolacci, E. and Neri, G. (2017). Chapter 6 - Epigenetic causes of intellectual disability—the fragile X syndrome paradigm. In *Neuropsychiatric Disorders and Epigenetics* (ed. Yasui, D. H.), Peedicayil, J.), and Grayson, D. R.), pp. 107–127. Boston: Academic Press.

Tamanini, F., Willemsen, R., van Unen, L., Bontekoe, C., Galjaard, H., Oostra, B. A. and Hoogeveen, A. T. (1997). Differential Expression of FMR1, FXR1 and FXR2 Proteins in Human Brain and Testis. *Human Molecular Genetics* **6**, 1315–1322.

Tenenbaum, C. M., Misra, M., Alizzi, R. A. and Gavis, E. R. (2017). Enclosure of Dendrites by Epidermal Cells Restricts Branching and Permits Coordinated Development of Spatially Overlapping Sensory Neurons. *Cell Reports* **20**, 3043–3056.

Tessier, C. R. and Broadie, K. (2011). The Fragile X Mental Retardation Protein Developmentally Regulates the Strength and Fidelity of Calcium Signaling in Drosophila Mushroom Body Neurons. *Neurobiol Dis* **41**, 147–159.

Tokuda, S., Higashi, T. and Furuse, M. (2014). ZO-1 Knockout by TALEN-Mediated Gene Targeting in MDCK Cells: Involvement of ZO-1 in the Regulation of Cytoskeleton and Cell Shape. *PLOS ONE* **9**, e104994.

Torres-Vazquez, J., Warrior, R. and Arora, K. (2000). schnurri Is Required for dpp-Dependent Patterning of the Drosophila Wing. *Developmental Biology* **227**, 388–402.

Tracy Cai, X., Li, H., Safyan, A., Gawlik, J., Pyrowolakis, G. and Jasper, H. (2019). AWD regulates timed activation of BMP signaling in intestinal stem cells to maintain tissue homeostasis. *Nat Commun* **10**, 2988.

Tsang, B., Arsenault, J., Vernon, R. M., Lin, H., Sonenberg, N., Wang, L.-Y., Bah, A. and Forman-Kay, J. D. (2019). Phosphoregulated FMRP phase separation models activity-dependent translation through bidirectional control of mRNA granule formation. *PNAS* **116**, 4218–4227.

Tsou, W.-L., Ouyang, M., Hosking, R. R., Sutton, J. R., Blount, J. R., Burr, A. A. and Todi, S. V. (2015). The deubiquitinase ataxin-3 requires Rad23 and DnaJ-1 for its neuroprotective role in Drosophila melanogaster. *Neurobiology of Disease* **82**, 12–21.

Tsurudome, K., Tsang, K., Liao, E. H., Ball, R., Penney, J., Yang, J.-S., Elazzouzi, F., He, T., Chishti, A., Lnenicka, G., et al. (2010). The Drosophila miR-310 cluster negatively regulates synaptic strength at the neuromuscular junction. *Neuron* **68**, 879–893.

Turola, E., Furlan, R., Bianco, F., Matteoli, M. and Verderio, C. (2012). Microglial microvesicles secretion and intercellular signalling. *Frontiers in Physiology* **3**,.

Upadhyay, A., Moss-Taylor, L., Kim, M.-J., Ghosh, A. C. and O'Connor, M. B. (2017). TGF-β Family Signaling in Drosophila. *Cold Spring Harb Perspect Biol* **9**,.

Urrutia, H., Aleman, A. and Eivers, E. (2016). Drosophila Dullard functions as a Mad phosphatase to terminate BMP signaling. *Sci Rep* **6**, 32269.

Vandenberg, G. G., Dawson, N. J., Head, A., Scott, G. R. and Scott, A. L. (2021). Astrocyte-mediated disruption of ROS homeostasis in Fragile X mouse model. *Neurochemistry International* **146**, 105036.

Vanlandingham, P. A., Fore, T. R., Chastain, L. R., Royer, S. M., Bao, H., Reist, N. E. and Zhang, B. (2013). Epsin 1 Promotes Synaptic Growth by Enhancing BMP Signal Levels in Motoneuron Nuclei. *PLOS ONE* **8**, e65997.

Vats, S. and Galli, T. (2022). Role of SNAREs in Unconventional Secretion—Focus on the VAMP7-Dependent Secretion. *Frontiers in Cell and Developmental Biology* **10**,.

Verheij, C., Bakker, C. E., de Graaff, E., Keulemans, J., Willemsen, R., Verkerk, A. J. M. H., Galjaard, H., Reuser, A. J. J., Hoogeveen, A. T. and Oostra, B. A. (1993).

Characterization and localization of the FMR-1 gene product associated with fragile X syndrome. *Nature* **363**, 722–724.

Verkerk, A. J., Pieretti, M., Sutcliffe, J. S., Fu, Y. H., Kuhl, D. P., Pizzuti, A., Reiner, O., Richards, S., Victoria, M. F. and Zhang, F. P. (1991). Identification of a gene (FMR-1) containing a CGG repeat coincident with a breakpoint cluster region exhibiting length variation in fragile X syndrome. *Cell* **65**, 905–914.

Vinayagam, A., Kulkarni, M. M., Sopko, R., Sun, X., Hu, Y., Nand, A., Villalta, C., Moghimi, A., Yang, X., Mohr, S. E., et al. (2016). An integrative analysis of the InR/PI3K/Akt network identifies the dynamic response to Insulin signaling. *Cell Rep* **16**, 3062–3074.

Vita, D. J., Meier, C. J. and Broadie, K. (2021). Neuronal fragile X mental retardation protein activates glial insulin receptor mediated PDF-Tri neuron developmental clearance. *Nat Commun* **12**, 1160.

Walsh, C. M. and Carroll, S. B. (2007). Collaboration between Smads and a Hox protein in target gene repression. *Development* **134**, 3585–3592.

Wan, H. I., DiAntonio, A., Fetter, R. D., Bergstrom, K., Strauss, R. and Goodman, C. S. (2000). Highwire Regulates Synaptic Growth in Drosophila. *Neuron* **26**, 313–329.

Wang, T., Li, L. and Hong, W. (2017). SNARE proteins in membrane trafficking. *Traffic* **18**, 767–775.

Ward IV, R. E., Lamb, R. S. and Fehon, R. G. (1998). A Conserved Functional Domain of Drosophila Coracle Is Required for Localization at the Septate Junction and Has Membrane-organizing Activity. *J Cell Biol* **140**, 1463–1473.

Wegel, E., Göhler, A., Lagerholm, B. C., Wainman, A., Uphoff, S., Kaufmann, R. and Dobbie, I. M. (2016). Imaging cellular structures in super-resolution with SIM, STED and Localisation Microscopy: A practical comparison. *Sci Rep* **6**, 27290.

Wegner, W., Steffens, H., Gregor, C., Wolf, F. and Willig, K. I. (2022). Environmental enrichment enhances patterning and remodeling of synaptic nanoarchitecture as revealed by STED nanoscopy. *eLife* **11**, e73603.

Weimer, R. M. and Jorgensen, E. M. (2003). Controversies in synaptic vesicle exocytosis. *Journal of Cell Science* **116**, 3661–3666.

Westmark, C. J. (2019). Fragile X and APP: A Decade in Review, A Vision for the Future. *Mol Neurobiol* **56**, 3904–3921.

Westmark, C. J. and Malter, J. S. (2007). FMRP Mediates mGluR5-Dependent Translation of Amyloid Precursor Protein. *PLOS Biology* **5**, e52.

Westmark, C. J., Westmark, P. R. and Malter, J. S. (2010). MPEP Reduces Seizure Severity in Fmr-1 KO mice over Expressing Human Aβ. *Int J Clin Exp Pathol* **3**, 56–68.

Westmark, C. J., Chuang, S.-C., Hays, S. A., Filon, M. J., Ray, B. C., Westmark, P. R., Gibson, J. R., Huber, K. M. and Wong, R. K. S. (2016). APP Causes Hyperexcitability in Fragile X Mice. *Frontiers in Molecular Neuroscience* **9**,.

White, R. and Krämer-Albers, E.-M. (2014). Axon-glia interaction and membrane traffic in myelin formation. *Front Cell Neurosci* **7**, 284.

Willert, K., Brown, J. D., Danenberg, E., Duncan, A. W., Weissman, I. L., Reya, T., Yates, J. R. and Nusse, R. (2003). Wnt proteins are lipid-modified and can act as stem cell growth factors. *Nature* **423**, 448–452.

Wong, J. J. L., Li, S., Lim, E. K. H., Wang, Y., Wang, C., Zhang, H., Kirilly, D., Wu, C., Liou, Y.-C., Wang, H., et al. (2013). A Cullin1-Based SCF E3 Ubiquitin Ligase Targets the InR/PI3K/TOR Pathway to Regulate Neuronal Pruning. *PLOS Biology* **11**, e1001657.

Wu, H., Xiong, W. C. and Mei, L. (2010). To build a synapse: signaling pathways in neuromuscular junction assembly. *Development* **137**, 1017–1033.

Wu, Z., Xiao, L., Wang, H. and Wang, G. (2021). Neurogenic hypothesis of positive psychology in stress-induced depression: Adult hippocampal neurogenesis, neuroinflammation, and stress resilience. *International Immunopharmacology* **97**, 107653.

Xu, S., Lu, J., Shao, A., Zhang, J. H. and Zhang, J. (2020). Glial Cells: Role of the Immune Response in Ischemic Stroke. *Front Immunol* **11**, 294.

Xue, M., Lin, Y. Q., Pan, H., Reim, K., Deng, H., Bellen, H. J. and Rosenmund, C. (2009). Tilting the Balance between Facilitatory and Inhibitory Functions of Mammalian and Drosophila Complexins Orchestrates Synaptic Vesicle Exocytosis. *Neuron* **64**, 367–380.

Yilmazer, Y. B., Koganezawa, M., Sato, K., Xu, J. and Yamamoto, D. (2016). Serotonergic neuronal death and concomitant serotonin deficiency curb copulation ability of Drosophila platonic mutants. *Nat Commun* **7**, 13792.

Yu, J. S. L. and Cui, W. (2016). Proliferation, survival and metabolism: the role of PI3K/AKT/mTOR signalling in pluripotency and cell fate determination. *Development* **143**, 3050–3060.

Yu, Z., Fan, D., Gui, B., Shi, L., Xuan, C., Shan, L., Wang, Q., Shang, Y. and Wang, Y. (2012). Neurodegeneration-associated TDP-43 Interacts with Fragile X Mental Retardation Protein (FMRP)/Staufen (STAU1) and Regulates SIRT1 Expression in Neuronal Cells. *Journal of Biological Chemistry* **287**, 22560–22572.

Zhang, Y. Q., Bailey, A. M., Matthies, H. J. G., Renden, R. B., Smith, M. A., Speese, S. D., Rubin, G. M. and Broadie, K. (2001). Drosophila Fragile X-Related Gene Regulates the MAP1B Homolog Futsch to Control Synaptic Structure and Function. *Cell* **107**, 591–603.

Zhang, M., Chen, D., Xia, J., Han, W., Cui, X., Neuenkirchen, N., Hermes, G., Sestan, N. and Lin, H. (2017). Post-transcriptional regulation of mouse neurogenesis by Pumilio proteins. *Genes Dev.* **31**, 1354–1369.

Zhang, F., Kang, Y., Wang, M., Li, Y., Xu, T., Yang, W., Song, H., Wu, H., Shu, Q. and Jin, P. (2018). Fragile X mental retardation protein modulates the stability of its m6A-marked messenger RNA targets. *Hum Mol Genet* **27**, 3936–3950.

Zhou, Z., Hartwieg, E. and Horvitz, H. R. (2001). CED-1 Is a Transmembrane Receptor that Mediates Cell Corpse Engulfment in C. elegans. *Cell* **104**, 43–56.